EVOLUTIONARY AND PULSATIONAL CONSTRAINTS FOR SUPER-METAL-RICH STARS WITH Z=0.04

Giuseppe Bono
Osservatorio Astronomico di Trieste, Via G.B. Tiepolo 11, 34131 Trieste, Italy;
bono@oat.ts.astro.it

Filippina Caputo
Osservatorio Astronomico di Capodimonte, Via Moiariello 16, 80131 Napoli, Italy;
caputo@astrna.na.astro.it

Santi Cassisi[1]
Osservatorio Astronomico di Teramo, Via M. Maggini, 64100 Teramo, Italy;
cassisi@astrte.te.astro.it

Vittorio Castellani[2]
Dipartimento di Fisica, Univ. di Pisa, Piazza Torricelli 2, 56100 Pisa, Italy;
vittorio@astr1pi.difi.unipi.it

and

Marcella Marconi
Dipartimento di Fisica, Univ. di Pisa, Piazza Torricelli 2, 56100 Pisa, Italy;
marcella@astr1pi.difi.unipi.it

ABSTRACT

We investigate the evolutionary behavior of stellar structures with metallicity Z=0.04 in order to disclose theoretical expectations for both evolutionary and pulsational behaviors of Super-Metal-Rich (SMR) objects, which are found in the solar neighborhood, in the Galactic bulge and in elliptical galaxies. A suitable set of stellar models is presented for the given metallicity value but for two alternative assumptions about the amount of original He, namely Y=0.34 and Y=0.37. Theoretical isochrones for H burning evolutionary phases are

[1]Dipartimento di Fisica, Università de L'Aquila, Via Vetoio, 67100 L'Aquila, Italy

[2]Osservatorio Astronomico di Teramo, Via M. Maggini, 64100 Teramo, Italy

presented for ages ranging from 18 to less than 1 Gyr. The evolutionary behavior of He burning structures is discussed for suitable assumptions about the mass of the progenitors and the amount of mass loss. For both quoted assumptions of original He abundance we confirm that at metal contents larger than the solar value the luminosity of the Horizontal Branch (HB) at the RR Lyrae gap increases as the metal content increases, a direct consequence of the expected simultaneous increase of original He. We find that at the exhaustion of central helium SMR stars definitely undergo the gravonuclear instabilities previously found in some He burning structures with solar metallicity (Bono et al. 1997b). On the basis of such an evolutionary scenario, we investigate the expected pulsational behavior of He burning SMR stars for suitable assumptions on the pulsators evolutionary parameters. Linear blue boundaries for pulsational instability in the fundamental and in the first overtone modes are derived and their dependence on stellar mass and chemical composition is investigated. Nonlinear, nonlocal, and time-dependent convective models are discussed, the modal stability is investigated for the first two modes, and the theoretical predictions about the period distribution inside the instability strip and the shape of both light and velocity curves are presented. Full amplitude, nonlinear envelope models show that the range of effective temperatures where SMR RR Lyrae variables present a stable limit cycle is smaller in comparison with pulsators characterized by lower metal abundances. In fact, the width of the instability strip at the Zero Age Horizontal Branch (ZAHB) luminosity level decreases from 1400 K to 1100 K. Taking also into account the peculiar narrow mass range characterizing SMR pulsators we estimate that these two factors alone cause a decrease in the occurrence of RR Lyrae pulsators by a factor of seven in comparison with metal-poor, globular cluster-like stellar populations. We find that canonical analytical relations connecting the nonlinear periods of metal-poor variables to their luminosity, mass and effective temperature cannot be safely extrapolated to the range of SMR pulsators.

We show that gravonuclear instabilities largely increase the lifetimes of stars crossing the instability strip at luminosity levels higher than the HB luminosity, thus increasing the expected occurrence of luminous low-mass variables. We show that both periods and light curves of different groups of type II Cepheids with periods shorter than six days, presented by Diethelm (1983,1990), can be all reproduced by suitable variations in the effective temperature or in the luminosity level of our SMR post-HB models, supporting evidence of a substantial homogeneity of these variables. On the basis of both evolutionary and pulsation findings we finally predict the rate of period change for a typical

field, metal-rich type II Cepheid across the instability strip and discuss an observational test for validating the present theoretical scenarios. In the Appendix we discuss in detail the physics of gravonuclear instabilities, which appear as a surprisingly exact confirmation of the theoretical predictions given by Schwarzschild and Harm as early as 1965.

Subject headings: galaxies: stellar content – field stars – stars: evolution – stars: horizontal branch – stars: variables: RR Lyrae, Type II Cepheids

1. INTRODUCTION

Almost thirty years ago Spinrad & Taylor (1969), discussing a large sample of narrow-band spectral indices for field and cluster G and K stars, identified a class of giants characterized by very strong line absorption and by an excess of UBV blanketing and suggested that similar features are the signature of an overabundance of metals up to 4 times larger than the solar metal content. Accordingly, they revealed the existence of a population of "Super-Metal-Rich" (SMR) stars, a name that we adopt here for all stars more metal-rich than the Sun. Much more recently, Rich (1988) first disclosed that the Galactic bulge population does contain a substantial fraction of SMR giants. Sadler, Rich and Terndrup (1996), discussed an impressive amount of spectroscopic observations of K and M giants in the Baade's Window, finding that more than 50% of their sample was characterized by metal abundances in the range $[Fe/H] \sim 0.3 - 0.4$. By relying on Strömgren photometry, Rocha-Pinto & Maciel (1996) have recently obtained a quite similar metallicity distribution for G dwarfs in the solar neighborhood. Thus SMR stars appear to be a rather common stellar component of our Galaxy.

Of course the occurrence of SMR stars is not restricted to our Galaxy. As a matter of fact, the presence of SMR globular clusters in external galaxies is becoming a well-established observational evidence. Recent ground-based and HST integrated photometry of a large sample of globular clusters belonging either to a peculiar (Minniti et al. 1996) or to an elliptical galaxy (Geisler, Lee & Kim 1996, hereinafter referred to as GLK) has firmly brought out the existence of a radial metallicity gradient between the inner and the outer regions of these galaxies, with the tail of the metallicity distribution which may reach very large metal abundances ($[Fe/H] \approx 0.5 - 1.0$).

According to this evidence, theoretical constraints on the evolutionary behavior of SMR stars have received increasing attention. After some pioneering papers (Torres Peimbert 1971; Caloi, Castellani & Di Paolo 1974) the attention of theoreticians has been mainly devoted to investigate the behavior of SMR He burning stars in connection with the problem of UV excesses in elliptical galaxies. The first exploratory papers on this matter (Brocato et al. 1990; Castellani & Tornambé 1991) were followed by more extensive investigations of HB structures by Horch, Demarque & Pinsonneault (1992, hereinafter referred to as HDP) and, more recently and more detailed, by Dorman, Rood & O'Connell (1993, hereinafter referred to as DRO).

However, SMR stellar tracks which cover not only helium burning but also the previous H burning evolutionary phases are a fundamental ingredient for approaching the problem of the age distribution in both bulge and solar neighborhood stars and in turn for constraining the formation history and the chemical evolution of the Galaxy. Moreover, and maybe more

relevantly, theoretical constrains concerning the whole evolutionary history of SMR stars will disclose the evolutionary scenario of similar stellar populations in external galaxies, allowing for the evaluation of integrated colors of SMR globular clusters and supplying useful clues for the spectral evolution codes which provide the integrated spectral energy distributions of multipopulation models (Magris & Bruzual 1993; Bressan et al. 1994; Weiss, Peletier & Matteucci 1995; Pozzetti, Bruzual & Zamorani 1996).

In this context, it is worth noting that detailed estimates of the metallicities of extra galactic SMR globular clusters based on the Washington index $(C - T_1)$ may still present problems. In fact, even though GLK evaluated an internal accuracy of metallicity estimates roughly of the order of 0.2 dex, the empirical metallicity calibration of the Washington index relies on a sample of Galactic clusters with $(-2.25 < [Fe/H] < -0.25)$. Therefore extrapolations at much larger metallicities could be risky. As an alternative approach, the problem of empirical calibrations could be overcome by evaluating the predicted integrated colors of a template globular cluster sequence by using evolutionary population synthesis models (Brocato et al. 1990; Buzzoni 1995; Cellone & Forte 1997) for which full coverage of the main evolutionary phases is obviously needed.

In order to provide such a theoretical framework for the evolution of SMR stars, in this paper we present an evolutionary investigation performed at fixed metal abundance, namely Z=0.04. In order to properly settle the chemically homogeneous models on their ZAMS, a suitable assumption concerning the ratio between the helium and the heavy elements enrichment ($\Delta Y/\Delta Z$) has to be provided as well. The evaluations of the parameter $\Delta Y/\Delta Z$ based on observations of HII regions present large uncertainties. On the basis of observations of emission lines in HII galaxies, Pagel et al. (1992) obtained $\Delta Y/\Delta Z \approx 6$, whereas Maeder (1992) by adopting a homogeneous and complete library of evolutionary models suggested for this parameter a value between 1.1 and 1.8 for metal-poor stars and a value between 1.5 and 2.2 for metal-rich stars. However, as Peimbert & Torres-Peimbert (1974) first claimed, the value of the enrichment parameter should be cautiously treated, since at present both theoretical and observational data seem to suggest the possible lack of an universal linear regression between Y and Z (see also Bertelli et al. 1996). Therefore the evaluation of $\Delta Y/\Delta Z$ seems to be a really thorny problem. The reader interested in recent discussions on this matter is referred to Peimbert (1993), Carigi et al. (1995), Traat (1995), and Dorman, O'Connell & Rood (1995 hereinafter referred to as DOR).

On the basis of the photometric database collected by the OGLE microlensing survey in the Baade's Window, Renzini (1994) has recently discussed the parameter R_c, i.e. the ratio between the number of HB clump stars and Red Giant Branch (RGB) stars, and suggested on this basis that in bulge stars the helium abundance should range from Y=0.30

to Y=0.35. Similar results were given by Terndrup (1988) and more recently by Minniti (1994, 1995). However, it should be mentioned that similar evaluations of the enrichment parameter take into account the "mean metallicity" of a stellar sample, so that no firm evaluations can be provided close to the tail of the metallicity distribution and in particular at very high metallicities. According to this contradictory situation, we choose Y=0.34 as a reasonable guess for the original amount of He, which allows for a direct comparison with previous SMR computations by DOR. A second alternative choice, Y=0.37, has to be regarded as a temptative but again reasonable upper limit for the amount of He, as produced by a value of $\Delta Y/\Delta Z$ approximately of the order of 5.

In §2 we present the physical and chemical assumptions adopted for constructing the evolutionary tracks. Section 2.1 deals with H burning stellar models and with their comparison with similar data already appeared in the literature. Selected results of these H burning models, namely the He core mass at the He ignition (M_{cHe}) and the extra-helium (ΔY_{du}) dredged up at the base of the RGB, allow for a proper evaluation of He burning models presented in section 2.2, where we discuss the occurrence of gravonuclear instabilities affecting the phase of central helium exhaustion. He burning models of SMR stars will be used for providing some fundamental input parameters such as the mass/luminosity ratio for both linear and nonlinear pulsation investigations which are presented in §3. The modal behavior of SMR RR Lyrae pulsators at the ZAHB luminosity level and the dependence of the width of the instability strip on the metal content are presented.

The pulsation properties and the modal behavior of envelope models for post-HB stars are compared with the observed scenario of field, metal-rich type II Cepheid stars (Diethelm 1990 and references therein) for which up to now there is no detailed theoretical investigation available in the literature. The dependence of the light curves of fundamental pulsators on effective temperature and on the appearance of the Hertzsprung progression in this group of variable stars are discussed in section 3.2. A brief summary of the results obtained in this investigation and the overall conclusions concerning both evolutionary and pulsational properties of SMR stellar populations are reviewed in §4.

Finally, the physical parameters which govern the appearance of "gravonuclear loops" -GNL- and a thorough analysis of the physical mechanisms which drive and/or inhibit the appearance of the gravonuclear instability are presented and discussed in the Appendix.

2. THEORETICAL STELLAR MODELS

Theoretical stellar models have been computed by adopting the FRANEC evolutionary code, whose structure has been discussed in Chieffi & Straniero (1989). As for the input physics, OPAL radiative opacity tables (Iglesias, Rogers & Wilson 1992; Rogers & Iglesias 1992) were adopted for temperatures higher than 10,000 K, while for lower temperatures were adopted the molecular opacities provided by Alexander & Ferguson (1994). Both high and low temperature opacity tables assume a solar scaled heavy element distribution (Grevesse 1991). The equation of state has been taken from Straniero (1988), supplemented by a Saha EOS at lower temperatures. The outer boundary conditions have been evaluated by assuming the $T(\tau)$ relation provided by Krishna-Swamy (1966). In the superadiabatic region of the stellar envelope a mixing length value of ml=2.25 H_p has been assumed, according to the calibration on the solar standard model (Salaris & Cassisi 1996).

Moreover, near the core helium exhaustion we inhibited the so-called "breathing pulses" (Castellani et al. 1985) by adopting the procedure suggested by Caputo et al. (1989). In this approach the onset of "breathing pulses" is avoided on the basis of a straightforward assumption concerning the size of the convective core. In other words, the extent of the convective core is checked so that the central helium abundance cannot increase between consecutive models.

2.1. H BURNING EVOLUTIONARY PHASES

Evolutionary tracks for the H burning phase have been computed for a fixed metal content (Z=0.04) and for the two quoted initial helium abundances, namely Y=0.34 and 0.37. For each given chemical composition calculations have been provided for a set of stellar masses ranging from $M/M_{\odot}$=0.7 to $M/M_{\odot}$=3.0. Table 1 reports the masses of all computed models and from left to right, for each mass, the luminosity of the model igniting He, the lifetime in H burning phase (i.e. the time at the onset of He burning) and the mass of the He core and the extra-helium brought to the surface respectively. The last two parameters are the ingredients needed to evaluate the behavior of our models during the subsequent phase of He burning evolution.

As it is well known, for each given stellar population (i.e. for each assumed value of chemical composition and age) we can define a critical mass value, i.e. the transition mass M_{tr}, as the upper mass limit of stars which experience strong electron degeneracy into the He core during the phase of H shell burning and which, in turn, ignite He through one or more violent off-center He flashes at the tip of the RGB. Around this value, in a mass range of

only few tenths of solar mass, stars undergo a sudden variation in the maximum luminosity reached by H shell burning structures known as the *Red Giant Transition Phase* (RGTP, for a detailed discussion see Sweigart, Greggio & Renzini 1989, hereinafter referred to as SGR, Sweigart, Greggio & Renzini 1990; Castellani, Chieffi & Straniero 1992). Note that the RGTP also plays a key role in theoretical studies of binary evolution (Tornambè 1982) and in the age evaluation of populous stellar clusters.

The fine grid of evolutionary H burning sequences computed up to the helium ignition allows for a detailed investigation of the RGTP for a SMR stellar population. Figure 1 shows the behavior of the He core mass, of the luminosity and of the age at the He ignition as a function of the total mass of the evolving star. We find that the RGTP occurs, for Y=0.34, at an age of t$\approx 7.95 \times 10^8$ yrs. At this age the stellar mass of the stars at the RGB tip is $M_{tr} \approx 2.1 M_{\odot}$ and the He core mass is $M_{cHe} \approx 0.40 M_{\odot}$. For the larger helium content, Y=0.37, we find $M_{tr} \approx 2.0 M_{\odot}$ with once again a He core mass at the RGB tip $M_{cHe} \approx 0.40 M_{\odot}$ and an age $\approx 8.12 \times 10^8$ yrs. Figure 2 compares the present evaluation of the transition mass (Y=0.34) with previous evaluations obtained for lower metallicities, as given by Cassisi & Castellani (1993), Cassisi, Castellani & Castellani (1997), and Bono et al. (1997b, hereinafter referred to as Paper I). Data plotted in this figure confirm that M_{tr} is not a monotonic function of the metal content. For metallicity values larger than Z=0.01 the transition mass decreases as the metal content increases, a feature to be connected with the corresponding increase in He abundance which plays a major role in decreasing the degree of electronic degeneracy inside the core of RG stars, decreasing in turn the value of the transition mass at a given metallicity. This occurrence provides, at the same time, a plain explanation for the increase shown by the ZAHB luminosity level at high metal contents (for a discussion see Paper I and *infra*).

Present results about the transition mass can be usefully compared with similar values provided by SGR for the same metallicity but for different assumptions on the initial helium abundance, namely Y=0.20 and Y=0.30. SGR found for Y=0.20 a $M_{tr} \approx 2.75 M_{\odot}$ and a RGTP age approximately equal to 540 Myr, whereas for Y=0.30 and the same evolutionary parameters they give $M_{tr} \approx 2.33 M_{\odot}$ and an age $\approx$ 510 Myr, respectively. The large difference being easily attributed to the different assumptions about the helium abundance. As a result, we find that with our assumptions about the correlation between He and metals, a SMR stellar population is expected to spend a longer time interval before its integrated light becomes red.

Data in Table 1 show that the extra-helium brought by the first dredge up into the stellar envelope attains a minimum for $M \approx 2 M_{\odot}$ and increases again when the stellar mass is further increased. The behavior of the extra-helium in the range of low mass stars and, in

particular, the sudden decrease of such an evolutionary parameter at the RGTP have been recently discussed by Castellani & Degl'Innocenti (1995) (but see also Cassisi, Castellani & Castellani 1997) and they will be not discussed further. However, here is interesting to underline that with a further increase of the stellar mass the amount of extra-helium starts increasing again as a consequence of the deepening convective zone in structures whose H burning evolution was already constantly dominated by CNO burning, but in which external convection succeeds in dredging up the He formed in the original ZAMS convective core.

Evolutionary tracks covering H burning phases have been used for computing H burning isochrones, which are presented in Figure 3 for selected assumptions on the stellar age. Data concerning these isochrones are reported in Table 2, in which, from left to right, are listed the age (Gyr), the mass of the stellar structure at the bluest point of the isochrone, and both luminosity and effective temperature of this point. Columns (5) and (6) give the M_V magnitude and the $(B-V)$ color of the same point respectively, evaluated by adopting bolometric corrections and color-temperature relations provided by Kurucz (1992), with $M_{Bol,\odot} = 4.75$ mag.

Figure 3 quite clearly shows the RG giant clump marking the encounter of the H burning shell with the chemical discontinuity produced in the stellar interior by the first dredge up. This figure reveals a rather curious feature: a decrease of the stellar mass implies, as expected (see for example Castellani, Chieffi & Norci 1989), a decrease of the bump luminosity which appears to move in such a way that the effective temperature of the bump keeps roughly constant over the whole range of the investigated isochrones. A similar feature can be also detected in the isochrones for Z=0.01 and Z=0.02 presented in Paper I. As a further point, we find that the clump is barely notable in the age range from 2 to 4 Gyr. By recalling that the clump is originated from the chemical discontinuity at the bottom of the mixed envelope, we can easily relate such a behavior to the already discussed occurrence of a minimum in the surface extra-helium, since a lower extra-helium implies a reduced chemical discontinuity and, in turn, a smaller evidence for the RG clump.

2.2. HE BURNING EVOLUTIONARY PHASES

On the basis of the evolutionary values of both the He core mass, M_{cHe}, and the surface He abundance at the RGB tip obtained by means of the H burning stellar models discussed in the previous section, we now investigate the evolution of He burning stars for selected assumptions about the RG progenitor mass, i.e. about the age of the stellar population. In the case Y=0.34 we choose RGB progenitors with masses $M/M_{\odot}$ =1.0,1.8,2.0 which

correspond to ages (see Table 1) ranging from 11.8 Gyr to 985 Myr. However, data listed in Table 1 point out that RG stars with masses smaller than $1.5M_{\odot}$ have all electron degenerate cores, so that the mass of the He core at the He ignition presents rather negligible variations. As a consequence, He burning models originated from a 1.5 $M_{\odot}$ progenitor can be considered representative of He burning stars with ages larger than about 2.5 Gyr, provided that the variation of the progenitor mass with age is taken into account and the small variations in the surface extra-helium are neglected (see Table 1).

For each given progenitor mass, i.e. for each assumed value of the He core mass at the He ignition, a suitable set of ZAHB models has been computed for different assumptions about the mass of the H rich stellar envelope (i.e. about the efficiency of mass loss during the RGB phase). Figure 4a shows the HR diagram location of these ZAHB models, whereas Table 3 gives related quantities for the computed models. In the same Table we report the expected difference in V magnitude between the magnitude of the ZAHB at the effective temperature typical of the RR Lyrae instability strip ($\log T_e = 3.85$) and the bluest point of the isochrone.

The computations have been extended up to very hot (i.e. with thin stellar envelopes) ZAHB models in order to investigate the evolutionary behavior of the expected progenitors of hot AGB-manqué and Early post-AGB stars (Greggio & Renzini 1990; DRO) which, according to current suggestions (see e.g. DOR) are regarded as the main sources of ultraviolet emission in elliptical galaxies. Similar computations have been performed under the alternative assumption Y=0.37. Figure 4b shows the ZAHB models referred to the quoted helium abundance, while the leading physical quantities are listed in Table 3. Figure 5 shows the comparison between the two ZAHB sequences characterized by the same RG progenitor mass but with alternative assumptions about the original He content. For a discussion of the differential effect of the He abundance on the ZAHB location the interested reader is referred to Caloi, Castellani & Tornambé (1978) and to DRO.

As already known, the ZAHB effective temperatures of metal-rich stars are strongly dependent on the ratio between the mass of the envelope and the total mass of the star: $q = M_{env}/M_{tot}$ (see also HDP and DRO). For SMR stars we find that this dependence is further enhanced, so that a variation of only 0.02-0.03 solar masses is sufficient for shifting a ZAHB model from a low effective temperature region ($T_e \approx 5500$ K) to a very high effective temperature region ($T_e \approx 22,000 - 25,000$ K). As a consequence, in a metal-rich stellar population the number of stars in the intermediate range of effective temperatures and thus the expected number of RR Lyrae variables should be quite small, as already discussed in Paper I (see also the discussion in §3.2). At the same time, if SMR stars are old enough (and therefore with low evolving masses), we expect the easy occurrence of Extremely Hot

HB (EHHB) stars with their progeny AGB-manqué stars.

Since EHHB objects spend a relevant fraction of their lifetime as very luminous blue stars, they are presently considered (see e.g. Greggio & Renzini 1990 and references therein; DOR) the dominant source for the phenomenon of UV upturn observed in elliptical galaxies (Code 1969) and in galactic bulges. As a matter of fact, a high frequency of EHHB stars and of their progeny in SMR stellar populations is expected on twofold grounds, namely: i) the increased helium abundance speeds up the evolution and therefore less massive stars, for a given age, are evolving off the main sequence; ii) metal-rich stars should lose their mass more efficiently than metal-poor ones (D'Cruz et al. 1996). In fact, at fixed stellar mass and luminosity level the metal-rich stars present larger radii and therefore lower gravities and lower escape velocities in comparison with metal-poor structures. As a consequence, the classical Reimers's (1975) relation and/or other empirical estimates (Goldberg 1979; Nieuwenhuijzen & de Jager 1990 and references therein) predict larger mass loss rates for metal-rich stars.

Present off-ZAHB computations have been extended either to the onset of thermal pulses for more massive models, or until the luminosity along the cooling sequence of white dwarfs decreases to $\log L/L_{\odot} \approx -2.5$ for less massive models. The evolutionary path in the HR diagram of these models during their He burning evolution is reported in Figures 6 and 7 for the labeled assumptions on the RG progenitor mass. The main evolutionary properties of He burning stars with metallicities equal and/or larger than the solar value have been already discussed in several investigations (Brocato et al. 1990; Castellani & Tornambé 1991; HDP; DRO; D'Cruz et al. 1996; Paper I) and they not deserve detailed discussion here. As expected, the computed set of models allow for a rather detailed investigation of the various evolutionary phases which follow the exhaustion of the central He burning. Three different cases are presented: i) Extremely Hot Horizontal Branch stars which do not reach the Asymptotic Giant Branch (AGB) and evolve as AGB-manqué stars; ii) Post Early AGB stars, which leave the AGB before the onset of thermal pulses, and iii) *bona fide* AGB stars, i.e. stars which are massive enough to experience the evolutionary phase of thermal pulses along the AGB.

For each given assumption about chemical composition and age, we report again in Table 3 the value of the stellar mass (M^{AGB}) separating AGB-manquè models from models approaching the AGB, together with the value (M^{TP}) for the less massive stars experiencing thermal pulses. Thanks to the fine grid of stellar models, we estimate that the formal uncertainty for both these parameters is of the order of $0.003 M_{\odot}$. As expected, we confirm that in SMR stellar populations the maximum stellar mass of AGB-manqué stars is remarkably increased, an occurrence to be related to the increased efficiency of the

H burning shell during the central He burning phase. As a consequence, a larger range of stellar structures exhausts hydrogen during central He burning, being forced to spend all their He burning phase near the He main sequence (i.e. at very high effective temperatures) and therefore as hot UV sources.

A sound comparison between our predictions on M^{AGB} and the results recently obtained by HDP for the same metallicity is made difficult by the different values adopted by the quoted authors for the He abundance and the progenitor mass. However, we can compare the value of $M^{AGB} = 0.62M_{\odot}$ as given by HDP for Y=0.37, $M_{cHe} = 0.455M_{\odot}$ with our value $M^{AGB} = 0.477M_{\odot}$ obtained for Y=0.37 and $M_{cHe} = 0.457M_{\odot}$ as given by the $1.8M_{\odot}$ progenitor. We attribute the discrepancy mainly to the coarse step in the mass value adopted by HDP, with only a minor influence of the restricted difference in both the adopted chemical and physical inputs. A more meaningful comparison can be made with a model by DRO, who give for $M_{cHe} = 0.454M_{\odot}$ and for $Y_{HB} = 0.356$ the value $M^{AGB} \approx 0.480M_{\odot}$. Our model with $M_{cHe} = 0.454M_{\odot}$, $Y_{HB} = 0.347$ predicts $M^{AGB} \approx 0.473M_{\odot}$. This remarkable agreement, with a difference of the order of only 0.007 solar masses, can be regarded as an evidence of the accuracy achieved in the investigation of the evolutionary properties of He burning stellar models.

As discussed by DRO, a further relevant evolutionary parameter is given by the maximum stellar mass M^{TP} which skips the phase of thermal pulses before leaving the AGB. By definition this parameter marks the transition between stars which evolve as Post-Early AGB and stars which climb up the AGB experiencing recursive flashes in both H and He burning shells. The values of M^{TP} listed in Table 3 show that this parameter attains values of the order of $0.54 - 0.55M_{\odot}$ for all models. Quite similar values have been found by DRO even for quite different assumptions about RG progenitor masses and initial helium abundances. We conclude that M^{TP} appears fairly independent of evolutionary parameters other than the metal content.

As a relevant point, Figures 6 and 7 show that after the exhaustion of central He many of our models undergo the gravonuclear instabilities we shortly discussed in Paper I for a few "young" solar metallicity HB stars. The evolutionary tracks plotted in the quoted figures show that gravonuclear instabilities are a rather common feature of the off-ZAHB evolution of less massive SMR HB models. As a matter of fact, for Y=0.34 we find that all the models with mass lower than $M/M_{\odot} \approx 0.52 \div 0.53$, either AGB-manquè or evolving toward the AGB, undergo this kind of instability. Accordingly, gravonuclear instabilities appear for Y=0.37 in all models less massive than $M/M_{\odot} \approx 0.51 \div 0.52$. This small difference in the limiting stellar mass which experience gravonuclear instabilities can be easily connected with the parallel evidence that moving from Y=0.34 to Y=0.37 the He core masses decrease

of approximately 0.01 $M_{\odot}$. This evidence indicates that the mass of the stellar envelope plays a key role in the onset of gravonuclear instabilities.

Owing to the intrinsic relevance of this finding, the physics of gravonuclear instabilities will be discussed with some details in the Appendix to this paper. Here we briefly note that, as a consequence of gravonuclear instabilities, many HB models experience GNL (see also Paper I), which slow down the off-ZAHB evolutionary phases. As already discussed in Paper I, such an occurrence obviously appears relevant for the evaluation of UV radiation from hot He burning stars. However, both Figs. 6 and 7 show that during the blueward and/or the redward excursions GNL also succeed in pushing some HB models into the region of pulsation instability at luminosities much larger than the original HB luminosity. The expected observational relevance of such an occurrence is disclosed for a helium abundance Y=0.34 in Figure 8, in which we report the time behavior of both effective temperature and luminosity for a "cool" model with mass equal to $0.510 M/M_{\odot}$ and $M_{cHe} = 0.454 M/M_{\odot}$ during the GNL phase.

For the sake of this discussion, let us assume here the interval $3.806 < \log T_e < 3.690$ (see below) as the region where stars experience pulsational instabilities. As shown in this figure, we find that the model along its "natural" trajectory toward the AGB spends about 1.6 10^5 years in that region. Taking into account that for such model the He central burning lifetime is about 1.6 10^8 yrs, this occurrence implies that only 1 star out of about 1000 stars on the HB should be expected to be a pulsator. However, due to GNL, the star will spend further 2 10^6 yrs crossing the instability region, and the probability to detect a pulsator increases by more than one order of magnitude. According to such evidence, in the next section the expected pulsational behavior of these luminous post-HB pulsators will be investigated.

3. SMR VARIABLE STARS

According to theoretical predictions we foresee that SMR He burning stars could suffer pulsational instabilities either on their major phase of central helium burning or while crossing the instability strip above the ZAHB luminosity. In terms of a well established pulsational scenario, this suggests the occurrence of RR Lyrae and/or type II Cepheids produced by HB and/or post-HB stars, respectively. Curiously enough, current observational surveys of variable stars give scarce evidence, if any, of SMR RR Lyrae stars either in the Galactic field (Suntzeff et al. 1991; Layden 1995 and references therein) or in the solar neighborhood (Preston 1959; Kemper 1982). Most interesting, RR Lyrae stars in the Baade's Window present a narrow metallicity distribution with a mean value close to

[Fe/H]=-1 (Walker & Terndrup 1991), whereas the K giants have a metallicity distribution which ranges from [Fe/H]≈-1 to 0.5 (Terndrup, Sadler & Rich 1995 and references therein).

On the other hand, Harris & Wallerstein (1984) and Diethelm (1986) have recently reported the evidence for the occurrence of SMR type II Cepheids. Taken at its face value, this observational evidence appears as a rather strange occurrence. In fact, HB evolutionary times are in all cases much longer than post-HB times and therefore *prima facie* we should expect a larger evidence for RR Lyrae pulsators. We expect that the small range of masses producing RR Lyrae plus the occurrence of GNL should play a role in this matter. However, we will show in the following that there are further intrinsic pulsational reasons which reduce the probability for the occurrence of SMR RR Lyrae variables.

Several thorough analyses have been already devoted to type II Cepheids belonging to Galactic globular clusters (Wallerstein & Cox 1984; Harris 1985; Sandage, Diethelm & Tammann 1994 hereinafter referred to as SDT; Bono, Caputo & Santolamazza 1997 hereinafter referred to as BCS). Under this term are commonly classified old, low-mass variable stars with periods ranging from 1 to roughly 30 days. On the basis of their evolutionary properties, type II Cepheids are often divided into two different groups. The short-period group, called BL Herculis stars, is characterized by periods between 1 and approximately 10 days. Their progenitors are low-mass HB stars which, during their evolution, cross the instability strip moving from the blue tail of the HB toward the AGB. The long-period group, called W Virginis stars, is characterized by periods longer than 10 days with low-mass AGB progenitors which experience one or more loops inside the instability strip when starting their AGB evolution. As a whole, the evolutionary and pulsational properties for type II Cepheids in globular clusters emerging from the observational scenario appear in fairly satisfactory agreement with current theoretical predictions (see SDT, BCS and references therein).

The scenario for type II Cepheids in the field appears much less clear. The distinction between classical Cepheids and type II Cepheids is -first of all- a thorny problem since these two groups of variables present similar periods and effective temperatures. A detailed discussion concerning the limits of both photometric and spectroscopic classifications has been given by Harris (1985) and Diethelm (1986, 1990). According to the accepted evidence, field type II Cepheids are found over a very wide range of metallicities, from metal-poor up to SMR stars, with the period distribution for metal-rich type II Cepheids which differs from the distribution shown by similar variables in globular clusters. This feature, together with several observed properties of field, old-disk type II Cepheids still lacks a comprehensive and homogeneous explanation, indicating that moving from low to high metal contents the theoretical scenario will face some intrinsic differences.

In order to investigate on a quantitative basis the pulsational behavior of the evolutionary models presented in the previous sections, we computed a large set of both linear and nonlinear pulsation models for suitable assumptions about the stellar mass and the effective temperature of the stars. The results of these calculations together with some simple clues concerning the evolutionary status of these variable stars will be discussed in the following subsections.

3.1. LINEAR NONADIABATIC MODELS

During the last fifteen years several theoretical investigations on the pulsation properties of BL Her stars have been presented (Carson & Stothers 1982; Hodson, Cox & King 1982; Buchler & Buchler 1994; Bono, Castellani & Stellingwerf 1995 and references therein). They appear in good agreement with observational constraints concerning the modal stability as well as secondary features of both luminosity and velocity curves. However, the quoted surveys were mainly devoted to type II Cepheids in Galactic globular clusters with metal-poor chemical compositions. Up to now no investigation on the dependence of the pulsational behavior of BL Her stars on metal content and stellar masses has been provided. In order to approach the problem we investigate the pulsational behavior of He burning SMR variables at fixed chemical composition (Z=0.04, Y=0.34) and by assuming three suitable stellar mass values, namely $M/M_{\odot}$=0.520, 0.505 and 0.485, chosen as representative of He burning stars populating the instability strip either during their HB or their post-HB phases.

The linear modal stability was investigated by exploring a wide range of effective temperatures at three different luminosity levels ($\log L/L_{\odot}$=1.56, 2.0, 2.2), again chosen in such a way to cover theoretical expectations concerning HB and post-HB SMR variable stars. In order to provide a detailed analysis of the pulsation properties of SMR RR Lyrae variables we also computed, for $M/M_{\odot}$=0.505, a sequence of envelope models located at $\log L/L_{\odot}$=1.48. Models located close to the blue boundary of the instability strip were computed with a temperature step of 100 K in order to reach a sufficiently detailed information on the effective temperature of the linear blue edge. As it is well known, no information on the red edge can be obtained from linear radiative computations. Both linear and nonlinear calculations have been performed by assuming the same set of radiative opacity tables adopted in the evolutionary calculations, even though the method adopted for handling the tables is different (for more details see Bono, Incerpi & Marconi 1996 hereinafter referred to as BIM). According to the prescriptions suggested by Bono & Stellingwerf (1994 hereinafter referred to as BS), for each envelope model the number of

zones is of the order of 200. The boundary conditions -i.e. the optical depth at the outer boundary and the depth of the envelope- were chosen as in previous investigations (Bono et al. 1997c hereinafter referred to as BCCM).

Tables 4, 5, and 6 summarize the results of the linear nonadiabatic survey for the three different assumptions on the stellar mass value and for the labeled values of the luminosities. Columns (1) and (2) report the surface effective temperature (K) and the static gravity, whereas columns (3), (4) and (5) list, in the order, the period, the pulsation constant, and the growth rate of the fundamental mode. The growth rate - i.e. the fractional amount of energy added or subtracted to the pulsation in each period- is defined in such a way that negative values imply the pulsational stability of the stellar envelope for the given mode. In the same Tables, columns (6), (7) and (8) report the same quantities listed in the previous three columns, but referred to the first overtone mode. No attempt has been made for evaluating the modal stability of the second overtone since at large luminosities it is expected to be stable on the whole instability strip (Bono et al. 1997a).

As a first result, we find that models at luminosity levels close to $\log L/L_{\odot}$=2.0 reproduce with fairly good accuracy the effective temperatures, gravities and periods observed in field BL Her stars (Diethelm 1990). By a quick inspection of Figures 6 and 7 we note that the quoted luminosity level falls inside the luminosity interval where GNL tend to accumulate stars. On the contrary, in the case of a quiescent evolution such a luminosity would be attained only by hot HB stars in their final and rapid crossing of the instability strip (see Figure 3 in DRO). As a result, we find that the occurrence of GNL which push a larger amount of post-HB models inside the instability strip at large luminosity levels allows for a simple and homogeneous explanation of this group of variable stars. If this is the case, at the mean time we would also understand why field, metal-rich type II Cepheids present a larger period spread in comparison with the cluster type II Cepheids (Harris 1985), the instability strip of the former variables being populated by HB models characterized by a larger range of stellar masses.

Figure 9 shows the location of the blue boundaries of the instability strip in the HR diagram for the three different assumptions on the stellar masses, disclosing that in this mass range the modal stability of both fundamental and first overtone presents only a negligible dependence on stellar mass. As a consequence, the luminosity of the "intersection point", i.e. of the point where the First Overtone Blue Edge (FOBE) intersects the Fundamental Blue Edge (FBE) moves only from $\log L/L_{\odot}$=2.0 for the models with $M/M_{\odot}$=0.485 to $\log L/L_{\odot}$=2.05 for the models with $M/M_{\odot}$=0.505. As it is well known, only fundamental pulsators are allowed above the quoted luminosities. On this basis, it has been found (see BCS) that in galactic globular clusters blue ZAHB models evolving across the instability

strip should scarcely produce first overtone, metal-poor type II Cepheids (see BCS). On the contrary, we find that the location inside the HR diagram of SMR post-HB models during the phase of GNL should allow for the occurrence of both fundamental and first overtone pulsators.

The dependence of the blue boundaries on the chemical composition has been studied by computing selected linear models with a given mass ($M/M_{\odot}$ =0.505) and for two different "metal-rich" compositions, namely Z=0.02, Y=0.28, and Z=0.04, Y=0.34. However the investigation has been extended to models representative of metal-poor, globular cluster type II Cepheids, by investigating the case $M/M_{\odot}$ =0.58, Y=0.24, Z=0.001. The blue instability boundaries for these three assumptions are given in Figure 10. We find that moving from solar to super solar chemical compositions the increase in helium and metal content affects only marginally the location of the FBE at high luminosity levels, whereas FOBE moves toward large effective temperatures. Moreover, we find that the blue boundaries of metal-poor pulsators, and in particular the FBE, move toward hotter effective temperatures and hence toward larger gravities. Even tough the modal stability can be safely evaluated only through a nonlinear approach, the above linear analysis provides useful insights into the expected behavior of the dependence of blue edges on physical parameters. In particular, we find that the behavior depicted in Figure 10 would provide a sound explanation for the observational evidence, originally suggested by Diethelm (1990), according to which both temperatures and gravities of type II Cepheids decrease as soon as the metallicity increases.

The quoted linear computations allow for the analysis of the dependence of the modal stability of metal-rich pulsators on the chemical composition. Figure 11 shows the linear total work curves (W is the work integral per logarithmic temperature in units of the total kinetic energy) as a function of the logarithmic temperature for two models characterized by the same luminosity (log $L/L_{\odot}$ =2.0), temperature (6400 K) and stellar mass ($M/M_{\odot}$ =0.505) but with different chemical compositions, namely Y=0.28, Z=0.02 and Y=0.34, Z=0.04. The arrows mark the location of the driving regions, whereas the symbols indicate, according to the linear eigenfunctions, the location of the first overtone nodes. Note that Figure 11 displays $dW/d(logT)$ rather than the canonical $dW/d(logMe)$ (Me = exterior mass). Similar plots provide useful information concerning the sources which drive (positive values) or quench (negative values) the pulsation instability since they can be closely connected with the opacity features. At the same time this approach maintains the relative areas of both driving and quenching regions under the total work curve (Stellingwerf 1979).

As expected on the basis of the topology of the instability strip, the driving regions of the

fundamental mode, caused by the Hydrogen Ionization Region (HIR, $T \approx 1.3 \times 10^4$ K) and the Helium Ionization Region (HEIR, $T \approx 5.0 \times 10^4$ K) present only a negligible change moving from Y=0.28 to Y=0.34. The additional driving region located at $T \approx 2.0 \times 10^5$ K is caused by the iron opacity bump. The SMR model presents in this region a slight enhancement in comparison with the model at solar composition, but its contribution to the total driving is negligible. In envelope models characterized by larger stellar masses this driving region becomes more effective since the iron bump shifts toward the nonadiabatic region of the stellar envelope and therefore can supply a larger amount of net positive work.

The total work curves referred to the first overtone disclose a stronger dependence on the chemical composition and indeed the driving region caused by the HEIR is significantly larger in the SMR model than in the model with solar composition. In the latter model the driving region caused by the iron bump disappears almost completely since it is located quite close to the node of the luminosity eigenfunction and therefore an obvious reduction of the amount of driving takes place. A detailed discussion of the effects caused by this feature on modal stability of RR Lyrae and δ Scuti stars is given in BIM and Bono et al. (1997a), respectively. The strong dependence of the first overtone instability on the helium content explains why an increase of metals and helium moves the FOBE toward higher effective temperatures.

3.2. NONLINEAR LIMITING AMPLITUDE MODELS

To further investigate the behavior of SMR variables and, in particular, to attain information on both the red edge of the instability and the pulsational amplitudes, nonlinear, nonlocal and time-dependent convective models have been computed by assuming the same input physics adopted in the linear analysis. The envelope models were integrated in time until the radial displacements approach their asymptotic behavior, i.e. the nonlinear limit cycle stability, and the pulsation amplitudes attain a periodic similarity of the order of or lower than 10^{-4} over two consecutive full pulsation cycles. The initial velocity profiles were imposed by perturbing the linear radial eigenfunctions with a constant velocity amplitude ranging from 10 to 20 kms^{-1}.

We first explored the luminosity level of SMR HB stars by computing envelope models for $M/M_\odot$=0.505, log $L/L_\odot$=1.48 and for selected choices of stellar effective temperatures. As a relevant result, we found that the fundamental red edge slightly moves toward higher effective temperatures, whereas the first overtone blue edge moves in the opposite direction in comparison with RR Lyrae variables belonging to globular clusters. As a matter of fact, the fundamental red edge referred to SMR RR Lyrae variables is located at $T_e \sim 5950$ K,

whereas the first overtone blue edge is located at $T_e \sim 7050$ K. As a whole we find that the instability strip in the SMR case covers a smaller temperature range in comparison with pulsators characterized by lower metal contents, since from the canonical value of $\Delta T_e \sim$1400 K (see BCCM and Bono et al. 1997d) the width of the instability strip narrows down to $\Delta T_e \sim$1100 K. Such a result adds of course a further theoretical motivation to the observed paucity of SMR RR Lyrae stars, since the width of the instability strip remains almost constant from Z=0.0001 (Y=0.24) up to the solar chemical composition (Z=0.02, Y=0.28), whereas an increase of a factor of two of the metallicity (Z=0.04) together with a decrease of the order of 10% in the H abundance causes a narrowing of the intability strip of the order of 20%.

An estimate of the combined effects of metallicity on the occurrence of RR Lyrae pulsators has been obtained by distributing single models with a mass step $\Delta M = 0.005 M_{\odot}$ all over the ZAHB and evaluating the ratio between the sum of evolutionary times of models falling within the instability strip and the sum of evolutionary times for all ZAHB models (as far as the evolutionary time is concerned, we have taken into account the total central He burning lifetime). Figure 12 shows the ratio $\tau(RRLyrae)/\tau(HB)$ as a function of the metal content. Data plotted in this figure show that moving from metal-poor to metal-rich stellar populations the number of RR Lyrae variables, due to the narrowing of the mass range which populates the instability strip and the narrowing of the instability edges, decreases of a factor of seven. An occurrence which could play a not negligible role in the observed lack of metal-rich variables in the Galactic bulge (Walker & Terndrup 1991).

On theoretical grounds, as a final remark, one can notice that the origin of the narrowing of the instability strip can be found in the prediction already given in BS and BIM concerning the dependence of the boundaries of the RR Lyrae instability strip on the chemical composition and in particular the dependence of the fundamental red edge on the H abundance. If this is the case, we can predict that a further increase in the helium content over the adopted value Y=0.34 would cause a further narrowing of the strip and therefore a further decrease of the probability to detect HB pulsators. As for "theoretical" SMR RR Lyrae variables we report in Table 7 selected quantities depicting the pulsational behavior. We find that the pulsation amplitudes and the shape of both light and velocity curves do not present any peculiar feature in comparison with canonical RR Lyrae pulsators and therefore they are not further discussed. Detailed data are available upon request.

To explore the pulsational behavior of our theoretical BL Her candidates, a sequence of nonlinear fundamental models was computed by exploring at fixed stellar mass ($M/M_{\odot}$ =0.505), luminosity level ($\log L/L_{\odot} = 2.0$), and chemical composition (Y=0.34, Z=0.04) a wide range of effective temperatures. A fine temperature step ($\Delta T_e \leq 200$ K)

has been adopted to investigate the appearance of secondary features like bumps on light and velocity curves. Few selected models have been also computed at a larger luminosity level (log $L/L_{\odot}$=2.2) to explore the dependence of both light and velocity curves on this physical parameter. Selected results of the nonlinear survey of fundamental models located at log $L/L_{\odot}$=2.0 and 2.2 are also reported in Table 7. The pulsation amplitudes reported in this table are only for pulsators which show a pure single nonlinear limit cycle stability. The only exception is the model located at T_e=5700 K, log $L/L_{\odot}$ = 2.0 which at full amplitude presents a permanent mixture of fundamental and higher overtone(s) (mixed-mode pulsator). Columns (1) and (2) report the effective temperature (K) and the nonlinear period (days). The comparison between nonlinear periods and the periods listed in Table 5 shows that nonlinear effects only marginally affect this parameter. Columns (3), (4), and (5) list the fractional radial oscillation, the surface velocity amplitude, and the bolometric amplitude, respectively. Columns (6) and (7) present the static and the effective surface gravities, whereas columns (8) and (9) report the variation of surface and effective temperature throughout a full pulsation cycle. The overall trend of the pulsation amplitudes of BL Her fundamental pulsators present a peculiar feature. Unlike fundamental RR Lyrae variables the amplitudes are not strictly decreasing when moving from the blue to the red edge of the instability region. A relevant consequence of this new behavior will be discussed further on.

Figures 13 and 14 show the light curves at limiting amplitude for the sequence of fundamental pulsators computed at fixed luminosity level. A quick inspection of these figures shows that moving from the hot to the cool edge of the instability strip the shape of the bolometric light curves presents remarkable differences worth being discussed in detail. We find that the light curve of the model located close to the FBE (T_e=6400 K) shows almost a smooth sinusoidal luminosity variation throughout the pulsation cycle, whereas the light curves of models located at lower effective temperatures show the occurrence of bumps both before and after the main luminosity maximum. Moving from T_e=6300 K to T_e=6100 K the bump located at the base of the rising branch becomes more and more evident. At the same time, a second bump appears along the decreasing branch which moves toward earlier pulsation phases as the temperature decreases.

The light curve of the models located around T_e=5900 K presents even a different shape, with the luminosity that after the main maximum is strictly decreasing, and the disappearance of the second bump. Interesting enough, the model located at T_e =5700 K is a mixed-mode pulsator since the pulsation amplitudes of this model -followed over 3000 periods- fluctuate around a mean value over consecutive periods. The light curves of models located at even lower effective temperatures change once again: the second bump now takes place before the luminosity maximum and becomes the absolute luminosity maximum

at effective temperatures lower than 5500 K. In this temperature interval the first bump becomes less and less evident, and almost disappears for temperatures lower than 5200 K. Finally, the light curves of the models located between this temperature and the red edge of the instability strip are characterized by a smooth decreasing branch and by a small bump located between the flat "true" luminosity maximum and the phase of minimum radius.

This analysis of the dependence of the light curves on effective temperatures brings out some relevant results we will discuss in detail:

i) the varying shape of the light curve across the instability strip provides the theoretical evidence that, as originally suggested by Diethelm (1990), variable stars classified in the *General Catalog of Variable Stars* (GCVS, Kholopov et al. 1981 and references therein) as CW and BL Her may belong to the same family of radial pulsators. The two quoted classes have been indeed separated on the basis of the bump location, and now we find that, decreasing the star temperature, the bump appears first along the rising branch and then on the decreasing branch of the light curve. Due to the incomplete coverage of the possible pulsators parameters presented in this exploratory paper, we do not wish to push such a comparison too far. However, we note that bolometric curves in Figures 13 and 14 do show a remarkable similarity with the photoelectric V light curves reported in figures 2 and 3 of Diethelm (1983).

ii) The regular light curves of models located close to the red edge of the instability strip ($T_e \leq 5200$ K) supplies the intriguing suggestion that some of the variable stars classified as "Classical Cepheids", (Cδ) in GCVS, when characterized by relatively short periods (2-6 days) could have been misclassified. As a matter of fact, both the range of periods and the shapes of the light curves reported in figure 4 of Diethelm (1983) appear in fairly good agreement with theoretical results for the reddest pulsators. If this is the case, similar radial pulsators would belong to the group of low-mass metal-rich type II Cepheids instead of belonging to the group of intermediate-mass classical Cepheids. Note that a similar suggestion has been already given by Petersen (1981) in discussing the light curves of classical Cepheids originally collected by Payne-Gaposchkin (1961).

iii) Finally we also note that the sample of "Sinusoidal Cepheids" (SA in the nomenclature of the GCVS) provided by Connolly (1980) and Diethelm (1990) presents periods and light curves which appear in close agreement with the models located near the blue or the red edge of our BL Her pulsating models. Thus once again we could speculate about the possible misclassification of at least a fraction of variable stars belonging to this group. Unfortunately, here as well as in the previous cases, observational light curves are characterized by low photometric accuracy and poor time resolution to allow for a detailed comparison with theoretical predictions. Even though several methods have been proposed

for discriminating among the pulsational properties of short period Cepheids (Simon 1986; Morgan 1995), a general and meaningful classification scheme of these objects needs further spectroscopic and photometric data which could cast light on their pulsational behavior.

The regular progression of the bump disclosed by the light curves of BL Her stars across the instability strip presents a close similarity to the well known Hertzsprung (1926) progression of classical Cepheids. This is the first time such a phenomenon appears in full amplitude nonlinear pulsation models. We suggest that this finding could be connected with the discussed theoretical evidence according to which the bolometric amplitudes of fundamental BL Her pulsators attain an absolute maximum right at the period ($\approx$ 1.7 d) in which the second bump is in phase with the "true" luminosity maximum. The physical mechanisms governing the appearance of such a phenomenon and a detailed analysis of the region inside the instability strip where it appears will be addressed in a forthcoming paper (Bono et al. 1997e).

The appearance of the Hertzsprung progression among type II Cepheids supports the theoretical prediction by Christy (1970) for a period-phase-of-bump relation in this group of pulsators, as well as the results presented by Stobie (1973) for a small sample of halo/old disk Cepheids. More recently Petersen (1981) investigated the linear period limits, predicting a bump progression closely connected with the results of our nonlinear theoretical scenario. Finally we note that our mixed-mode pulsator located at T_e=5700 K presents a linear period ratio P(FO)/P(F) = 0.687, smaller than the ratios observed for TU Cas and U TrA (P(FO)/P(F)=0.710), the only presently known mixed-mode pulsators belonging to the group of classical Cepheids with fundamental periods shorter than three days (Hoffmeister, Richter & Wenzel 1985). The agreement could be possibly achieved by tuning the luminosity and/or the mass of the pulsators.

Figures 15 and 16 show the radial velocity curves of the sequence of fundamental pulsators presented in Figs. 13 and 14. An interesting feature is that the BL Her pulsators which present the second bump along the decreasing branch of the light curve *attain the luminosity maximum almost at the same phase of the velocity maximum*, i.e. luminosity and velocity variations are correlated throughout the pulsation cycle. On the contrary, models located at effective temperatures lower than 5600 K which have the second bump along the increasing branch of the light curve *attain the "true" luminosity maximum* before *the phase of velocity maximum*. In particular, models located between 5400 K and 5200 K reach the absolute luminosity maximum at the phase of minimum radius, whereas for cooler models this maximum takes place *after* the phase of minimum radius and *before* the phase of maximum outward excursion. All these features suggest that the Hertzsprung progression in BL Her stars should be tightly connected with a substantial variation in the physical properties of

the outermost layers which cause in turn a variation in both the thermal and the dynamical timescales of these pulsators.

The dependence of the light curve on the assumed luminosity level has been investigated by constructing two models at log $L/L_{\odot}$ =2.2 and for two given effective temperatures, namely 5700 K and 5500 K. Figure 17 shows both the light (top panels) and the velocity (bottom panels) curves for these models. Comparison with Figures 13 and 14 shows a large similarity with less luminous models. As a main difference, we find that the first bump precedes the rising branch, whereas the same feature appears along the rising branch of models located at lower luminosities. However, this result appears in agreement with the discussion given in BCCM, where we found that a small increase in the luminosity level of RR Lyrae pulsators involves almost a rigid shift of the pulsation behavior toward higher effective temperatures, i.e. the same shape of the light curve can be found at higher luminosity but in hotter models. If this is the case, now we expect that while the luminosity of BL Her stars increases, the Hertzsprung progression is only shifted toward larger temperatures.

As already discussed, on the basis of linear evaluations (and thanks to the occurrence of GNL) we expect the occurrence of BL Her first overtone pulsators. In order to verify the occurrence of a stable FO limit cycle at the same luminosity level of F pulsators, we computed three first overtone models located at T_e=6300, 6000, and 5700 K respectively. However, the radial motions of these models, soon after an initial transient phase, during which slow low-amplitude modes appear, undergo a sudden transition toward the fundamental mode. As soon as the mode switching takes place the oscillations rapidly approach pure fundamental periodic motions and eventually the nonlinear limit cycle stability. Figure 18 shows for a first overtone model the changes in period (top panel), bolometric amplitude (middle panel), and total kinetic energy (bottom panel) as a function of the integration time. The time behavior of these quantities shows quite clearly both the mode switching shown by the steplike adjustment of the period at $t = 0.3$ yrs ($P(FO) = 1.2354d \Rightarrow P(F) = 1.7952d$), and the approach of dynamical motions to the fundamental asymptotic amplitude (see the arrow plotted in the bottom panel). At least for this luminosity level we conclude that predictions of linear computations are not supported by the nonlinear approach, and that only the fundamental mode is a stable attractor of the system. However, the occurrence of FO pulsators cannot be ruled out at luminosity levels lower than the explored one.

3.3. PERIODS AND PERIOD CHANGES

The period of radial pulsators is one of the most common parameters adopted in the comparison between theoretical predictions and observations. Accordingly, here we will investigate *in primis* the difference between linear and nonlinear periods and *in secundis* the dependence of nonlinear periods on the chemical composition.

Figure 19 shows both linear (solid line) and nonlinear (dotted line) periods as a function of the effective temperature for the labeled values of stellar masses and luminosities. The nonlinear periods refer to the sequence of fundamental models reported in Figs. 13 and 14, whereas the linear ones come from data listed in Table 5. We find that the difference between linear and nonlinear periods can be barely noted. Only close to the red edge of the instability strip nonlinear periods become systematically shorter due to the nonlinear effects introduced by the increased efficiency of convective motions on the "average" density profile (see BS).

However, the same figure shows the periods evaluated according to the analytical relation given by BCCM for metal-poor cluster variables (dashed line), which reproduce the results of nonlinear models with an accuracy better than 1 percent. A similar formula but based on linear, nonadiabatic models was originally derived by van Albada & Baker (1971). The discrepancy between periods from the present investigation and from the analytical relation appears almost constant and of the order of 15 percent in the logarithm of period. This difference has to be obviously attributed to the remarkable difference in the chemical composition. Thus it appears that a general fitting formula which can safely represent the actual periods of both metal-poor and metal-rich variable stars would require an extra term also taking into account the dependence on the helium content.

Among the plentiful astrophysical legacy left by Eddington (1918), one of the most simple and weighty insights connecting stellar evolution and stellar pulsation was the evaluation of period changes due to evolutionary effects. Period changes can provide not only useful clues about the variation of the density distribution caused by the evolution, as suggested by Eddington, but can be also connected with the evolutionary rates inside the HR diagram. Even though the measurement of this quantity is quite simple in principle, reliable estimates are often a tantalizing problem due to the systematic errors and in turn to the spurious effects introduced by different sets of old photographic data. Several investigations have been devoted to both theoretical and observational aspects connected with the evaluation of the evolutionary period changes (Sweigart & Renzini 1979; Wehlau & Bohlender 1982; Lee, Demarque & Zinn 1990; SDT).

To cast light on the effects of different evolutionary scenarios for low-mass He burning

stars, we computed the evolutionary rate of fundamental periods for selected physical structures, taking into account three different prototypes: a metal poor RR Lyrae variable ($M/M_{\odot}$=0.65, Y=0.23, Z=0.001), a globular cluster type II Cepheid ($M/M_{\odot}$=0.58, Y=0.23, Z=0.001), and a field metal-rich type II Cepheid ($M/M_{\odot}$=0.51, Y=0.34, Z=0.04). Note that the RR Lyrae prototype is given by a moderately blue ZAHB model which crosses the strip moving to the red during its off-ZAHB evolutionary phases.

Figure 20 shows the predicted rates of period change for the three prototypes. The top panel discloses the large and repeated variation of the rate of period change caused by the GNL. Positive values denote a redward evolution, whereas the negative ones mark the evolution in the opposite direction. The asymmetry between positive and negative values prompts a substantial difference in the time spent by this evolutionary track during the redward and the blueward excursions, showing that the latter is a factor of two faster in comparison with the former one. The curves plotted in the middle and in the bottom panels show that the rate of period change for both RR Lyrae and globular cluster type II Cepheid prototypes keeps increasing, as expected, across the instability strip. According to data in Figure 20, one would predict that type II Cepheids should show rates of period change as a function of time two orders of magnitude larger in average when compared to canonical RR Lyrae stars, as already suggested by SDT (and references therein) on the basis of the HB evolutionary tracks provided by Dorman (1992). However, the rate of period change of a BL Her star would be at least a further order of magnitude larger in comparison with type II Cepheids. As a result, if GNL are at work the rate of period change in BL Her stars should be much easier to detect, thus providing a test for the suggested evolutionary scenario.

4. SUMMARY AND CONCLUSIONS

In this paper we present a homogeneous theoretical scenario covering both evolutionary and pulsation properties of a SMR stellar population. In order to provide a proper investigation of the main evolutionary phases two extensive sets of H burning evolutionary tracks have been computed by adopting different assumptions on the initial helium content. The results of these calculations allow for the evaluation of detailed grids of hydrogen burning isochrones covering a wide range of stellar ages, as well as for a sound estimate of several astrophysical parameters such as the transition mass, the He core mass at the He ignition and the amount of extra-helium dredged up during RGB evolution.

On the basis of these results we investigated the He burning evolutionary phases. The HB promenade has been investigated assuming different initial helium abundances (Y=0.34, Y=0.37) and adopting different values of the RG progenitor mass (i.e. different cluster

ages). Evolutionary ZAHB have been populated assuming an increasing amount of mass loss until the bluest ZAHB models have been almost completely peeled of the stellar envelope. This approach supplied a fine coverage of the various evolutionary phases which follow the exhaustion of the central He burning, allowing for a sound evaluation of several astrophysical parameters connected with the ZAHB and the off-ZAHB evolutionary phases.

As a relevant result, we found widespread appearance of gravonuclear instabilities at the ignition of the He shell burning, according to a mechanism already found in some "young" HB models at solar metallicity. Since the occurrence of gravonuclear loops may play a crucial role in understanding the evolutionary status of field, metal-rich type II Cepheids, in the Appendix to this paper we discuss the physical mechanisms which drive their appearance.

Evolutionary results for SMR He burning models have been used to investigate the pulsational behavior of models crossing the instability strip, either as HB or post-HB structures. Linear nonadiabatic computations disclose a reasonable agreement between the present estimates of periods and gravities of stars at the luminosity level of GNL with the observational value for BL Her variables.

The dependence of the blue boundaries on stellar mass and chemical composition was approached again in the frame of linear nonadiabatic computations, investigating the modal stability of both fundamental and first overtone modes for solar and super solar metallicities. We find that the HR diagram location of the instability boundaries presents a negligible dependence on the stellar mass at least in the range of stellar masses typical of SMR He burning stars. A sequence of linear nonadiabatic models representative of metal-poor type II Cepheids was also computed. The results provide a sound explanation for the observed decrease of both effective temperature and gravities for increasing metal abundances.

In order to better investigate the expected properties of SMR stars we have also carried out the computation of a sequence of nonlinear, nonlocal and time-dependent convective models at given stellar mass and chemical composition: Z=0.04, Y=0.34. The computations were mainly aimed at predicting both the modal stability and the shape of both light and velocity curves across the instability strip. We found that the range of effective temperatures covered by the instability strip for SMR RR Lyrae pulsators is sensibly reduced in comparison with less metallic pulsators, an occurrence which can play a not negligible role in the observed lack of SMR RR Lyrae variables.

The theoretical investigation of a selected sample of pulsational models suitable for BL Her pulsators revealed some important findings concerning the nature of these objects. The agreement between the shape of bolometric light curves and observational data is

quite reasonable. The appearance of the bump after the luminosity maximum in models located close to the blue edge and its shift at pulsation phases which precede the luminosity maximum in models characterized by lower effective temperatures suggests that the group of variables classified as CW and BL Her stars in the GCVS may refer to very similar stellar structures. The close similarity between the light curves of models located close to the red edge and the light curves observed for classical Cepheids with periods lower than six days suggests that out of this sample at least some variables could be low-mass, metal-rich type II Cepheids.

The nonlinear analysis has also qualitatively suggested a theoretical framework concerning the appearance of the Hertzsprung progression among present BL Her models, due to a substantial difference in the dependence of both thermal and dynamical timescales on the effective temperature. Further theoretical investigations aimed at producing an extended survey of limiting amplitude, nonlinear models covering a wider range of luminosities and stellar masses are needed to establish an exhaustive pulsational scenario. However, in view of the rather encouraging and plausible results given by the adopted theoretical approach, we suggest that observational data for the rate of period change could be a relevant test for the theory. In fact, we predict that for SMR BL Her this rate should be at least an order of magnitude larger in comparison with the corresponding values for metal-poor type II Cepheids in globular clusters. Moreover, we predict that BL Her would show both positive and negative rates, due to the occurrence of GNL, whereas only positive values are expected in metal-poor Cepheids, due to the evolution of these metal-poor, hot HB stars toward the Hayashi track.

Theoretical luminosity and radial velocity curves reveal a plethora of interesting features that cannot be soundly compared with observational data due to the paucity of extensive and accurate photometric data presently available. We expect that the impressive database of photometric data collected by recent international collaborations (MACHO, EROS, OGLE) devoted to the search for microlensing events in the bulge and in the halo of the Galaxy will not only improve the accuracy of the light curves but also increase the present sample of BL Her stars. However, the problem in which the data of microlensing experiments will certainly play a role of paramount importance is the comprehensive evaluation of the evolutionary rate of period change among type II Cepheids. In fact, the long set of observational runs which characterize these databases will provide useful insights on the detection of this effect which can be barely accomplished, in spite of its inherent simplicity, on the basis of data available at present.

It is a real pleasure to thank L. Rusconi for a detailed reading of an early draft of this paper and A. Tornambé and O. Straniero for several interesting discussions on this topic. We

wish also to acknowledge the referee, R. T. Rood, for his careful reading of the manuscript and for the pertinence of his suggestions which substantially improved the content and the readability of the appendix. The evolutionary tracks, the isochrones, the ZAHBs, as well as the linear nonadiabatic blue boundaries and both light and velocities curves can be found in http://terri1.te.astro.it/oact-home/cassisi.html. This research has made use of NASA's Astrophysics Data System Abstract Service and of SIMBAD database operated at CDS, Strasbourg, France. This work was partially supported by MURST, CNR-GNA and ASI.

A. GRAVONUCLEAR LOOPS AND SCHWARZSCHILD-HARM INSTABILITIES

Even though a large amount of theoretical investigations has been recently devoted to the evolution of HB structures (Castellani, Chieffi & Pulone 1991; HDP; DRO; Bertelli et al. 1996), only in Paper I we found that in some HB models with solar metallicity the He shell ignition is affected by what we named gravonuclear instability, an occurrence which appears to be a rule for super-metal-rich He burning structures. According to this evidence, the related appearance of *gravonuclear loops* -GNL- in the HR diagram is dependent on the metal content and on the mass of the H rich envelope. In this Appendix we discuss in more detail the physical mechanisms which govern the appearance of this phenomenon in metal-rich HB models and its dependence on astrophysical parameters.

As reported in Figure 8 the time behavior of surface luminosity and effective temperature for the "cool" 0.51 $M_{\odot}$ model shows that at the ignition of the He shell this model spends roughly 3 million years showing periodic drops in luminosity accompanied by a contraction of the structure which drives the increase in the effective temperature. Eventually, the model succeeds in quietly burning He in the shell as a red Asymptotic Branch structure. Figure 21, where we report the same data but for the "hot" 0.48 $M_{\odot}$ model, shows that the phenomenon is remarkably similar even in much hotter models: in both cases, before quietly burning He in a shell, the models approximatively experience 20 loops with quite similar timescales. In order to better define the occurrence of this phenomenon, Figure 22 discloses the energetics of the "hot" model during the GNL phase. We find that the loops are driven by a sequence of periodic switching off/on of both H and He burning shells, which in turn drives the expansion of the structure: the majority of the energy produced by nuclear reactions is absorbed by the expansion which succeeds in cooling the stellar interior, switching off the shells. This phase is obviously followed by a contraction which raises internal temperatures, reigniting the shells and reiterating the process.

In order to disentangle the effects of gravitational energy, ϵ_g, from the nuclear energy

sources, on the development of GNL we performed, as suggested by the referee, a numerical experiment in which the ϵ_g term in the equation for energy conservation has been artificially switched off throughout the stellar structure. A similar approach was originally suggested by Sweigart (1971) for suppressing the thermal instability in helium shell burning stars. The consequence of assuming a vanishing ϵ_g term on the appearance of GNL are shown in Fig. 22 for the "hot" 0.48 $M_\odot$ model previously discussed. The energetics of this model (dashed lines) show quite clearly that after the ignition of helium shell burning the gravitational energy rules the onset of gravonuclear instability, and indeed this model does not present any cyclic change in the energy sources. At the same time, it turns out that this model does not experience the luminosity and temperature excursions typical of GNL and hence the evolutionary track moves along its canonical phases.

Moreover, we also note that the occurrence of GNL does not depend on the chemical composition profile of the region located between the hydrogen and helium burning shells, since as pointed out by Sweigart (1971) the SH instabilities are not affected by the abundance profile of this region.

The smooth variation of all physical quantities along the evolutionary phases during which the model undergoes the loop can be taken as a plane evidence that we are dealing with a real phenomenon rather than with a numerical instability. Initially we thought about a possible interaction between the two shells, producing an oscillatory overstability. However, we early found the evidence that the H shell can play quite a negligible role on that matter, as shown in Figure 23 where we report the energetics of GNL in a less massive 0.457 $M_\odot$ HB model, where the H shell burning plays a negligible contribution to the onset and development of GNL. This difference in the efficiency of the CNO cycle is mainly caused by the location of the H burning shell, and indeed in hot models is closer to the surface than it is in the cool models. As a consequence we reach the conclusion that GNL deal with the occurrence of a thermal instability in the He burning shell. However, inspecting the literature on this subject we disclose that this is not an unexpected finding, since it was predicted by Schwarzschild & Härm in a beautiful paper dating back to 1965 (hereinafter referred to as SH), in which they discuss the instability of a $M/M_\odot$=1.0 model *in the phase of He burning shell*. In that paper the authors demonstrated that non-degenerate shells containing a highly temperature-sensitive nuclear energy source (as triple alpha reactions are) can undergo thermal runaways provided that the temperature drop across the shell is sufficiently large (eq. [12] in SH).

It is not necessary to repeat here the elegant discussion given by SH in their pioneering paper. The philosophy is that, in that case, the ignition of the shell is not efficiently counteracted by the local expansion, inducing an increase in the local temperature which

leads to a thermal runaway. We find that this prediction is nicely confirmed by the behavior of the model shown in Figure 24. This figure shows the time behavior of temperature and density at both the stellar center and the He burning shell. At the same time, these quantities are compared with gravitational and neutrino luminosities of the structure. We find that the exhaustion of the central He is followed by an overall contraction phase, where the increase of central temperature is partially dumped by the increased efficiency of neutrino cooling. The ignition of the shell is marked by the sequence of peaks in the shell temperature, which points out the positive feed back affecting this parameter until the expansion of the structure first cools and then switches off the shell. As a consequence, we find that our models follow closely SH predictions. However, we find that stellar matter at the shell location appears affected by moderate electron degeneracy, which contributes with a further 40% to the perfect gas pressure, possibly playing a role in favoring the onset of gravonuclear instabilities. Without further details, it is worth underlining that the scenario outlined by SH casts light only on the appearance of GNL in metal-rich stars, since the increased opacity steepens the temperature gradients in the stellar interior, which, as already discussed, is the parameter governing the onset of this instability.

SH only speculated about the consequence of these thermal instabilities, suggesting that the thermal perturbation would likely increase the He burning rates by more than a factor of 10 over its normal value, possibly inducing deep mixing and, although not likely, dynamical effects. However, their best guess was that since the runaway: *"would probably not alter the star basically and hence may be repetitive, one might guess that a thermal instability of the type here considered may lead to a kind of relaxation oscillation, a thermal flicker. Whether the convective mixing could reach an extent sufficient to have substantial evolutionary consequences seems at present an entirely open question"*. We find that such a scenario appears soundly confirmed by our detailed computations. In fact, He burning rates reach a factor of 10 over their normal values and the phenomenon is indeed repetitive, producing a sequence of relaxation oscillations. However, convection is damped since energy is converted into radial expansion, and no substantial mixing occurs. As shown in the same Figure 24, we can only add that the transient flickering succeeds in affecting the whole stellar structure, and indeed central conditions also flicker as a function of time until the steady burning in the He shell is reached.

As a whole, we note that helium burning shells, due to both the strong dependence of triple alpha reactions on local temperature and the sudden decrease of the temperature across the shell, cause the onset of SH instability during the AGB thermal pulses (AGB-TP) and the post-HB phases (GNL). However, the GNL are tightly connected with the envelope opacity and indeed the appearance of this phenomenon is a common feature of metal-rich HB models. On the other hand, both metal-poor and metal-rich stars which evolve along

the AGB experience the phase of thermal pulses. Moreover, we find that during the GNL the helium burning shells are characterized by a moderate amount of electron degeneracy, whereas the AGB-TP are only marginally affected by this phenomenon. Even though the hydrogen and helium burning shells govern the morphology of GNL, the helium shell, in contrast with the AGB-TP, never approaches the hydrogen shell. Finally, we note that the timescale of AGB-TP is ruled by the efficiency of H burning shell, whereas the GNL are ruled by the thermal timescale of the envelope.

We have already outlined the role played by envelope opacities on the appearance of GNL (see section 2.1 in Paper I). However, in order to assess in more detail the effects of new radiative opacities on this phenomenon, Figure 25 shows the opacity distribution in the stellar layers located above the H burning shell for several envelope models computed at different effective temperatures (see labeled values) but at fixed luminosity level (log $L/L_{\odot}$ =1.90) and stellar mass ($M/M_{\odot}$ =0.48). According to the data plotted in this figure we find that the iron bump is the main opacity source of the stellar envelopes located in the high temperature region of the SMR horizontal branch stars. At effective temperatures lower than log $T_e = 4.6$ the opacity bump due to the second HEIR appears and it becomes a non-negligible opacity source for effective temperatures of the order of 25,000 K. At even lower effective temperatures the opacity bumps due to both hydrogen and first helium ionization become the main opacity sources of the envelope. Moreover, it is worth mentioning that the opacity peak due to iron, in contrast with the helium peak, remains almost constant over the whole range of effective temperatures. The old opacities (Huebner et al. 1977, dashed lines), as it is well known, do not show the Z-bump close to log T=5.3.

On the basis of these non trivial differences we computed an evolutionary track by assuming the same input parameters of the "hot" model shown in Fig. 21 but by adopting the old opacities together with both a coarse and a fine zoning throughout the envelope regions. Oddly enough, the coarse zoning evolutionary track evolves toward the white dwarf cooling sequence and does not show the appearance of GNL, whereas the fine zoning evolutionary track presents the GNL. In order to provide a comprehensive analysis of the opacity effects, we performed the same numerical experiments but by adopting the input parameters of the "cool" model shown in Fig. 8. In this case we find that both the coarse and the fine zoning evolutionary tracks do not experience at all the gravonuclear instability.

As a consequence, we think it right to stress that the new opacities are not a sufficient condition for the appearance of this phenomenon. In fact, several numerical experiments performed to evaluate the effect of spatial resolution on the onset and development of gravonuclear instability disclose that a decrease of the spatial resolution connected with the iron bump and with the H and He ionization regions causes a substantial increase of the

transparency in the outermost regions. Therefore the energy released by the He shell is substantially reduced, and in turn the radius and luminosity excursions of GNL are reduced and/or inhibited.

The increase of spatial resolution in the iron bump and in the ionization regions causes a decrease of the time step since in the fine zoning models it is ruled by the pressure gradient in the stellar envelope and not by nuclear reactions in H and He burning shells. SH already suggested that the instability we are dealing with will not be necessarily noted in stellar evolutionary computations, since it will be passed without notice as long as the adopted time step is twice the e-folding time of the instability. Luckily, we approached the phase of central He exhaustion with time steps of the order of few thousand years for following in detail the He exhaustion and the ignition of the H burning at first and then of the He burning shells. Similar time steps are much shorter than the Kelvin-Helmotz timescale which governs thermal runaways, and thus provide a detailed coverage of the onset and development of the gravonuclear instability. However, if time steps are evaluated according to the much longer nuclear timescales, the GNL will be largely smoothed away. We suggest that the use of old opacities and of a coarse zoning in the envelope regions could be the reasons why DRO did not find GNL in their recent computations of metal-rich HB structures.

In order to speed up the calculations required to approach the post-AGB evolutionary phases, we decreased the spatial resolution in the opacity bumps (increase of the time step) for artificially switching off the GNL. Note that for a proper treatment of GNL at least 20,000 models for each track would be needed.

REFERENCES

Alexander, D. R., & Ferguson, J. W. 1994, ApJ, 437, 879

Bertelli, G., Bressan, A., Chiosi, C., & Ng, Y. K. 1996, A&A, 310, 115

Bono, G., Caputo, F., Cassisi, S., Castellani, V., & Marconi, M. 1997b, ApJ, 479, 279 (Paper I)

Bono, G., Caputo, F., Cassisi, S., Castellani, V., Marconi, M., & Stellingwerf, R. F. 1997a, ApJ, 477, 346

Bono, G., Caputo, F., Cassisi, S., Incerpi, R., & Marconi, M. 1997d, ApJ, 483, July 10

Bono, G., Caputo, F., Castellani, V., & Marconi, M. 1997c, A&AS, 121, 327 (BCCM)

Bono, G., Caputo, F., & Santolamazza, P. 1997, A&A, 317, 171, (BCS)

Bono, G., Castellani, V., & Stellingwerf, R. F. 1995, ApJ, 445, L145

Bono, G. et al. 1997e, in preparation

Bono, G., Incerpi, R., & Marconi, M. 1996, ApJ, 467, L97 (BIM)

Bono, G., & Stellingwerf, R. F. 1994, ApJS, 93, 233 (BS)

Bressan, A., Chiosi, C., & Fagotto, F. 1994, ApJS, 94, 63

Brocato, E., Matteucci, F., Mazzitelli, I., & Tornambé A. 1990, ApJ, 349, 458

Buchler, J. R., & Buchler, N. E. G. 1994, A&A, 391, 736

Buzzoni, A. 1995, ApJS, 98, 69

Caloi, V., Castellani, V., & Di Paolo, N. 1974, A&A, 30, 349

Caloi, V., Castellani, V., & Tornambé. A. 1978, A&AS, 33, 169

Carigi, L., Colin, P., Peimbert, M., & Sarmiento A. 1995, ApJ, 445, 98

Carson, R., & Stothers, R. 1982, ApJ, 259, 740

Caputo, F., Castellani, V., Chieffi, A., Pulone, L., & Tornambé, A. 1989, ApJ, 340, 241

Cassisi, S., & Castellani, V. 1993, ApJS, 88, 509

Cassisi, S., Castellani, M., & Castellani, V. 1997, A&A, 317, 108

Castellani, M., & Tornambé, A. 1991, ApJ, 381, 393

Castellani, V., Chieffi, A., & Norci, L. 1989, A&A, 216, 62

Castellani, V., Chieffi, A., & Pulone, L. 1991, ApJS, 76, 911

Castellani, V., Chieffi, A., Pulone, L., & Tornambé, A. 1985, ApJ, 296, 204

Castellani, V., Chieffi, A., & Straniero, O. 1992, ApJS, 78, 517

Castellani, V., & Degl'Innocenti, S. 1995, A&A, 298, 827

Cellone, S. A., & Forte, J. C. 1997, ApJ, in press

Chieffi, A., & Straniero, O. 1989, ApJS, 71, 47

Christy, R. F. 1970, QJRASC, 64, 8

Code, A. D. 1969, PASP, 81, 475

Connolly, L. P. 1980, PASP, 92, 165

Cox, A. N. 1991, ApJ, 381, L71

D'Cruz, N. L., Dorman, B., Rood, R. T., & O'Connell, R. W. 1996, ApJ, 466, 359

Diethelm, R. 1983, A&A, 124, 108

Diethelm, R. 1986, A&AS, 64, 261

Diethelm, R. 1990, A&A, 239, 186

Dorman, B. 1992, ApJS, 81, 221

Dorman, B., O'Connell, R. W. & Rood, R. T. 1995, ApJ, 442, 105 (DOR)

Dorman, B., Rood, R. T., & O'Connell, R. W. 1993, ApJ, 419, 596 (DRO)

Eddington, A. S., 1918, MNRAS, 79, 2

Geisler, D., Lee, M. G., & Kim, E. 1996, AJ, 111, 1529 (GLK)

Goldberg, L. 1979, QJRASC, 20, 361

Greggio, L., & Renzini, A. 1990, ApJ, 364, 35

Grevesse, N. 1991, in IAU Symp. 145, Evolution of Stars: the Photospheric Abundance Connection, eds. G. Michaud & A. Tutukov (Dordrecht: Kluwer), 63

Harris, H. C. 1985, in IAU Colloq. 82, Cepheids: Theory and Observations, ed. B.F. Madore (Cambridge: Cambridge Univ. Press), 232

Harris, H. C., & Wallerstein, G. 1984, AJ, 89, 379

Hertzsprung, E. 1926, BAIN, 3, 115, (96)

Hodson, S. W., Cox, A. N., & King, D. S. 1982, ApJ, 253, 260

Hoffmeister, C., Richter, G., & Wenzel, W. 1985, Variable Stars, (Berlin: Springer-Verlag), 38

Horch, E., Demarque, P., & Pinsonneault, M. 1992, ApJ, 388, L53 (HDP)

Huebner, W. F., Merts, A. L., Magee, N. H., & Argo, M. F. 1977, Los Alamos Sci. Lab. Rep., No. LA-6760-M

Iglesias, C. A., Rogers, F. J., & Wilson, B. G. 1992, ApJ, 397, 717

Kemper, E. 1982, AJ, 87, 1395

Kholopov, P. N. 1981, IBVS, 2042

Krishna-Swamy, K. S. 1966, ApJ, 145, 174

Kurucz, R. L. 1992, in IAU Symp. 149, The Stellar Populations of Galaxies, eds. B. Barbuy & A. Renzini (Dordrecht: Kluwer), 225

Layden, A. C. 1995, AJ, 110, 2288

Lee, Y. W., Demarque, P., & Zinn, R. 1990, ApJ, 350, 155

Maeder, A. 1992, A&A, 264, 105

Magris, G. C., & Bruzual, G. 1993, ApJ, 417, 102

Minniti, D. 1994, PASP, 106, 813

Minniti, D. 1995, A&A, 300, 109

Minniti, D., Alonso, M. V., Goudfrooij, P., Jablonka, P. & Meylan, G. 1996, AJ, accepted

Morgan, S. M. 1995, AJ, 109, 1263

Nieuwenhuijzen, H., & de Jager, C. 1990, A&A, 231, 134

Pagel, B. E. J., Simonson, E. A., Terlevich, R. J., & Edmunds, M. G. 1992, MNRAS, 255, 325

Payne-Gaposchkin, C. 1956, Vistas in Astron., 2, 1142

Peimbert, M. 1993, Rev. Mex. Astr. Astrofis., 27, 9

Peimbert, M., & Torres-Peimbert, S. 1974, ApJ, 193, 327

Petersen, J. O. 1981, A&A, 96, 146

Pozzetti, L., Bruzual, G., & Zamorani, G. 1996, MNRAS, 281, 953

Preston, G. W. 1959, ApJ, 130, 507

Reimers, D. 1975, Mém. Soc. Roy. Sci. Liége 6^e Ser., 8, 369

Renzini, A. 1994, A&A, 285, L5

Rich, R. M. 1988, AJ, 95, 828

Rocha-Pinto, H. J., & Maciel, W. J. 1996, MNRAS, 279, 447

Rogers, F. J., & Iglesias, C. A. 1992, ApJS, 79, 507

Sadler, E. M., Rich, R. M., & Terndrup, D. M. 1996, AJ, 112, 171

Salaris, M., & Cassisi S. 1996, A&A, 305, 858

Sandage, A., Diethelm, R., & Tammann, G. A. 1994, A&A, 283, 111 (SDT)

Schwarzschild, M., & Härm, R. 1965, ApJ, 142, 855 (SH)

Simon, N. R. 1986, ApJ, 311, 305

Spinrad, H., & Taylor, B. J. 1969, ApJ, 157, 1279

Stellingwerf, R. F. 1979, ApJ, 227, 935

Stobie, R. S. 1973, Observatory, 93, 111

Straniero, O. 1988, A&AS, 76, 157

Suntzeff, N. B., Kinman, T. D., & Kraft, R. P. 1991, ApJ, 367, 528

Sweigart, A. V. 1971, ApJ, 168, 79

Sweigart, A. V., Greggio, L., & Renzini, A. 1989, ApJS, 69, 911 (SGR)

Sweigart, A. V., Greggio, L., & Renzini, A. 1990, ApJ, 364, 527

Sweigart, A. V., & Renzini, A. 1979, A&A, 71, 66

Terndrup, D. M. 1988, AJ, 96, 884

Terndrup, D. M., Sadler, E. M., & Rich, R. M., 1995, AJ, 110, 1774

Tornambè, A. 1982, MNRAS, 239, 771

Torres-Peimbert, S. 1971, Bol. Obs. Tonantzintla y Tacubaya, 6, 113

Traat, P. 1995, in ESO/EIPC Workshop on "The Light Element Abundances", ed. P. Crane (Berlin: Springer & Verlag), 191

van Albada, T. S., & Baker, N. 1971, ApJ, 169, 311

Walker A. R., & Terndrup D. M., 1991, ApJ, 378, 119

Wallerstein, G. W., & Cox, A. N. 1984, PASP, 96, 677

Wehlau, A., & Bohlender, F. 1982, AJ, 87, 780

Weiss, A., Peletier, R. F., & Matteucci, F. 1995, A&A, 296, 73

This preprint was prepared with the AAS LaTeX macros v4.0.

Fig. 1.— Evolutionary parameters for structures at the RGB tip as a function of the stellar mass. From the top to the bottom are plotted: the stellar age, the luminosity and the mass of the He core. The solid and dashed lines are referred to data obtained by adopting an initial He abundance equal to Y=0.34 and Y=0.37, respectively.

Fig. 2.— Behavior of the transition mass M_{tr} as a function of the metallicity. The results shown in this figure have been derived by adopting, at lower metallicities, data from Cassisi & Castellani (1993), Cassisi et al. (1996), and Paper I.

Fig. 3.— Theoretical isochrones for the H burning phases for the labeled assumptions about the stellar age and for two different helium abundances, namely Y=0.34 (panel a) and Y=0.37 (panel b). The time interval between consecutive isochrones is 2 Gyr, with the exception of the four isochrones corresponding to 0.8, 0.9, 1.0 and 2.0 Gyr, respectively. The arrows mark the location of the RGB clump in both the youngest and the oldest isochrones.

Fig. 4.— ZAHB locations for the He burning stellar models for the labeled assumptions about the red giant progenitor masses and for the two different initial He abundances, namely Y=0.34 (panel a) and Y=0.37 (panel b).

Fig. 5.— ZAHB locations for the He burning models at fixed red giant progenitor mass ($M/M_{\odot}$ =1.8) and for the two quoted initial He abundances.

Fig. 6.— Evolutionary tracks in the HR diagram of He burning structures evaluated by assuming fixed metal content (Z=0.04) and initial helium abundance (Y=0.34). The sets of HB models have been computed by adopting three different values of the progenitor mass ($M_{pr} = 2.0, 1.8, 1.0 M_{\odot}$) and different assumptions concerning the efficiency of mass loss along the RGB.

Fig. 7.— Same as Fig. 6, but referred to HB models computed by adopting a different initial helium abundance, namely Y=0.37.

Fig. 8.— Time behavior of the surface luminosity (top panel) and effective temperature (bottom panel) for a "cool" model which presents gravonuclear loops. For this model the RG progenitor mass is $M_{pr} = 1.8 M_{\odot}$. The total mass value, the He core mass at the He ignition and the chemical composition are labeled.

Fig. 9.— HR diagram showing the linear blue boundaries of both fundamental and first overtone BL Herculis variable stars. The stability analysis has been performed by adopting a fixed chemical composition (Y=0.34, Z=0.04) and three different values of the stellar mass, namely $M/M_{\odot}$ =0.485, 0.505, 0.52.

Fig. 10.— HR diagram showing the linear blue boundaries of both fundamental and first overtone BL Herculis variable stars. The stability analysis has been performed by adopting a fixed stellar mass value ($M/M_{\odot}$ =0.505) and two different chemical compositions, namely Y=0.34, Z=0.04; and Y=0.28, Z=0.02. The dashed lines indicate the blue boundaries of the instability region connected with type II Cepheids belonging to globular clusters.

Fig. 11.— Linear work curves per logarithmic temperature versus the logarithmic temperature for two models computed by adopting the same luminosity (log $L/L_{\odot}$ =2.0), effective temperature (T_e=6400 K), and stellar mass ($M/M_{\odot}$ =0.505). The different chemical compositions are labeled. The top panel is referred to the fundamental mode, whereas the bottom one to the first overtone, surface at right. The arrows denote the position of the driving regions connected with the ionization regions (HIR, HEIR) and with the opacity bump caused by iron. The symbols plotted in the bottom panel mark the location of the first overtone nodes in radius (diamonds), temperature (triangles), and luminosity (squares). See text for further explanation.

Fig. 12.— Predicted ratio between the number of RR Lyrae variables and the total number of Horizontal Branch stars as a function of the metal content (see text).

Fig. 13.— Fundamental bolometric magnitude variation at limiting amplitude. This sequence of nonlinear models has been computed by adopting fixed luminosity (log $L/L_{\odot}$ =2.0), stellar mass ($M/M_{\odot}$ =0.505), and chemical composition (Y=0.34, Z=0.04). The nonlinear periods (days) and the effective temperatures (K) are labeled.

Fig. 14.— Same as Fig. 13, but referred to lower temperature models. The top panel shows quite clearly that the model located at T_e=5700 K is a mixed-mode pulsator, and indeed over subsequent periods both the shape of the light curve and the pulsational amplitude present substantial variations. The value of the nonlinear period labeled in the top panel is referred to the pulsation cycle between $\phi = 0.0$ and $\phi = 1.0$, whereas the period of the following cycle is P=2.1903 d.

Fig. 15.— Variation of the surface radial velocity at limiting amplitude. The velocity curves are referred to the sequence of fundamental nonlinear models described in the text. Positive values indicate expansion, whereas the negative ones contraction. The labels and the notation are the same as in Fig. 13.

Fig. 16.— Same as Fig. 15, but referred to lower temperature models.

Fig. 17.— Variation of both bolometric magnitude (top panels) and surface radial velocity at limiting amplitude. The curves are referred to two fundamental pulsators computed by

adopting the following input parameters: log $L/L_{\odot}$ =2.2, $M/M_{\odot}$ =0.505, Y=0.34, Z=0.04. Labels and notation are the same as in Fig. 13.

Fig. 18.— Time behavior along the integration of period (top panel), bolometric amplitude ($\Delta M = \Delta M_{bol}(max) - \Delta M_{bol}(min)$; middle panel), and kinetic energy (bottom panel) for a first overtone model located at T_e=6000 K. This model shows a mode switching to the fundamental mode. The arrow in the top panel indicates the time at which the radial pulsation switches toward the fundamental, whereas the arrow in the bottom panel marks the time at which the model approaches the asymptotic behavior. The initial velocity profile was obtained by perturbing the radial first overtone eigenfunction with a constant velocity amplitude of 10 kms^{-1}.

Fig. 19.— Comparison in a log-log plane between linear (solid line) and nonlinear (dotted line) fundamental periods as function of the effective temperature for the labeled value of stellar mass and luminosity level. The dashed line shows the fundamental periods obtained by adopting the analytical relation provided by BCCM.

Fig. 20.— The evolutionary rates of period change for selected evolutionary models: (panel a) super-metal-rich BL Herculis; (panel b) globular cluster type II Cepheid; (panel c) globular cluster RR Lyrae. The stellar mass and the chemical composition of the adopted models are labeled.

Fig. 21.— Same as Fig. 8, but referred to a "hot" less massive HB model, namely M=0.480$M_{\odot}$.

Fig. 22.— Time behavior of gravitational (panel a), hydrogen (panel b), and helium (panel c) luminosities during the GNL phase of the HB model in Fig. 21. The dashed lines are referred to a numerical experiment performed by assuming a vanishing gravitational energy term throughout the stellar structure. See text for further details.

Fig. 23.— Same as Fig. 22, but referred to a less massive HB model with M=0.457$M_{\odot}$.

Fig. 24.— Time behavior of selected structural parameters for the 0.457$M_{\odot}$ model from the exhaustion of central He up to the onset of steady He shell burning. Top to bottom: density, temperature, gravitational luminosity, and neutrino luminosity. In the top panels the heavy solid line is referred to the center, whereas the solid one is referred to the He shell.

Fig. 25.— Opacity distribution as a function of the logarithmic temperature for several envelope models computed by adopting a fixed luminosity level (log $L/L_{\odot}$ =1.90) and a wide range of effective temperatures. The total stellar mass and the chemical composition have been assumed equal to the HB model adopted in Fig. 21. The solid lines are referred to

the radiative opacities provided by Rogers & Iglesias (1992), while the dashed lines to the old opacities provided by Huebner et al. (1977). It is worth noting that moving from hot envelope models (top) to the cooler ones (bottom) the opacity scale increases of almost one order of magnitude. The surface effective temperature is labeled.

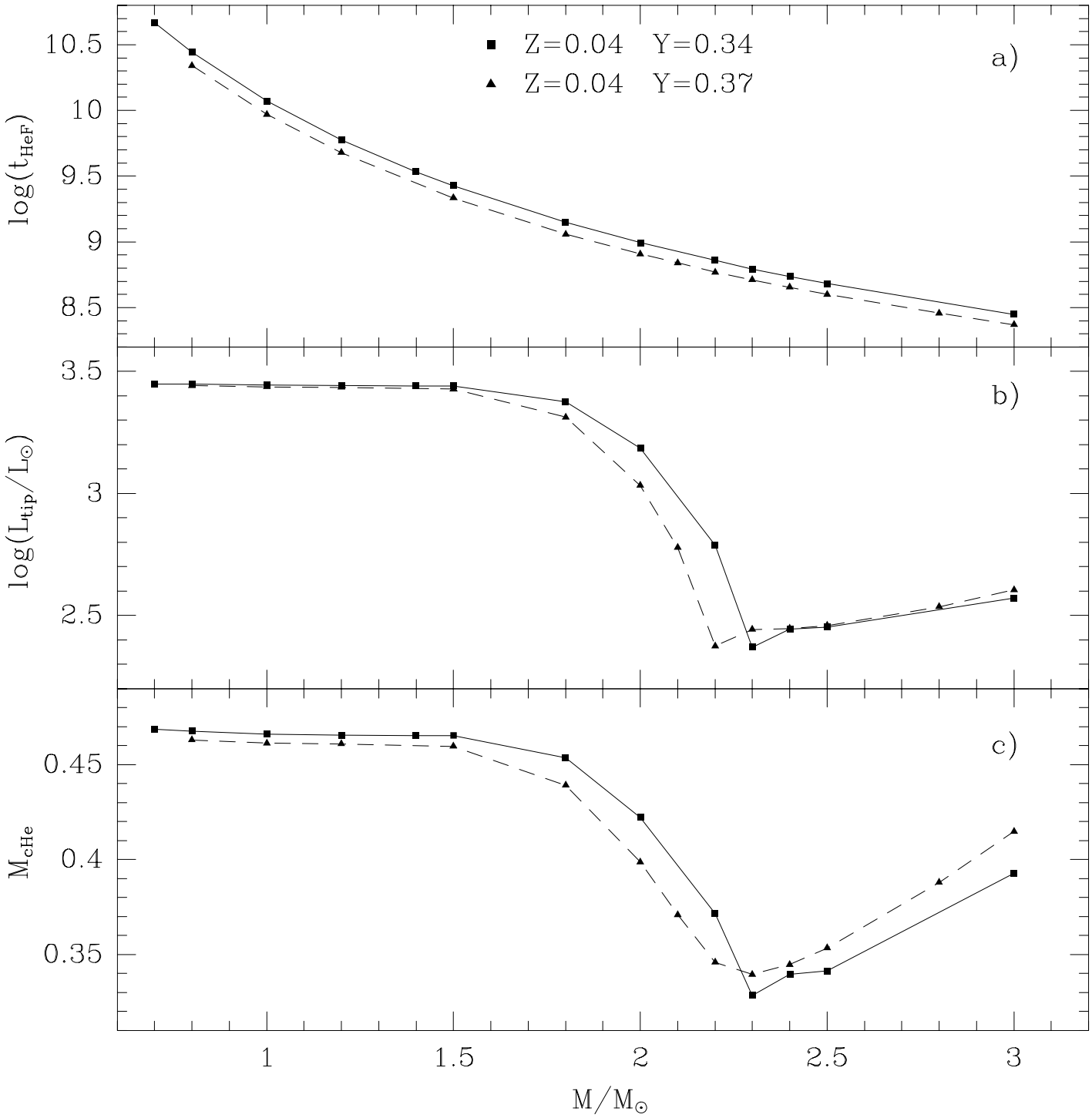
Z=0.04 Y=0.34
Z=0.04 Y=0.37
a)
b)
c)
log(t_HeF)
log(L_tip/L_⊙)
M_cHe
M/M_⊙
10.5
10
9.5
9
8.5
3.5
3
2.5
0.45
0.4
0.35
1
1.5
2
2.5
3

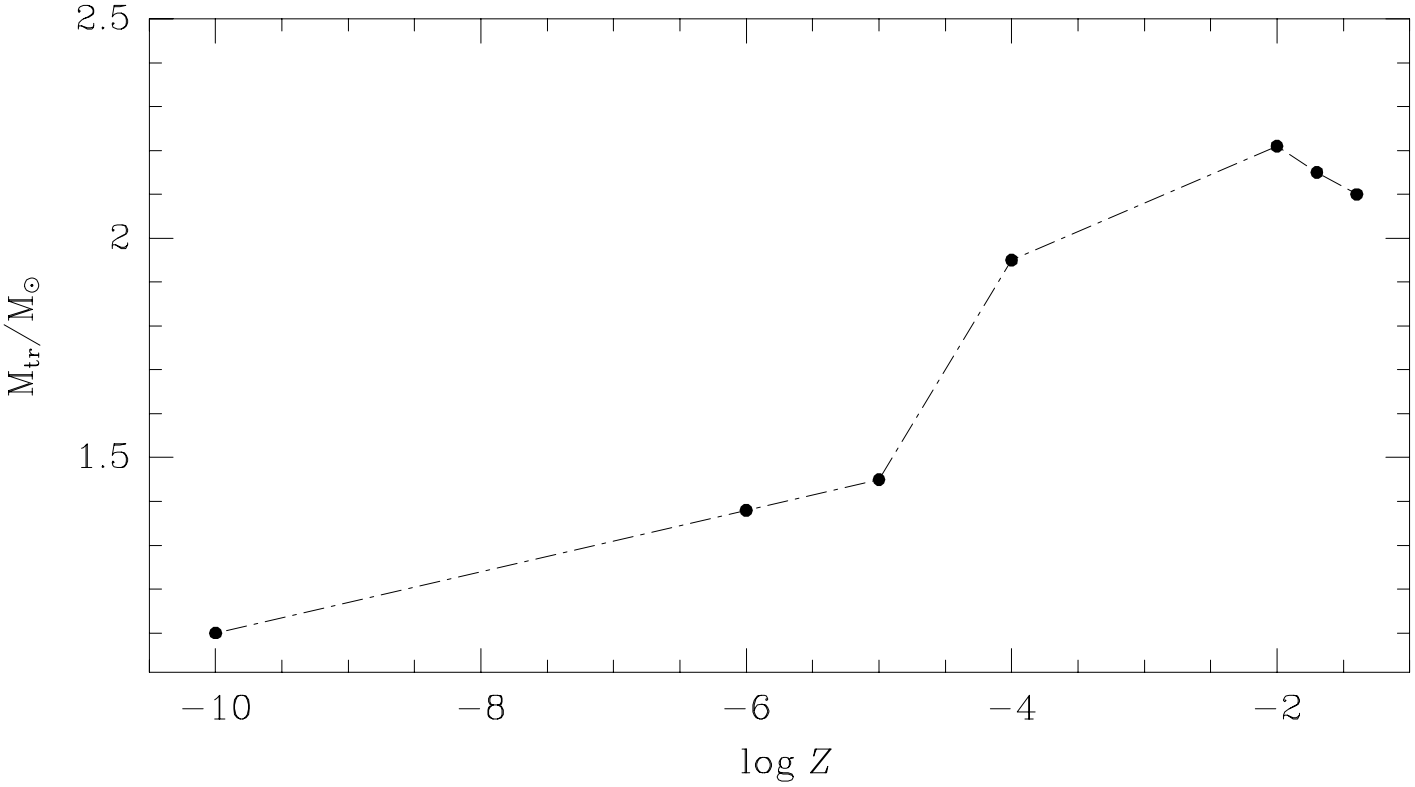
2.5
2
1.5
$M_{tr}/M_{\odot}$
−10
−8
−6
−4
−2
log Z

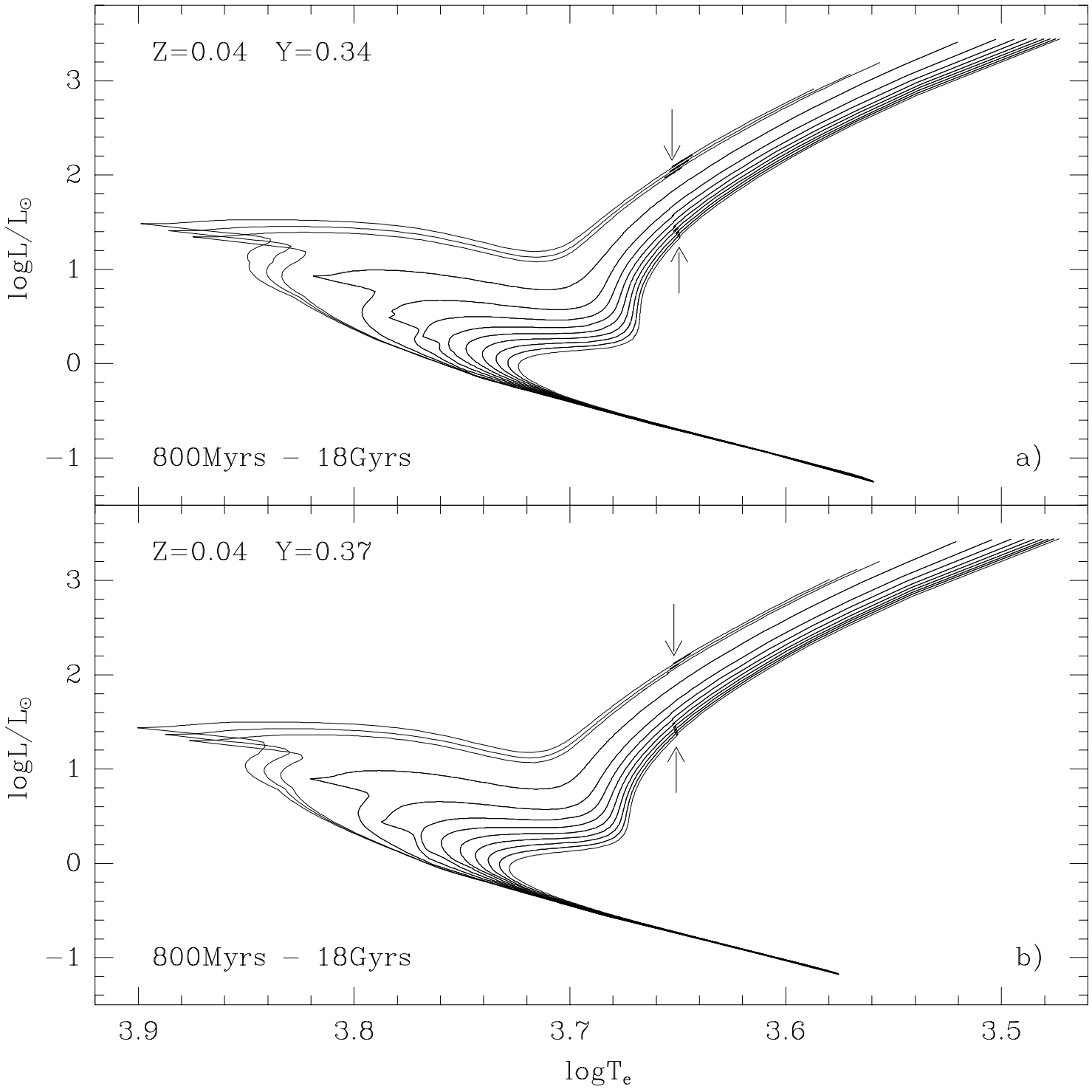
Z=0.04 Y=0.34
800Myrs – 18Gyrs
a)
Z=0.04 Y=0.37
800Myrs – 18Gyrs
b)
logL/L⊙
logT_e
3
2
1
0
−1
3.9
3.8
3.7
3.6
3.5

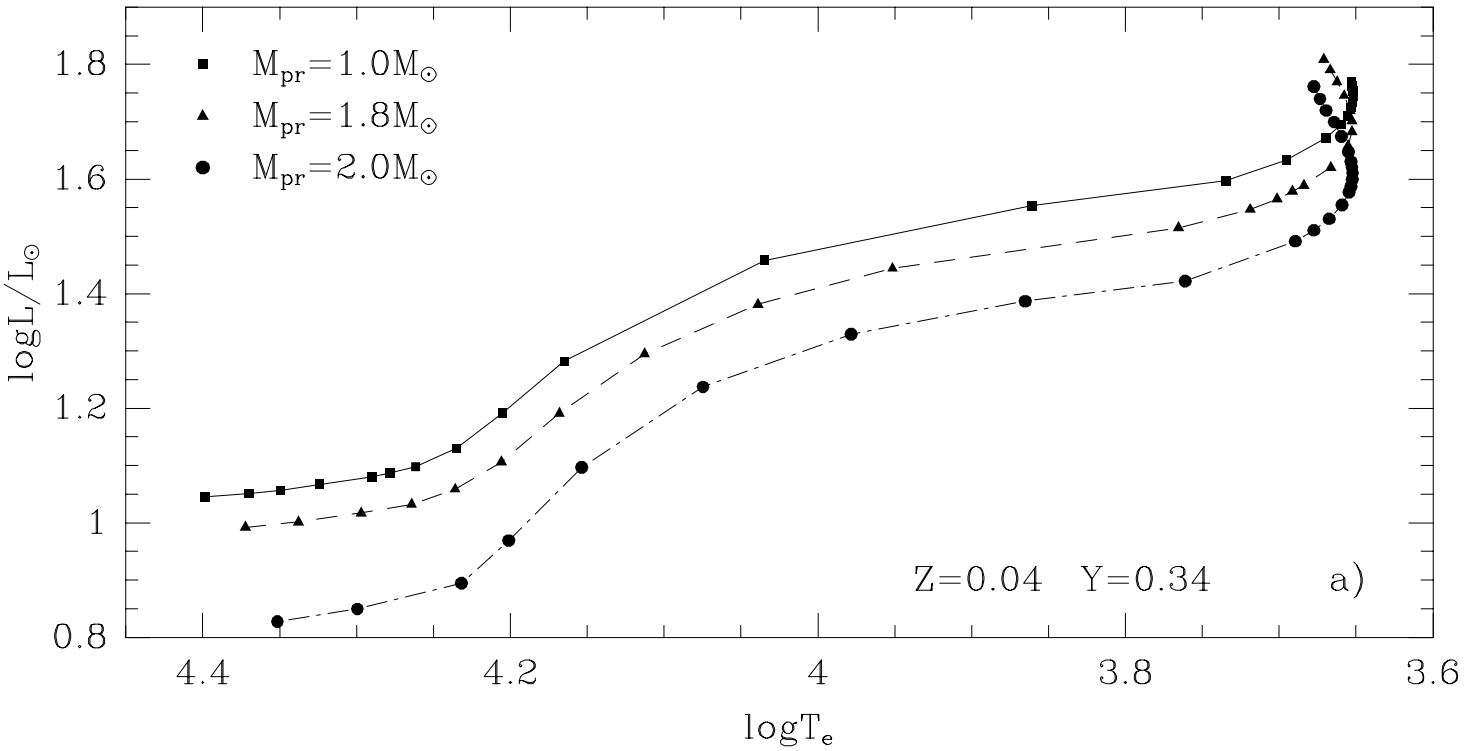
$M_{pr}=1.0M_\odot$
$M_{pr}=1.8M_\odot$
$M_{pr}=2.0M_\odot$
Z=0.04 Y=0.34
a)
$\log L/L_\odot$
$\log T_e$
1.8
1.6
1.4
1.2
1
0.8
4.4
4.2
4
3.8
3.6

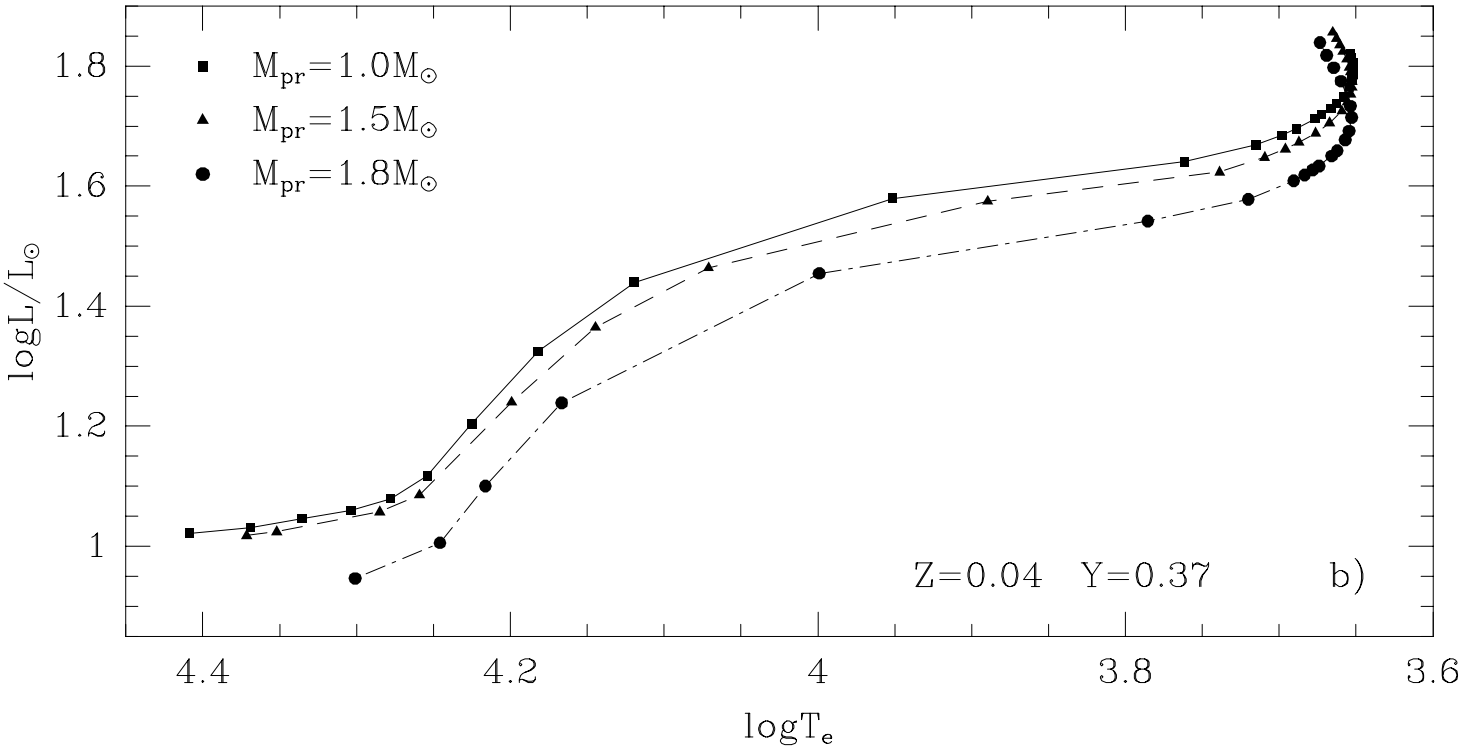
$M_{pr}=1.0M_\odot$
$M_{pr}=1.5M_\odot$
$M_{pr}=1.8M_\odot$
Z=0.04 Y=0.37
b)
$\log L/L_\odot$
$\log T_e$
1.8
1.6
1.4
1.2
1
4.4
4.2
4
3.8
3.6

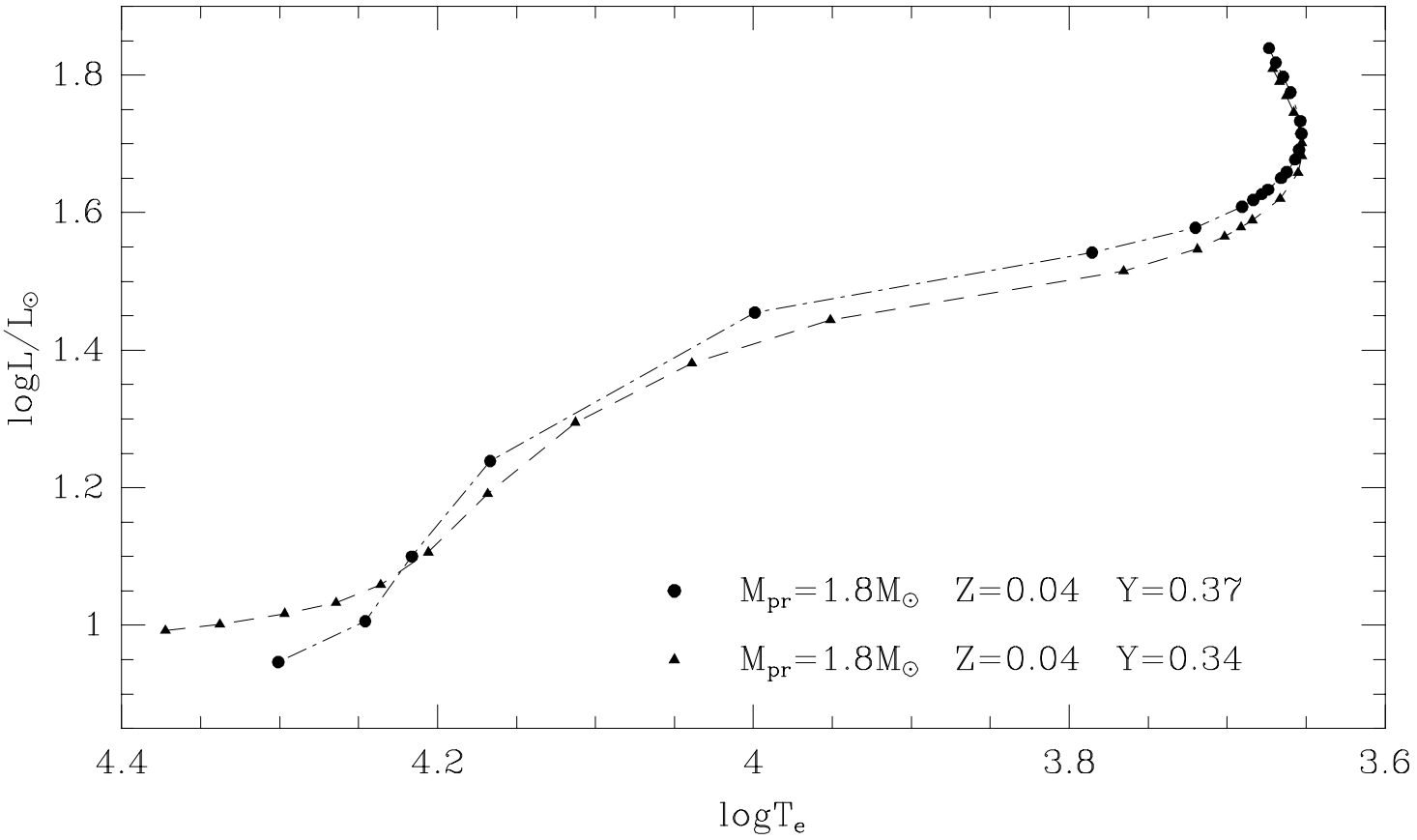
1.8
1.6
1.4
1.2
1
logL/L⊙
4.4
4.2
4
3.8
3.6
logT_e
M_pr=1.8M⊙ Z=0.04 Y=0.37
M_pr=1.8M⊙ Z=0.04 Y=0.34

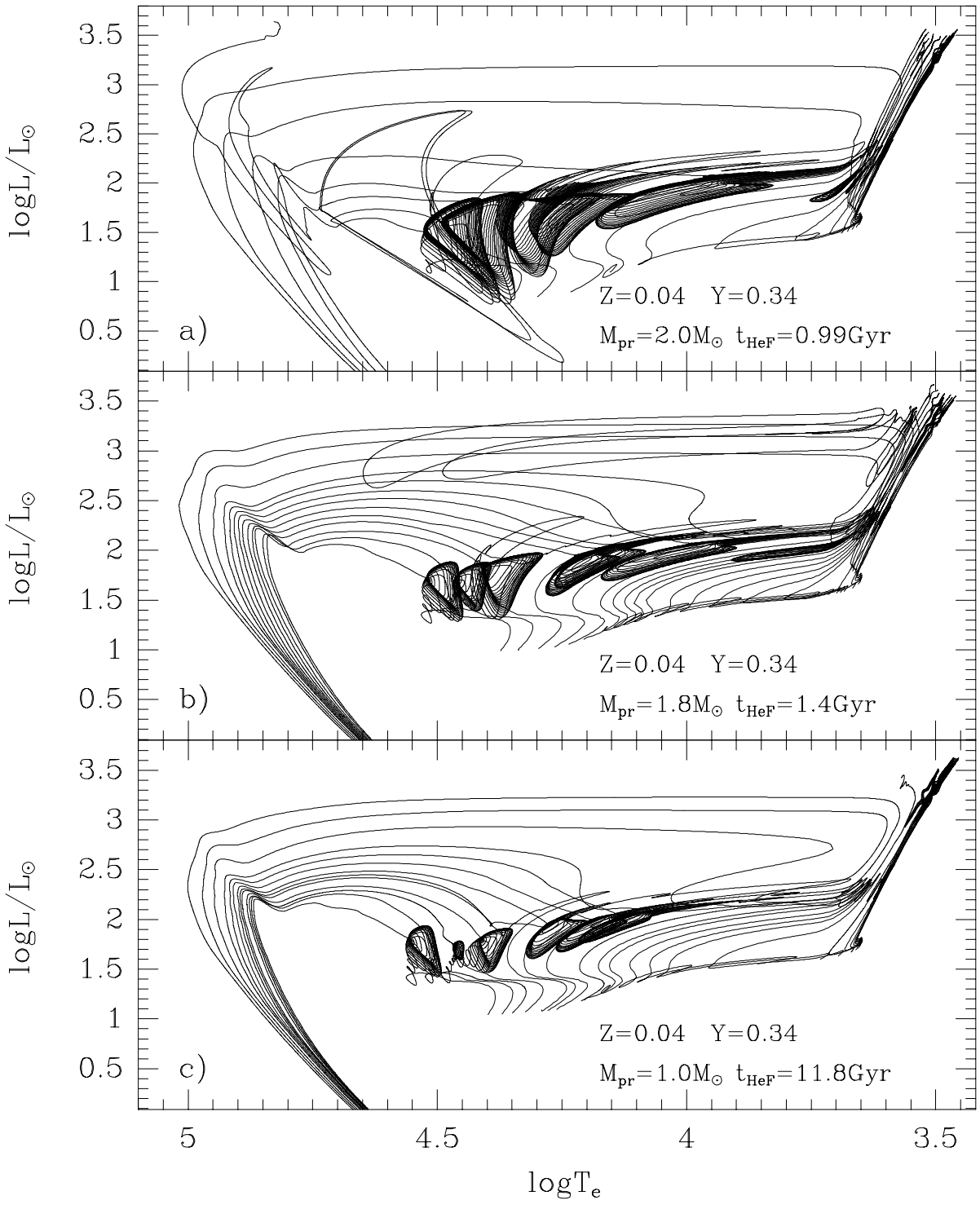
3.5
3
2.5
2
1.5
1
0.5
logL/L⊙
a)
Z=0.04 Y=0.34
M_pr=2.0M⊙ t_HeF=0.99Gyr
b)
Z=0.04 Y=0.34
M_pr=1.8M⊙ t_HeF=1.4Gyr
c)
Z=0.04 Y=0.34
M_pr=1.0M⊙ t_HeF=11.8Gyr
5
4.5
4
3.5
logT_e

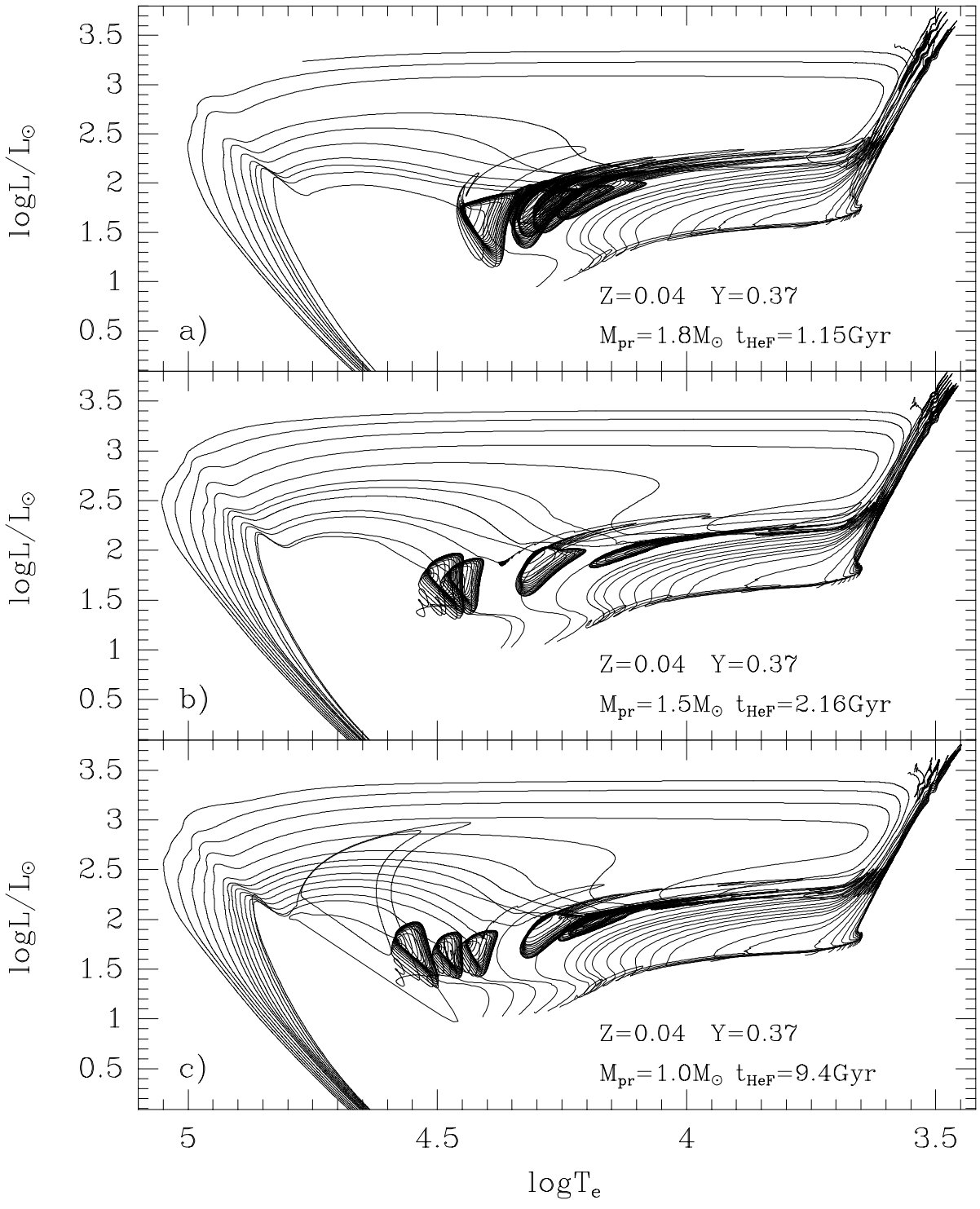
logL/L⊙
3.5
3
2.5
2
1.5
1
0.5
a)
Z=0.04 Y=0.37
M_pr=1.8M⊙ t_HeF=1.15Gyr
b)
Z=0.04 Y=0.37
M_pr=1.5M⊙ t_HeF=2.16Gyr
c)
Z=0.04 Y=0.37
M_pr=1.0M⊙ t_HeF=9.4Gyr
5
4.5
4
3.5
logT_e

TABLE 1

SELECTED THEORETICAL EVOLUTIONARY QUANTITIES AT FIXED METALLICITY (Z=0.04) AND TWO DIFFERENT HELIUM CONTENTS.

$M/M_{\odot}$[a]	$\log(L/L_{\odot})_{tip}$[b]	$\log t_{He}$[c]	M_{cHe}[d]	ΔY_{du}[e]
		Y=0.34		
0.7	3.449	10.668	0.469	0.014
0.8	3.448	10.444	0.468	0.017
1.0	3.445	10.072	0.466	0.019
1.2	3.442	9.775	0.466	0.015
1.4	3.441	9.533	0.465	0.011
1.5	3.440	9.427	0.465	0.010
1.8	3.376	9.147	0.454	0.007
2.0	3.186	8.994	0.422	0.005
2.2	2.788	8.861	0.372	0.007
2.3	2.370	8.792	0.328	0.007
2.4	2.445	8.736	0.340	0.007
2.5	2.453	8.682	0.341	0.008
3.0	2.571	8.449	0.393	0.010
		Y=0.37		
0.8	3.442	10.341	0.463	0.016
1.0	3.437	9.970	0.461	0.016
1.2	3.435	9.679	0.461	0.012
1.5	3.428	9.334	0.460	0.008
1.8	3.313	9.059	0.439	0.005
2.0	3.033	8.909	0.399	0.005
2.1	2.778	8.840	0.391	0.005
2.2	2.375	8.770	0.346	0.005
2.3	2.443	8.711	0.340	0.006
2.4	2.447	8.655	0.345	0.006
2.5	2.459	8.601	0.353	0.007
2.8	2.536	8.457	0.388	0.008
3.0	2.606	8.370	0.415	0.008

[a] Stellar mass value (solar units). [b] Logarithmic luminosity (solar units) at the RGB tip. [c] Logarithmic age (yrs) at the RGB tip. [d] He core mass values (solar units) at the He ignition. [e] Amount of extra helium dredged up during RGB evolution.

TABLE 2

SELECTED EVOLUTIONARY DATA CONCERNING THE ISOCHRONES FOR Z=0.04.

Age (Gyr)	$M/M_{\odot}$ [a]	$\log(L/L_{\odot})$ [b]	$\log T_e$ [c]	M_V [d]	$(B-V)$ [e]	ΔV_{HB}^{TO} [f]
			Y=0.34			
1.0	1.908	1.344	3.875	1.429	0.266	0.15
2.0	1.520	0.929	3.819	2.517	0.475	1.46
3.0	1.343	0.695	3.794	3.131	0.573	2.09
4.0	1.220	0.488	3.784	3.664	0.615	2.64
5.0	1.147	0.376	3.776	3.959	0.647	2.96
6.0	1.093	0.287	3.768	4.196	0.679	3.21
7.0	1.058	0.244	3.761	4.317	0.707	3.35
8.0	1.030	0.206	3.756	4.425	0.728	3.48
9.0	1.005	0.175	3.752	4.511	0.745	3.59
10.0	0.985	0.160	3.748	4.560	0.763	3.65
11.0	0.963	0.131	3.744	4.644	0.779	3.76
12.0	0.944	0.104	3.741	4.721	0.795	3.85
13.0	0.927	0.080	3.737	4.792	0.808	3.92
14.0	0.910	0.050	3.734	4.877	0.821	4.01
15.0	0.896	0.029	3.731	4.938	0.833	4.07
16.0	0.882	0.010	3.729	4.996	0.844	4.13
17.0	0.870	-0.009	3.726	5.051	0.854	4.18
18.0	0.859	-0.026	3.724	5.103	0.863	4.23
			Y=0.37			
1.0	1.789	1.300	3.876	1.539	0.262	0.59
2.0	1.435	0.898	3.820	2.593	0.470	1.80
3.0	1.255	0.643	3.802	3.250	0.543	2.46
4.0	1.138	0.439	3.787	3.782	0.601	3.00
5.0	1.074	0.329	3.775	4.078	0.650	3.30
6.0	1.039	0.290	3.769	4.186	0.675	3.42
7.0	1.000	0.226	3.765	4.356	0.694	3.60
8.0	0.979	0.223	3.750	4.375	0.714	3.62
9.0	0.952	0.185	3.755	4.479	0.733	3.73
10.0	0.927	0.142	3.751	4.597	0.751	3.85
11.0	0.907	0.113	3.747	4.680	0.767	3.94
12.0	0.890	0.086	3.744	4.756	0.781	4.01
13.0	0.873	0.062	3.741	4.826	0.794	4.08
14.0	0.858	0.032	3.738	4.910	0.806	4.17
15.0	0.844	0.012	3.735	4.970	0.817	4.23
16.0	0.831	-0.014	3.733	5.041	0.828	4.30
17.0	0.819	-0.037	3.730	5.107	0.837	4.37
18.0	0.809	-0.053	3.728	5.155	0.846	4.41

[a] Mass value at the TO point (solar units). [b] Logarithmic luminosity of the TO point (solar units). [c] Logarithmic effective temperature (K) of the TO point. [d] V magnitude of the TO point (mag). [e] B-V color of the TO point (mag). [f] V Magnitude difference between the TO point and the ZAHB at $\log T_e = 3.85$.

TABLE 3

Selected evolutionary parameters for the He burning phase for different assumptions on initial Helium abundance and RG progenitor masses.

M_{pr}[a]	Y_{HB}[b]	M_{cHe}[c]	M_{tot}[d]	M^{AGB}[e]	M^{TP}[f]
			Y_{ZAMS}=0.34		
1.0	0.359	0.466	0.468, 0.470, 0.472, 0.475, 0.480, 0.482 0.485, 0.490, 0.495, 0.500, 0.510, 0.520 0.530, 0.550, 0.600, 0.650, 0.700, 0.752 0.800, 0.850, 0.900, 0.950, 1.000	0.483	0.54
1.8	0.347	0.454	0.457, 0.460, 0.465, 0.470, 0.475, 0.480 0.485, 0.490, 0.495, 0.500, 0.510, 0.520 0.530, 0.540, 0.550, 0.600, 0.700, 0.800 0.900, 1.000, 1.200, 1.400, 1.600, 1.800	0.473	0.54
2.0	0.345	0.422	0.425, 0.430, 0.440, 0.450, 0.470, 0.500 0.520, 0.550, 0.600, 0.664, 0.700, 0.750 0.800, 0.850, 0.900, 1.000, 1.200, 1.400 1.600, 1.800, 2.000	0.436	0.54
			Y_{ZAMS}=0.37		
1.0	0.386	0.461	0.463, 0.466, 0.470, 0.475, 0.480, 0.485 0.490, 0.495, 0.500, 0.510, 0.520, 0.530 0.540, 0.550, 0.570, 0.580, 0.600, 0.620 0.650, 0.700, 0.750, 0.800, 0.850, 0.900 0.950, 1.000	0.477	0.55
1.5	0.378	0.460	0.463, 0.465, 0.475, 0.480, 0.490, 0.495 0.500, 0.510, 0.520, 0.530, 0.540, 0.550 0.570, 0.600, 0.650, 0.700, 0.750, 0.800 0.850, 0.900, 0.950, 1.000, 1.100, 1.200 1.300, 1.400, 1.500	0.476	0.55
1.8	0.375	0.439	0.450, 0.460, 0.465, 0.470, 0.480, 0.490 0.500, 0.520, 0.530, 0.540, 0.550, 0.580 0.600, 0.650, 0.700, 0.800, 0.900, 1.000 1.200, 1.400, 1.600, 1.800	0.457	0.55

[a] Stellar mass value for the RG progenitor (solar units). [b] Helium abundances adopted for HB models. [c] Evolutionary He core mass values (solar units) at the He ignition. [d] Total stellar mass values adopted for HB models (solar units). [e] Transition mass between AGB-manqué models and models which approach the AGB (solar units). [f] Mass value for the most massive structures which do not experience thermal pulses along the AGB (solar units).

TABLE 4

LINEAR NONADIABATIC PULSATION MODELS FOR $M = 0.485 M_{\odot}$

T_e[a]	$\log(g)$[b]	$P(F)$[c]	$Q(F)$[d]	$\eta(F)$[e]	$P(FO)$[f]	$Q(FO)$[g]	$\eta(FO)$[h]
			$\log L/L_{\odot}$=1.56				
7400	3.00	.3820	.0382	−.0097	.2680	.0268	.0035
7300	2.98	.3995	.0383	−.0080	.2805	.0269	.0120
7100	2.93	.4380	.0386	−.0041	.3081	.0272	.0280
7000	2.90	.4590	.0388	−.0020	.3233	.0273	.0351
6900	2.88	.4815	.0390	.0003	.3396	.0275	.0414
6700	2.83	.5309	.0394	.0051	.3754	.0278	.0506
6500	2.77	.5871	.0398	.0101	.4164	.0282	.0547
6300	2.72	.6515	.0402	.0151	.4632	.0286	.0536
6100	2.66	.7254	.0406	.0199	.5169	.0289	.0471
6000	2.64	.7665	.0408	.0222	.5466	.0291	.0418
5900	2.61	.8107	.0411	.0243	.5785	.0293	.0354
			$\log L/L_{\odot}$=2.0				
6500	2.33	1.3789	.0437	−.0073	.9696	.0307	.0023
6400	2.31	1.4553	.0440	.0064	1.0218	.0309	.0081
6300	2.28	1.5375	.0443	.0204	1.0774	.0311	.0115
6100	2.22	1.7214	.0451	.0494	1.1993	.0314	.0116
5900	2.17	1.9359	.0458	.0789	1.3376	.0317	.0030
5700	2.11	2.1878	.0467	.1079	1.4947	.0319	−.0135
			$\log L/L_{\odot}$=2.2				
6100	2.02	2.5758	.0477	.0242	1.7445	.0323	−.1014
6000	2.00	2.7345	.0482	.0506	1.8389	.0324	−.1023
5800	1.94	3.0929	.0493	.1042	2.0462	.0326	−.1106
5600	1.88	3.5164	.0504	.1576	2.2812	.0327	−.1272
5400	1.81	4.0212	.0517	.2084	2.5486	.0328	−.1514

[a] Effective temperature (K). [b] Logarithmic static gravity. [c] Fundamental period (days). [d] Fundamental pulsation constant (days). [e] Fundamental growth rate. [f] First overtone period (days). [g] First overtone pulsation constant (days). [h] First overtone growth rate.

TABLE 5

LINEAR NONADIABATIC PULSATION MODELS FOR $M = 0.505 M_{\odot}$

T_e[a]	$\log(g)$[b]	$P(F)$[c]	$Q(F)$[d]	$\eta(F)$[e]	$P(FO)$[f]	$Q(FO)$[g]	$\eta(FO)$[h]
			$\log L/L_{\odot}$=1.48				
7500	3.12	.3074	.0373	−.0060	.2164	.0263	.0018
7300	3.07	.3359	.0376	−.0039	.2366	.0265	.0136
7100	3.02	.3681	.0379	−.0015	.2594	.0267	.0250
7000	3.00	.3857	.0381	−.0001	.2720	.0269	.0300
6900	2.97	.4045	.0383	.0013	.2854	.0270	.0345
6800	2.95	.4245	.0384	.0028	.2997	.0271	.0382
6700	2.92	.4458	.0386	.0043	.3151	.0273	.0411
6600	2.90	.4685	.0388	.0058	.3315	.0274	.0429
6100	2.76	.6077	.0397	.0129	.4326	.0283	.0364
5900	2.70	.6786	.0401	.0151	.4841	.0286	.0263
			$\log L/L_{\odot}$=1.56				
7400	3.02	.3724	.0380	−.0084	.2614	.0266	.0038
7000	2.92	.4475	.0386	−.0017	.3150	.0272	.0330
6900	2.90	.4693	.0388	.0003	.3308	.0273	.0389
6800	2.87	.4925	.0390	.0024	.3476	.0275	.0438
6600	2.82	.5438	.0393	.0067	.3848	.0278	.0503
6400	2.76	.6023	.0397	.0110	.4274	.0282	.0519
6200	2.71	.6692	.0401	.0154	.4761	.0285	.0485
6000	2.65	.7463	.0406	.0193	.5320	.0289	.0401
			$\log L/L_{\odot}$=2.0				
6600	2.38	1.2730	.0431	−.0171	.8968	.0303	.0037
6500	2.35	1.3418	.0434	−.0053	.9448	.0305	.0119
6400	2.32	1.4158	.0437	.0071	.9958	.0307	.0178
6300	2.30	1.4954	.0440	.0198	1.0502	.0309	.0213
6100	2.24	1.6733	.0447	.0461	1.1697	.0312	.0215
5900	2.18	1.8807	.0454	.0730	1.3053	.0315	.0133
5700	2.12	2.1240	.0463	.0993	1.4595	.0318	−.0029
5600	2.09	2.2617	.0467	.1117	1.5445	.0319	−.0140
5400	2.03	2.5755	.0477	.1334	1.7321	.0321	−.0409
5200	1.96	2.9509	.0488	.1489	1.9469	.0322	−.0732
5000	1.90	3.4036	.0501	.1554	2.1936	.0323	−.1081
4900	1.86	3.6647	.0507	.1548	2.3305	.0322	−.1248
			$\log L/L_{\odot}$=2.2				
6200	2.07	2.3596	.0468	.0026	1.6160	.0321	−.0811
6000	2.01	2.6547	.0478	.0508	1.7963	.0323	−.0804
5800	1.95	3.0008	.0488	.1003	2.0001	.0325	−.0885
5700	1.92	3.1950	.0493	.1257	2.1101	.0325	−.0966
5500	1.86	3.6406	.0504	.1741	2.3562	.0327	−.1172
5450	1.85	3.7667	.0508	.2389	2.4254	.0327	−.0292

[a] Effective temperature (K). [b] Logarithmic static gravity. [c] Fundamental period (days). [d] Fundamental pulsation constant (days). [e] Fundamental growth rate. [f] First overtone period (days). [g] First overtone pulsation constant (days). [h] First overtone growth rate.

TABLE 6

LINEAR NONADIABATIC PULSATION MODELS FOR $M = 0.520 M_{\odot}$

T_e[a]	$\log(g)$[b]	$P(F)$[c]	$Q(F)$[d]	$\eta(F)$[e]	$P(FO)$[f]	$Q(FO)$[g]	$\eta(FO)$[h]
			$\log L/L_{\odot}$ =1.56				
7400	3.03	.3657	.0378	−.0076	.2568	.0266	.0039
7300	3.01	.3824	.0380	−.0062	.2686	.0267	.0112
7100	2.96	.4191	.0383	−.0031	.2948	.0269	.0251
6900	2.91	.4607	.0386	.0003	.3246	.0272	.0369
6700	2.86	.5078	.0390	.0041	.3587	.0275	.0454
6500	2.80	.5614	.0394	.0081	.3976	.0279	.0495
6300	2.75	.6227	.0397	.0120	.4422	.0282	.0488
6100	2.69	.6930	.0402	.0157	.4933	.0286	.0432
6000	2.67	.7321	.0404	.0175	.5216	.0288	.0387
			$\log L/L_{\odot}$ =2.0				
6600	2.39	1.2484	.0428	−.0149	.8799	.0302	.0097
6500	2.36	1.3157	.0431	−.0040	.9271	.0304	.0178
6400	2.34	1.3881	.0434	.0075	.9773	.0306	.0237
6200	2.28	1.5494	.0441	.0314	1.0878	.0310	.0284
6000	2.23	1.7367	.0448	.0562	1.2132	.0313	.0246
5900	2.20	1.8419	.0452	.0688	1.2822	.0314	.0196
5700	2.14	2.0791	.0460	.0933	1.4342	.0317	.0037
5650	2.12	2.1449	.0462	.0991	1.4755	.0318	−.0016
			$\log L/L_{\odot}$ =2.2				
6200	2.08	2.3108	.0465	.0050	1.5878	.0465	−.0666
6100	2.05	2.4491	.0470	.0275	1.6741	.0470	−.0649
6000	2.03	2.5986	.0474	.0504	1.7658	.0474	−.0657
5800	1.97	2.9360	.0484	.0972	1.9670	.0484	−.0736
5600	1.91	3.3346	.0495	.1438	2.1954	.0495	−.0902
5450	1.86	3.6825	.0504	.1771	2.3873	.0504	−.1077

[a] Effective temperature (K). [b] Logarithmic static gravity. [c] Fundamental period (days). [d] Fundamental pulsation constant (days). [e] Fundamental growth rate. [f] First overtone period (days). [g] First overtone pulsation constant (days). [h] First overtone growth rate.

TABLE 7

NONLINEAR SURVEY FOR $M = 0.505 M_{\odot}$

T_e [a]	P [b]	$\Delta R/R_{ph}$ [c]	Δu [d]	ΔM_{bol} [e]	$\Delta \log g_s$ [f]	$\Delta \log g_{eff}$ [g]	ΔT [h]	ΔT_e [i]
			$\log L/L_{\odot}$ =1.48		First Overtone			
7000	.2712	.036	25.94	.310	.03	.32	450	550
6900	.2847	.043	31.44	.345	.04	.40	450	600
6700	.3138	.040	28.25	.265	.03	.36	350	400
			$\log L/L_{\odot}$ =1.48		Fundamental			
6800	.4246	.120	69.12	1.023	.11	.71	1350	1650
6700	.4460	.126	69.63	.971	.11	.79	1250	1500
6600	.4681	.036	24.25	.214	.03	.32	300	350
6100	.6068	.090	39.18	.334	.08	.46	450	550
6000	.6405	.069	28.51	.218	.06	.33	300	400
			$\log L/L_{\odot}$ =2.0		Fundamental			
6400	1.4164	.098	32.59	.571	.08	.40	750	900
6300	1.4997	.156	52.49	1.033	.13	.69	1550	1750
6200	1.5959	.300	104.75	1.545	.25	1.57	2100	2550
6100	1.6910	.236	75.26	1.564	.20	1.34	2050	2500
5900	1.9077	.293	95.52	1.388	.24	1.30	1750	2150
5800	2.0258	.276	83.15	1.361	.24	1.34	1500	1800
5700 [j]	2.1392	.312	87.85	1.130	.28	1.41	1400	1750
5600	2.2761	.292	88.67	1.103	.25	1.29	1250	1550
5500	2.4144	.280	82.21	.968	.24	1.26	1150	1450
5400	2.5701	.254	62.05	.943	.22	1.28	1200	1450
5200	2.9040	.240	52.96	.742	.21	1.21	1000	1250
5000	3.2861	.207	41.99	.559	.18	.96	750	950
4900	3.5000	.155	30.31	.385	.14	.54	550	650
			$\log L/L_{\odot}$ =2.2		Fundamental			
5700	3.2305	.324	69.28	1.342	.28	1.51	1700	2100
5500	3.6369	.313	66.60	1.194	.27	1.54	1300	1600

[a] Effective temperature (K). [b] Period (days). [c] Fractional radius variation. [d] Radial velocity amplitude (Km/s). [e] Bolometric amplitude (mag.). [f] Amplitude of logarithmic static gravity. [g] Amplitude of logarithmic effective gravity. [h] Surface temperature variation. [i] Effective temperature variation. [j] Mixed-mode pulsator. The amplitudes referred to this model are the average values over the last twenty cycles.

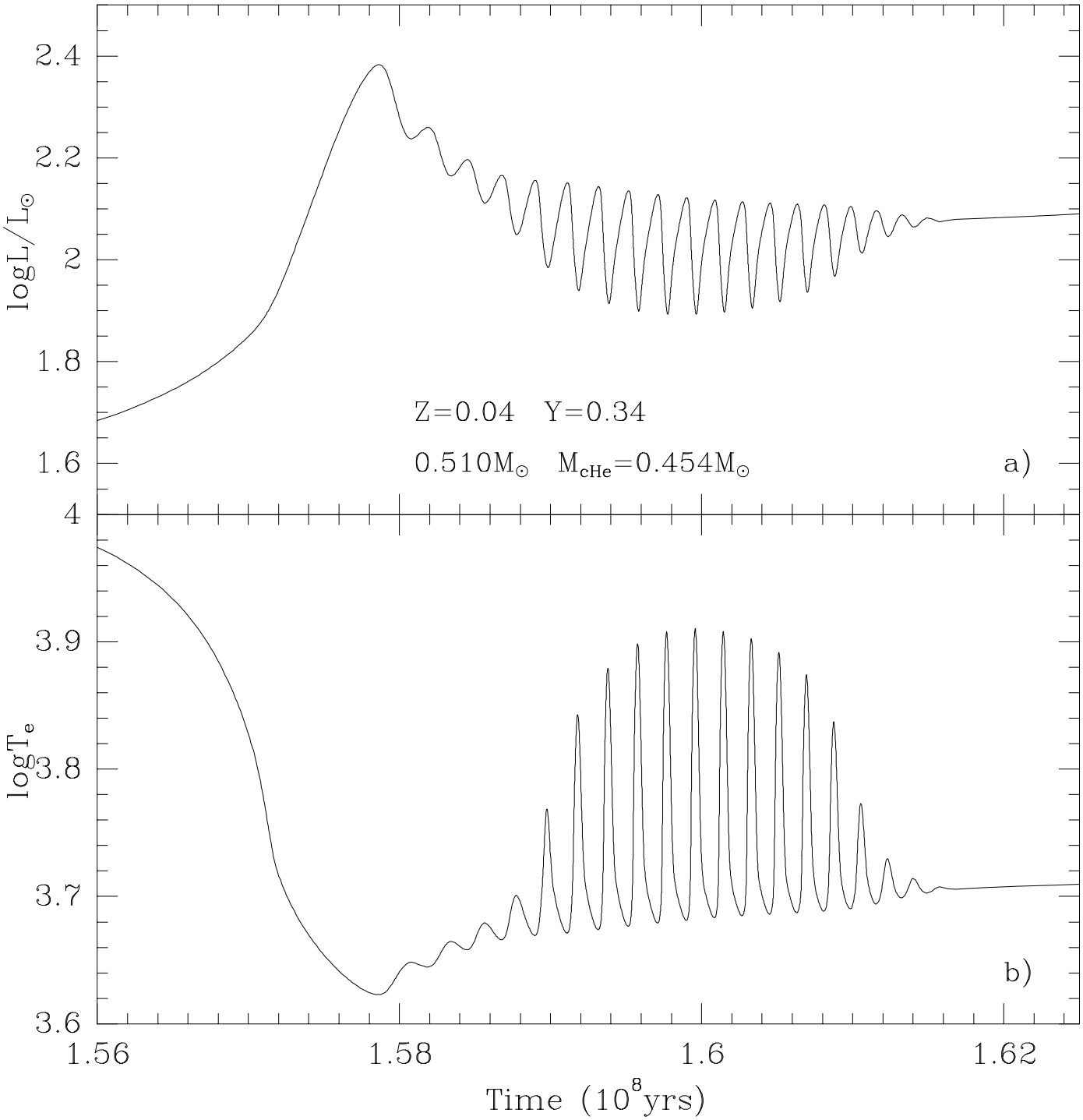
2.4
2.2
2
1.8
1.6
logL/L⊙
Z=0.04 Y=0.34
0.510M⊙ M_cHe=0.454M⊙
a)
4
3.9
3.8
3.7
3.6
logT_e
b)
1.56
1.58
1.6
1.62
Time (10^8 yrs)

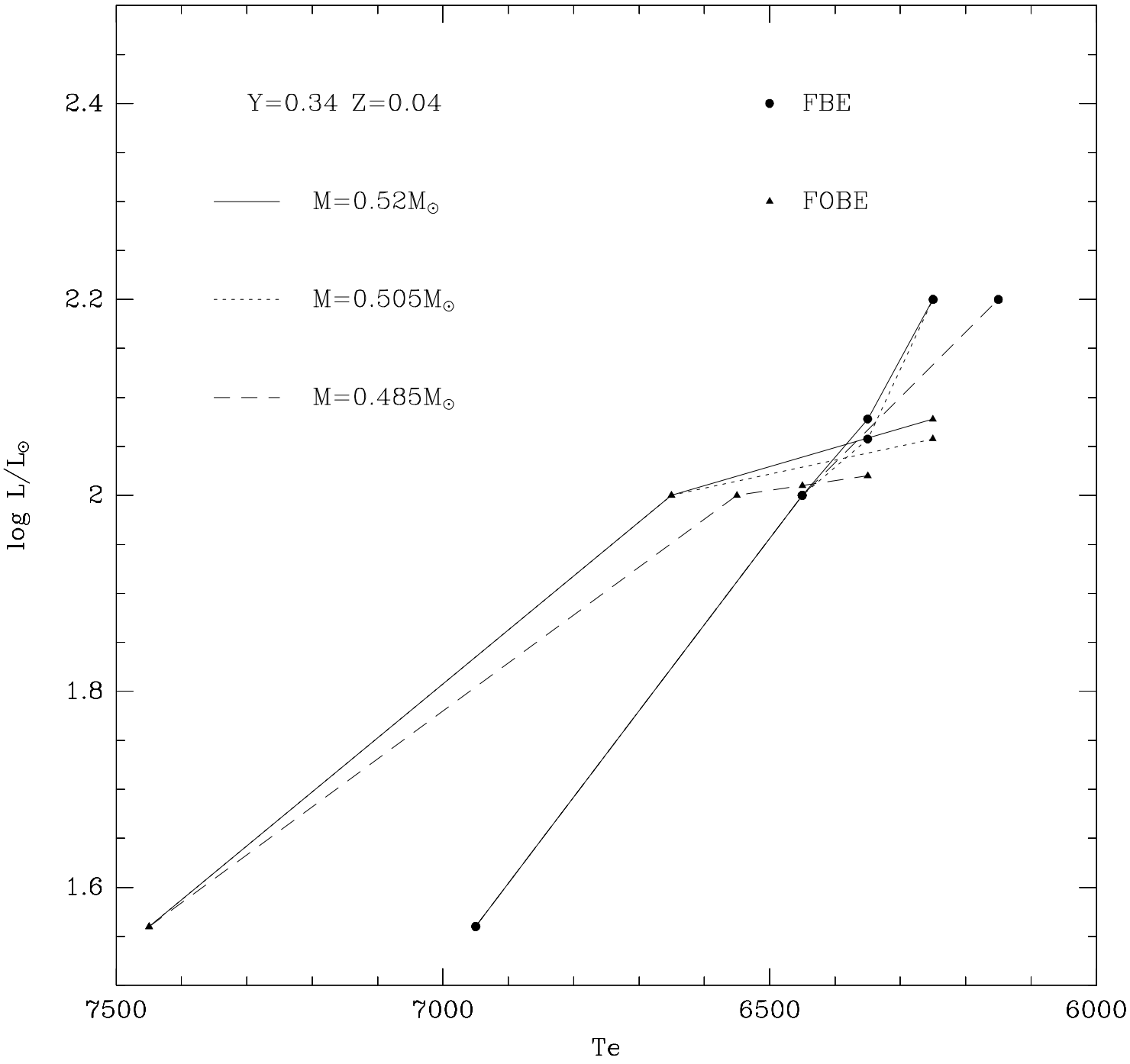
Y=0.34 Z=0.04
FBE
FOBE
M=0.52M⊙
M=0.505M⊙
M=0.485M⊙
log L/L⊙
2.4
2.2
2
1.8
1.6
7500
7000
6500
6000
Te

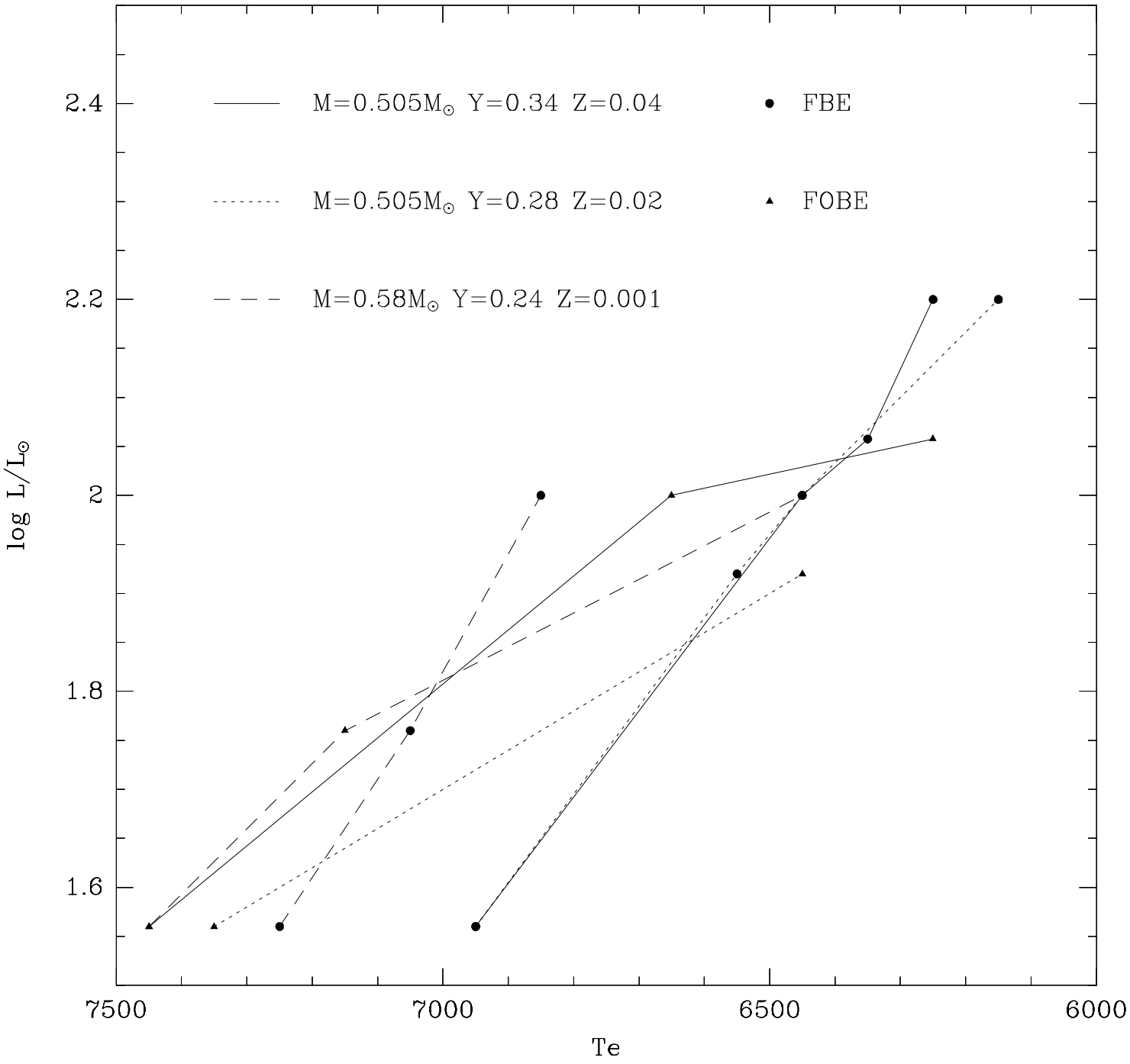
M=0.505M⊙ Y=0.34 Z=0.04
FBE
M=0.505M⊙ Y=0.28 Z=0.02
FOBE
M=0.58M⊙ Y=0.24 Z=0.001
2.4
2.2
2
1.8
1.6
log L/L⊙
7500
7000
6500
6000
Te

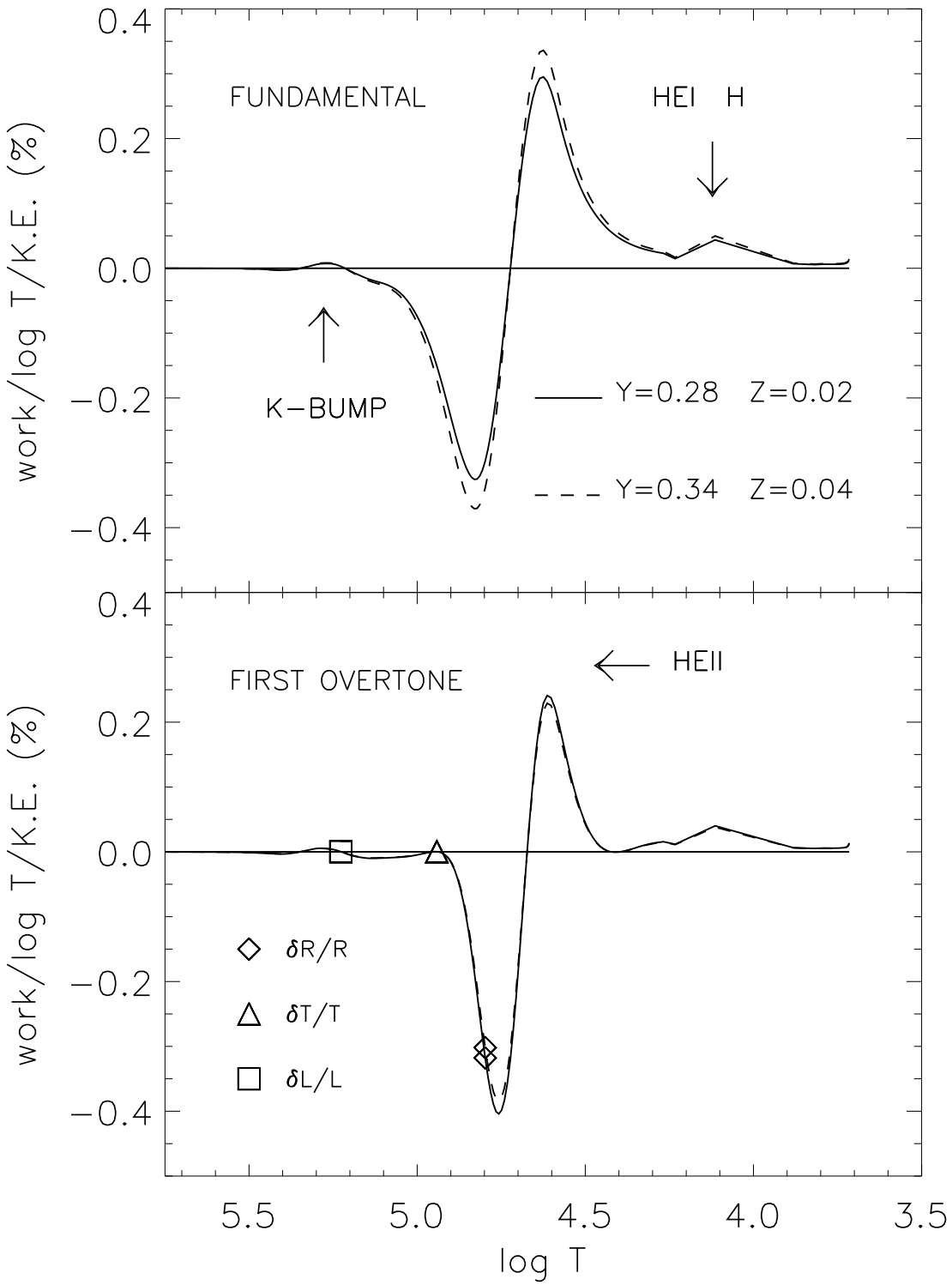
FUNDAMENTAL
HEI H
K−BUMP
Y=0.28 Z=0.02
Y=0.34 Z=0.04
FIRST OVERTONE
HEII
δR/R
δT/T
δL/L
work/log T/K.E. (%)
log T
0.4
0.2
0.0
−0.2
−0.4
5.5
5.0
4.5
4.0
3.5

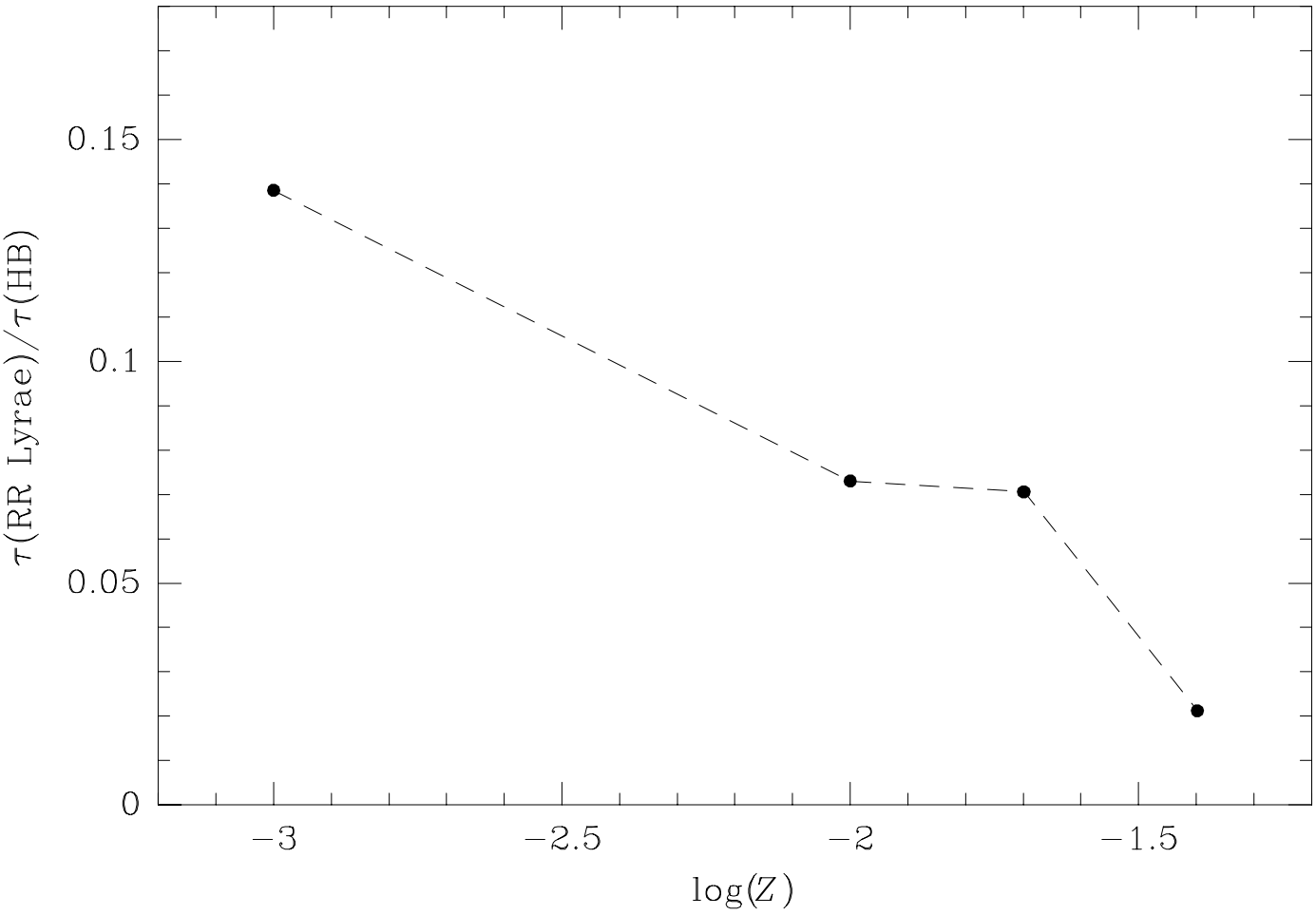
0.15
0.1
0.05
0
τ(RR Lyrae)/τ(HB)
−3
−2.5
−2
−1.5
log(Z)

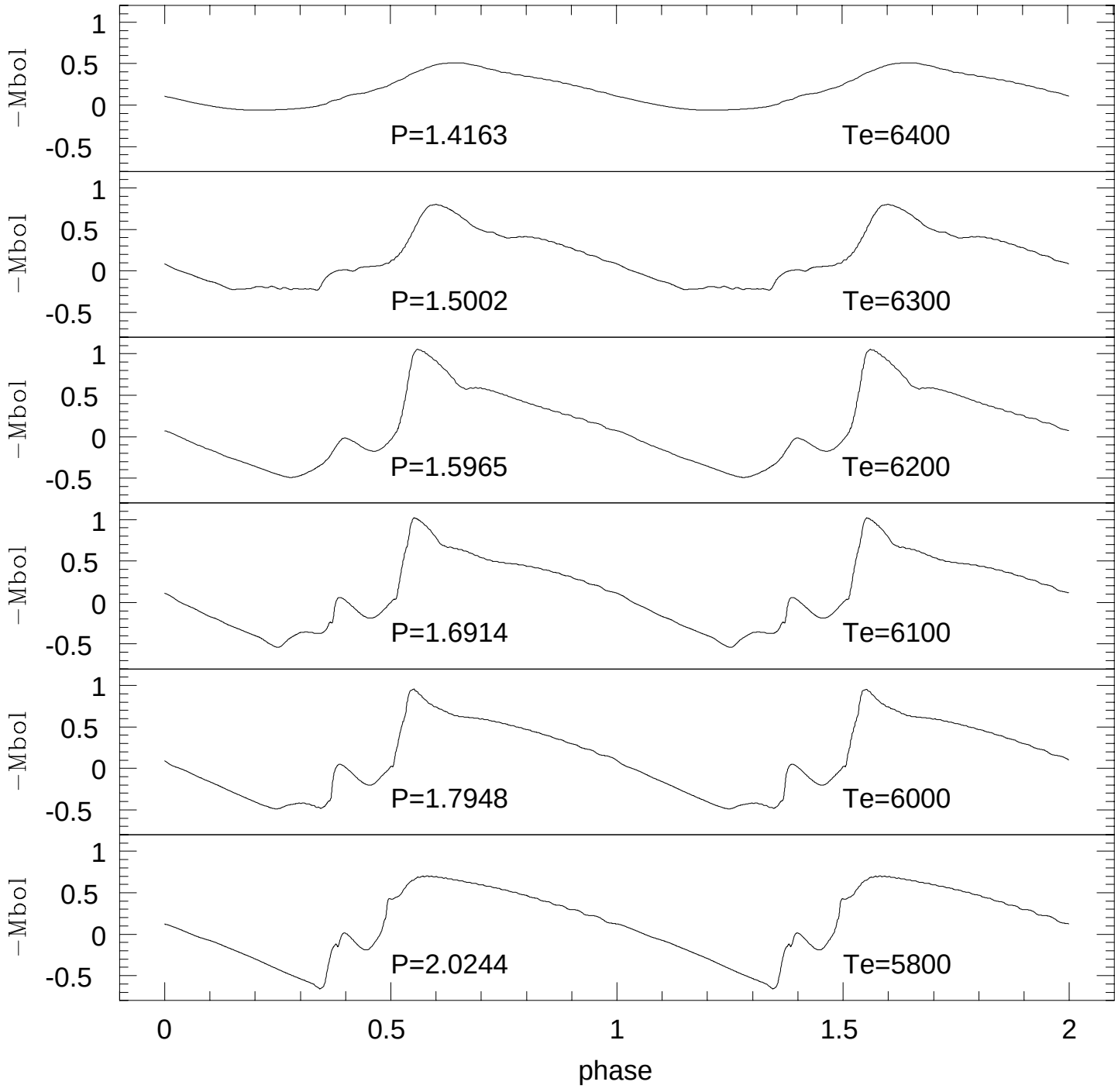
−Mbol
1
0.5
0
-0.5
P=1.4163
Te=6400
P=1.5002
Te=6300
P=1.5965
Te=6200
P=1.6914
Te=6100
P=1.7948
Te=6000
P=2.0244
Te=5800
0
0.5
1
1.5
2
phase

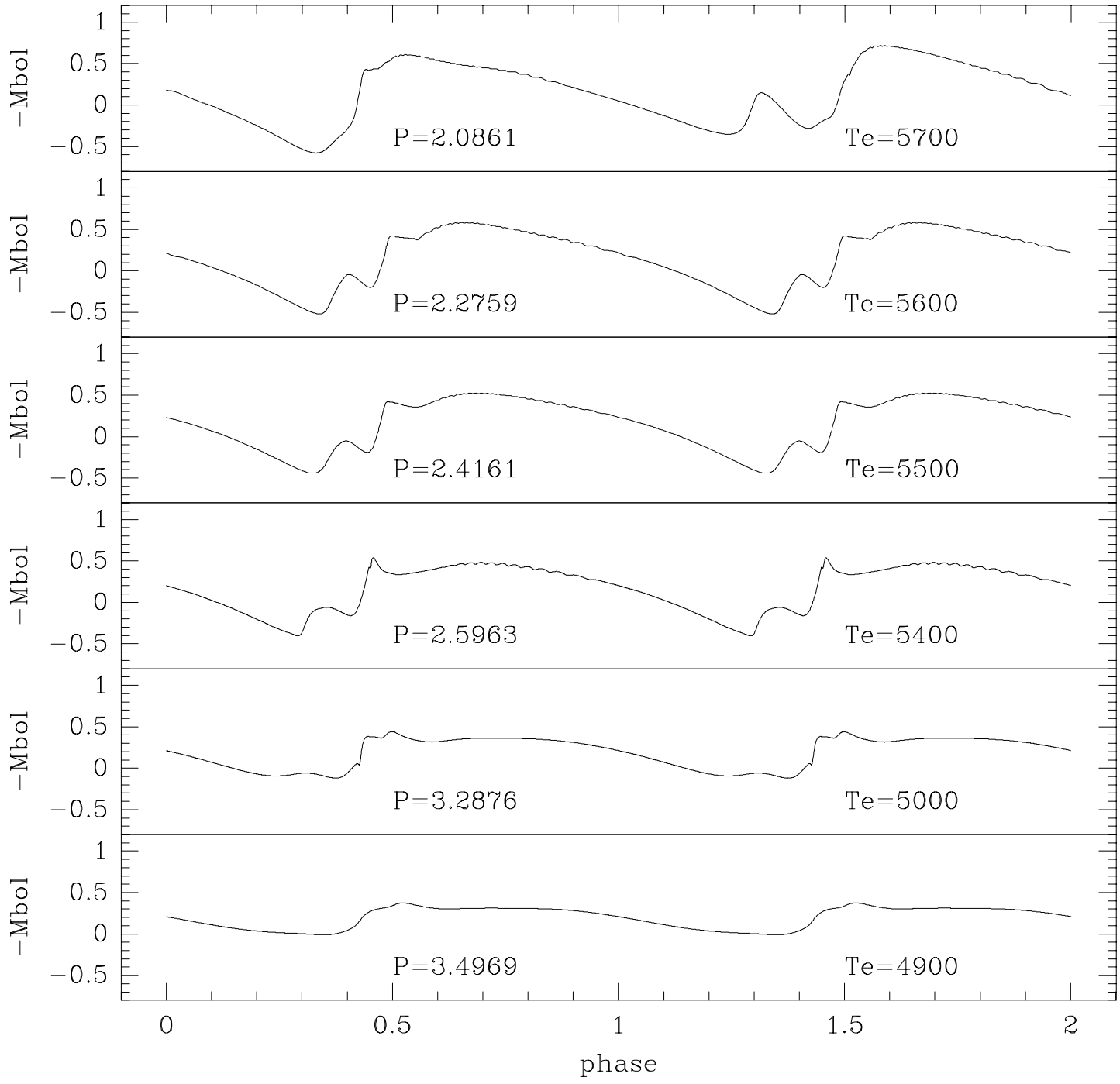
−Mbol
1
0.5
0
−0.5
P=2.0861
Te=5700
P=2.2759
Te=5600
P=2.4161
Te=5500
P=2.5963
Te=5400
P=3.2876
Te=5000
P=3.4969
Te=4900
0
0.5
1
1.5
2
phase

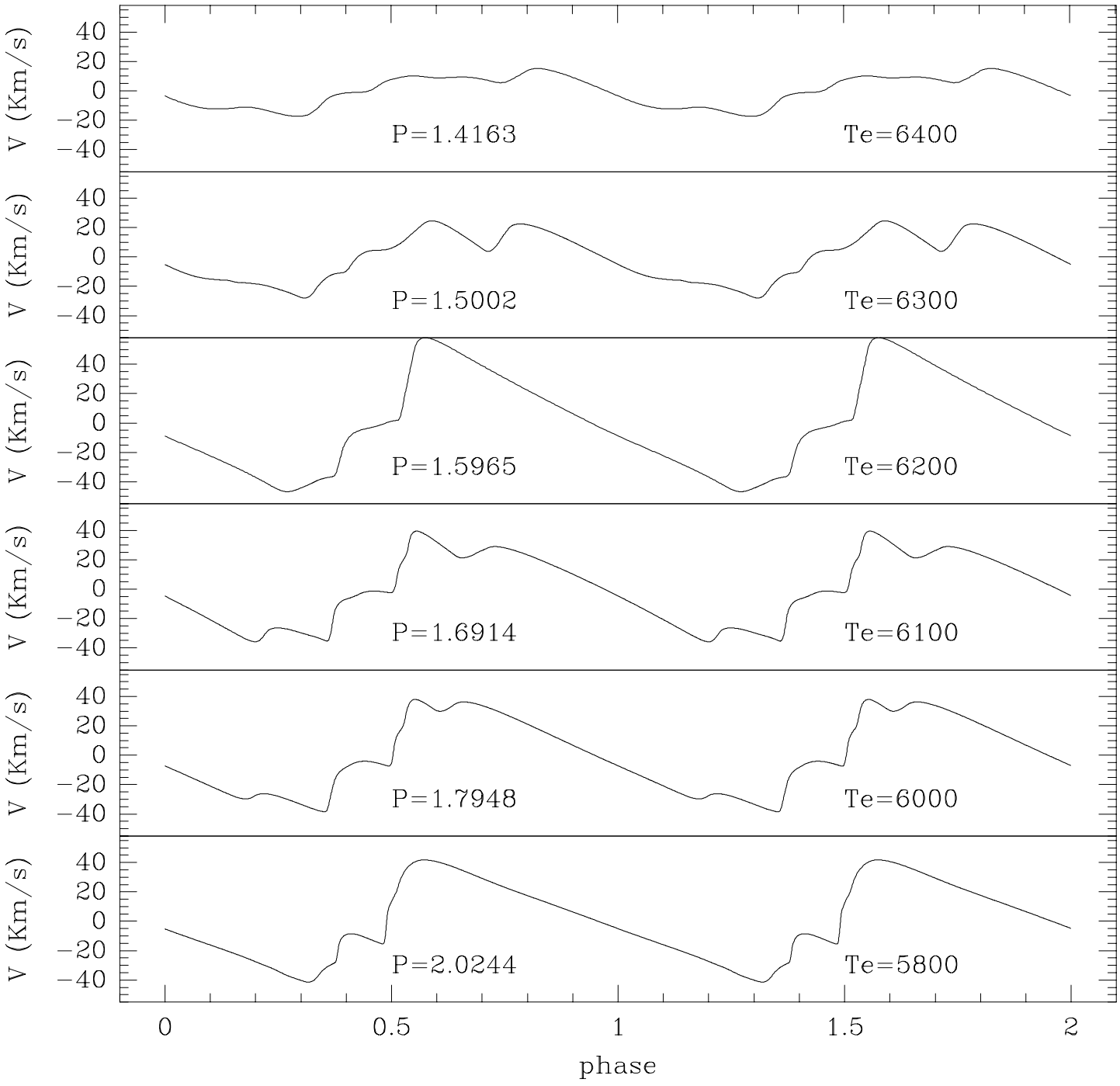
V (Km/s)
40
20
0
−20
−40
P=1.4163
Te=6400
P=1.5002
Te=6300
P=1.5965
Te=6200
P=1.6914
Te=6100
P=1.7948
Te=6000
P=2.0244
Te=5800
0
0.5
1
1.5
2
phase

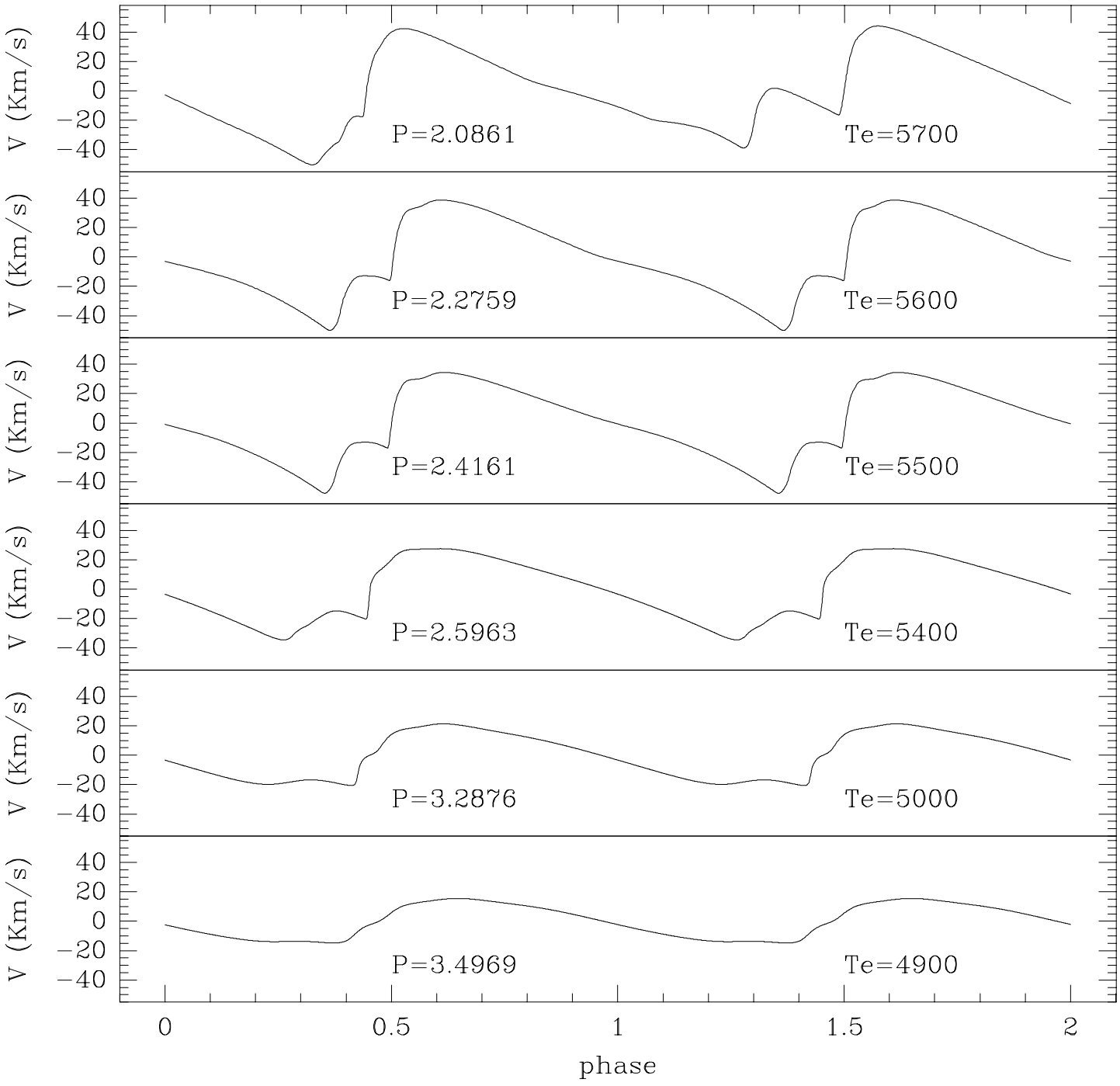
V (Km/s)
40
20
0
−20
−40
P=2.0861
Te=5700
P=2.2759
Te=5600
P=2.4161
Te=5500
P=2.5963
Te=5400
P=3.2876
Te=5000
P=3.4969
Te=4900
0
0.5
1
1.5
2
phase

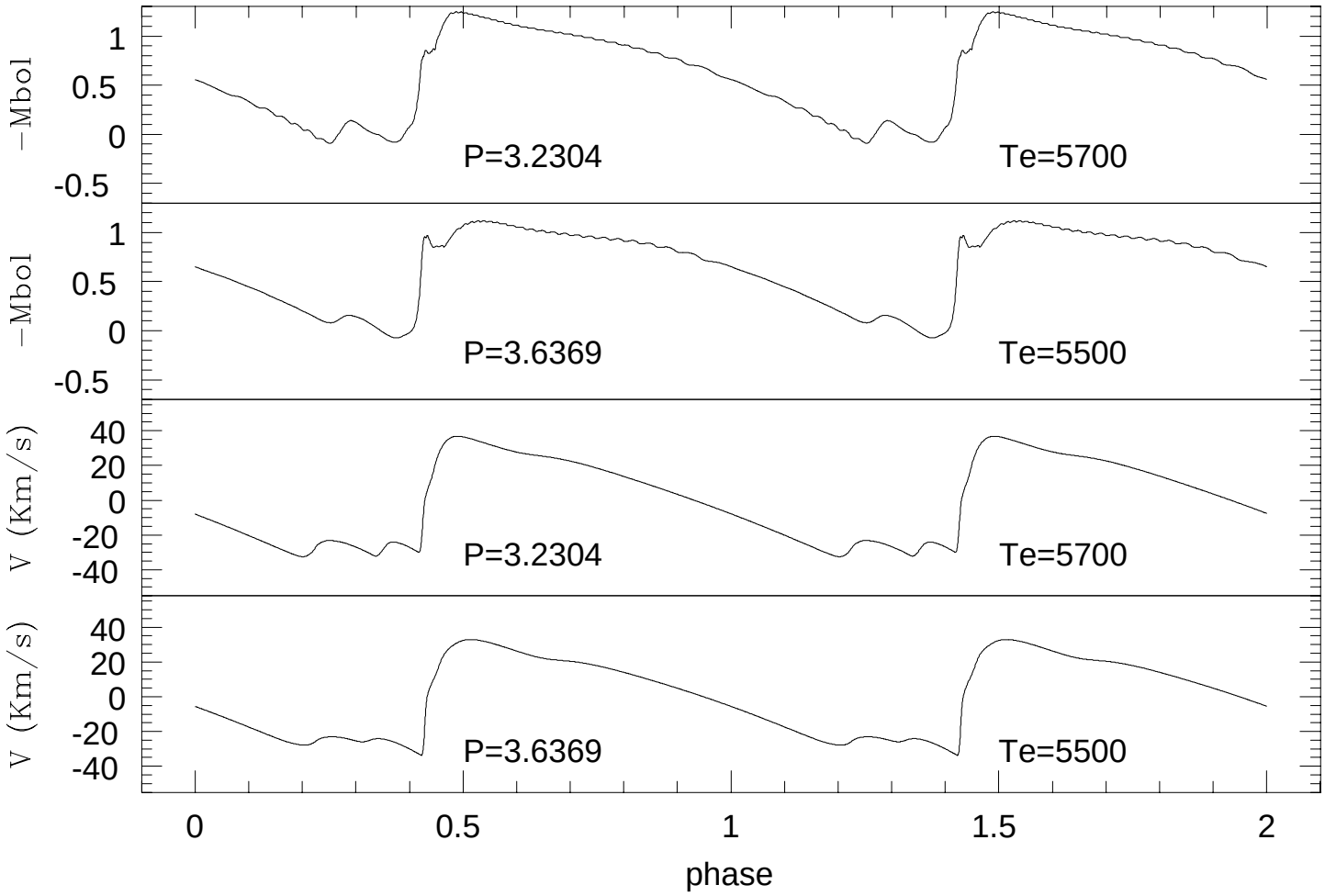
−Mbol
1
0.5
0
-0.5
P=3.2304
Te=5700
−Mbol
1
0.5
0
-0.5
P=3.6369
Te=5500
V (Km/s)
40
20
0
-20
-40
P=3.2304
Te=5700
V (Km/s)
40
20
0
-20
-40
P=3.6369
Te=5500
0
0.5
1
1.5
2
phase

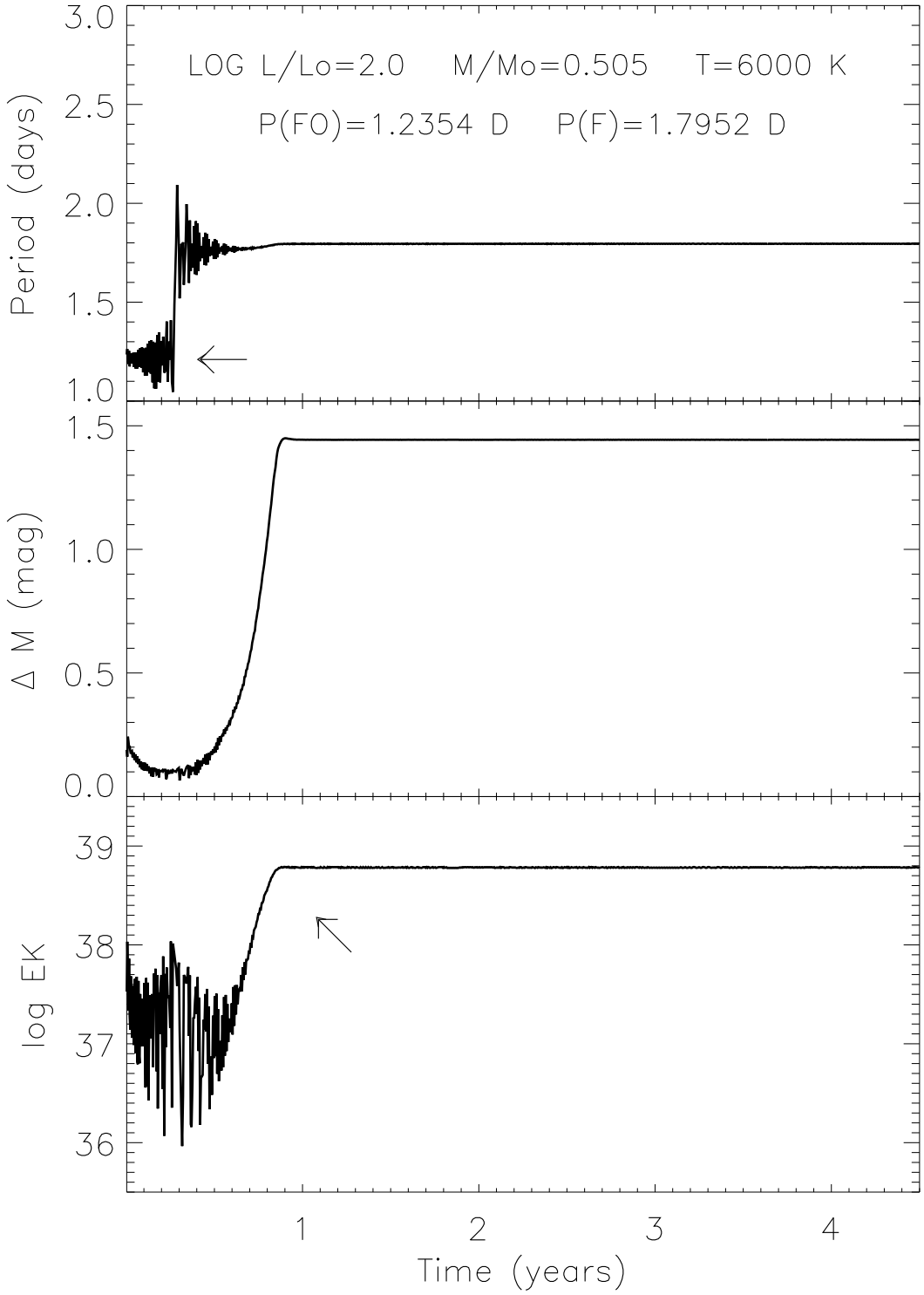
LOG L/Lo=2.0 M/Mo=0.505 T=6000 K
P(FO)=1.2354 D P(F)=1.7952 D
Period (days)
3.0
2.5
2.0
1.5
1.0
Δ M (mag)
1.5
1.0
0.5
0.0
log EK
39
38
37
36
1
2
3
4
Time (years)

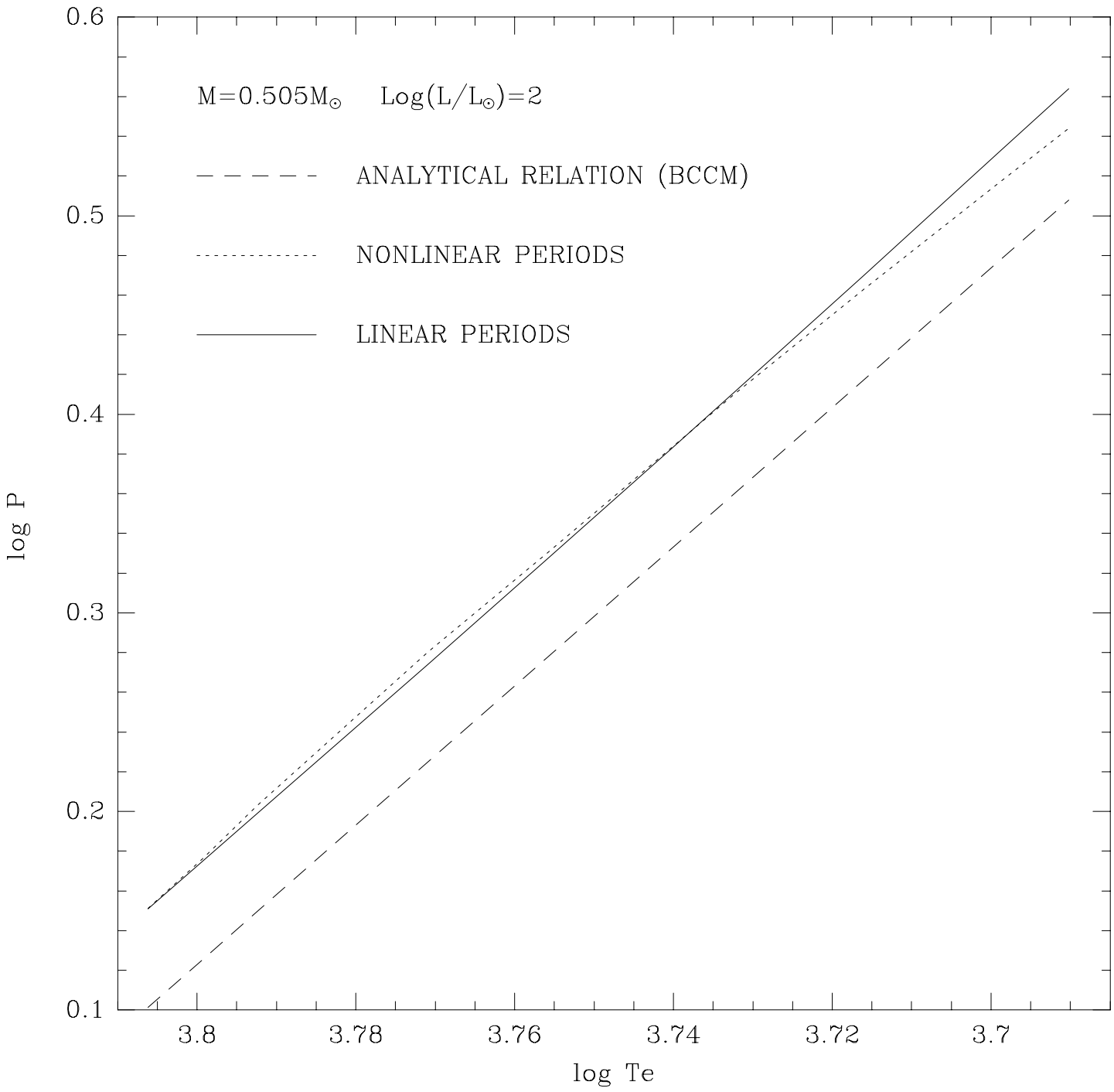
M=0.505M⊙ Log(L/L⊙)=2
ANALYTICAL RELATION (BCCM)
NONLINEAR PERIODS
LINEAR PERIODS
0.6
0.5
0.4
0.3
0.2
0.1
log P
3.8
3.78
3.76
3.74
3.72
3.7
log Te

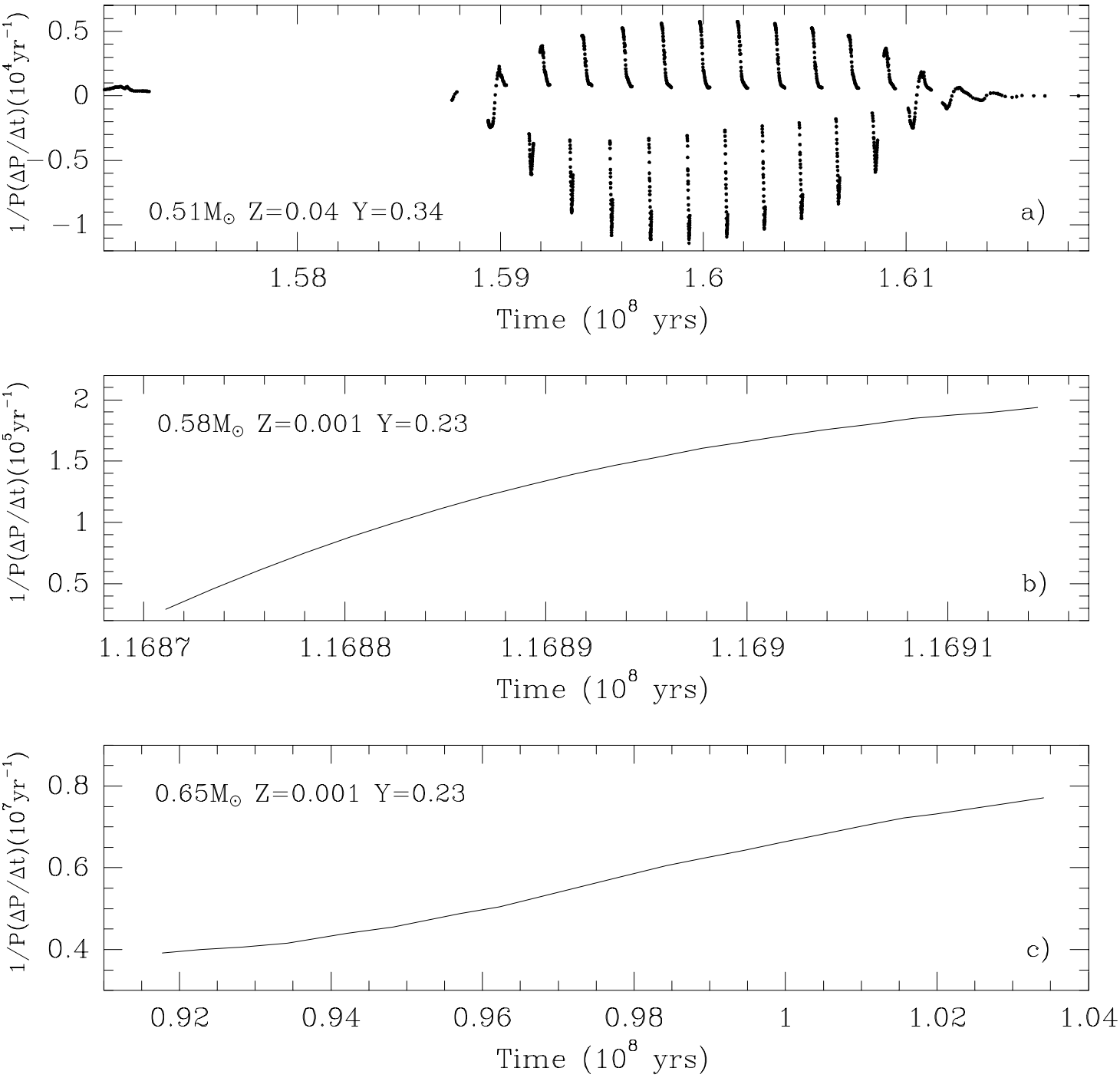
0.5
0
−0.5
−1
1/P(ΔP/Δt)(10^4yr^−1)
0.51M⊙ Z=0.04 Y=0.34
a)
1.58
1.59
1.6
1.61
Time (10^8 yrs)
2
1.5
1
0.5
1/P(ΔP/Δt)(10^5yr^−1)
0.58M⊙ Z=0.001 Y=0.23
b)
1.1687
1.1688
1.1689
1.169
1.1691
Time (10^8 yrs)
0.8
0.6
0.4
1/P(ΔP/Δt)(10^7yr^−1)
0.65M⊙ Z=0.001 Y=0.23
c)
0.92
0.94
0.96
0.98
1
1.02
1.04
Time (10^8 yrs)

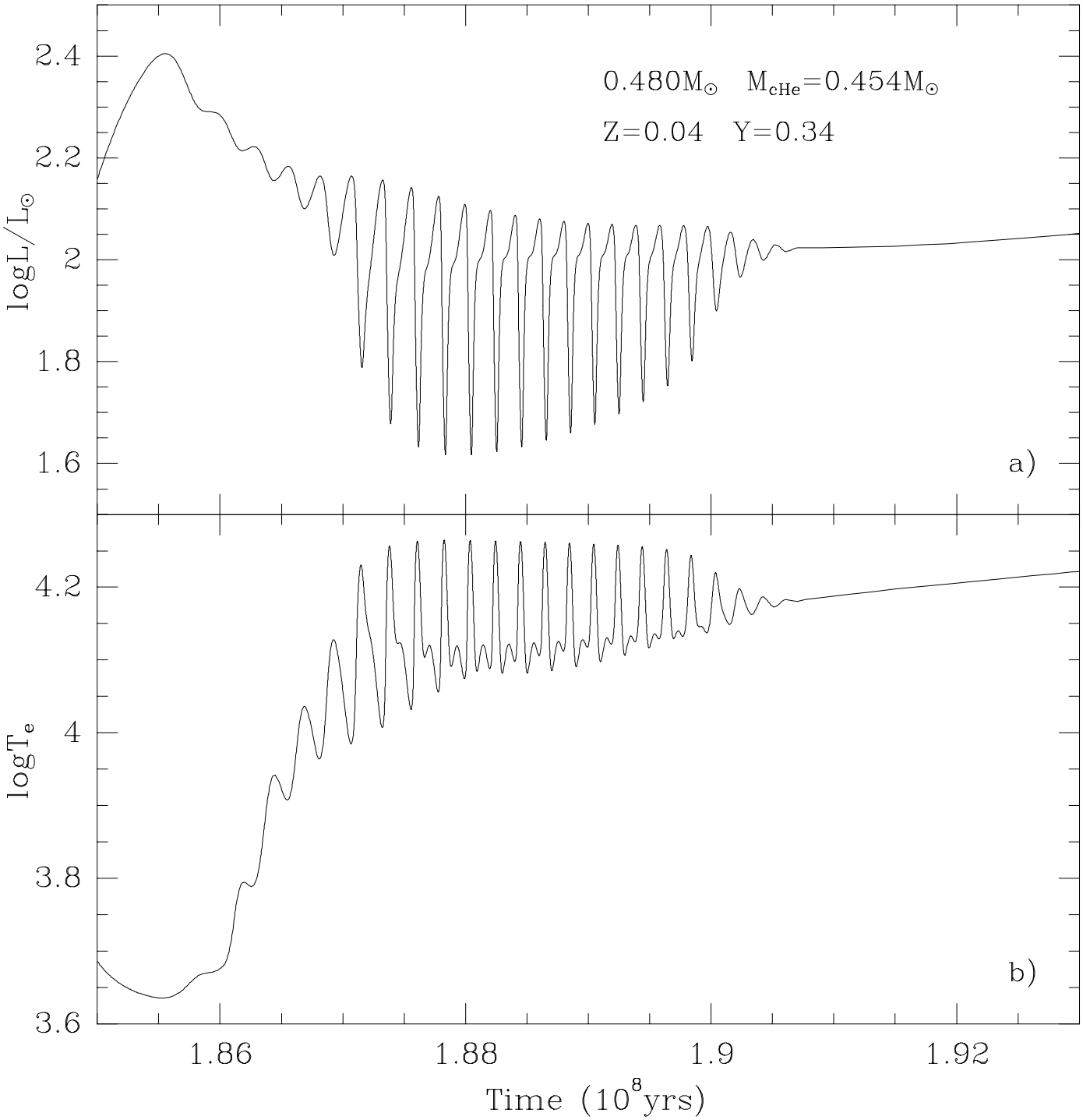
0.480M⊙ M_cHe=0.454M⊙
Z=0.04 Y=0.34
a)
b)
logL/L⊙
logT_e
Time (10^8 yrs)
2.4
2.2
2
1.8
1.6
4.2
4
3.8
3.6
1.86
1.88
1.9
1.92

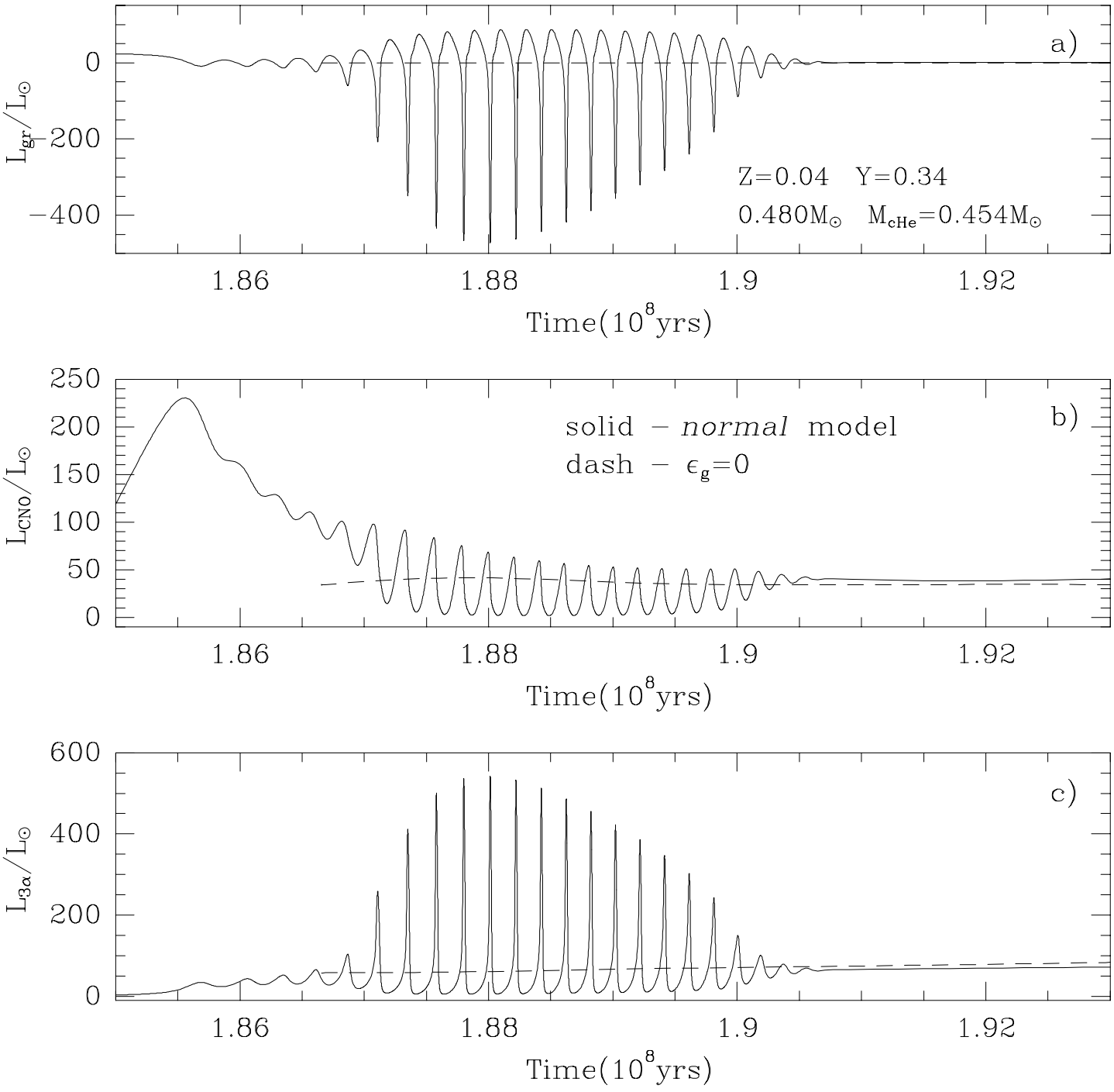
a)
0
−200
−400
$L_{gr}/L_\odot$
Z=0.04 Y=0.34
0.480$M_\odot$ M_{cHe}=0.454$M_\odot$
1.86
1.88
1.9
1.92
Time(10^8yrs)
b)
250
200
150
100
50
0
$L_{CNO}/L_\odot$
solid – *normal* model
dash – ϵ_g=0
1.86
1.88
1.9
1.92
Time(10^8yrs)
c)
600
400
200
0
$L_{3\alpha}/L_\odot$
1.86
1.88
1.9
1.92
Time(10^8yrs)

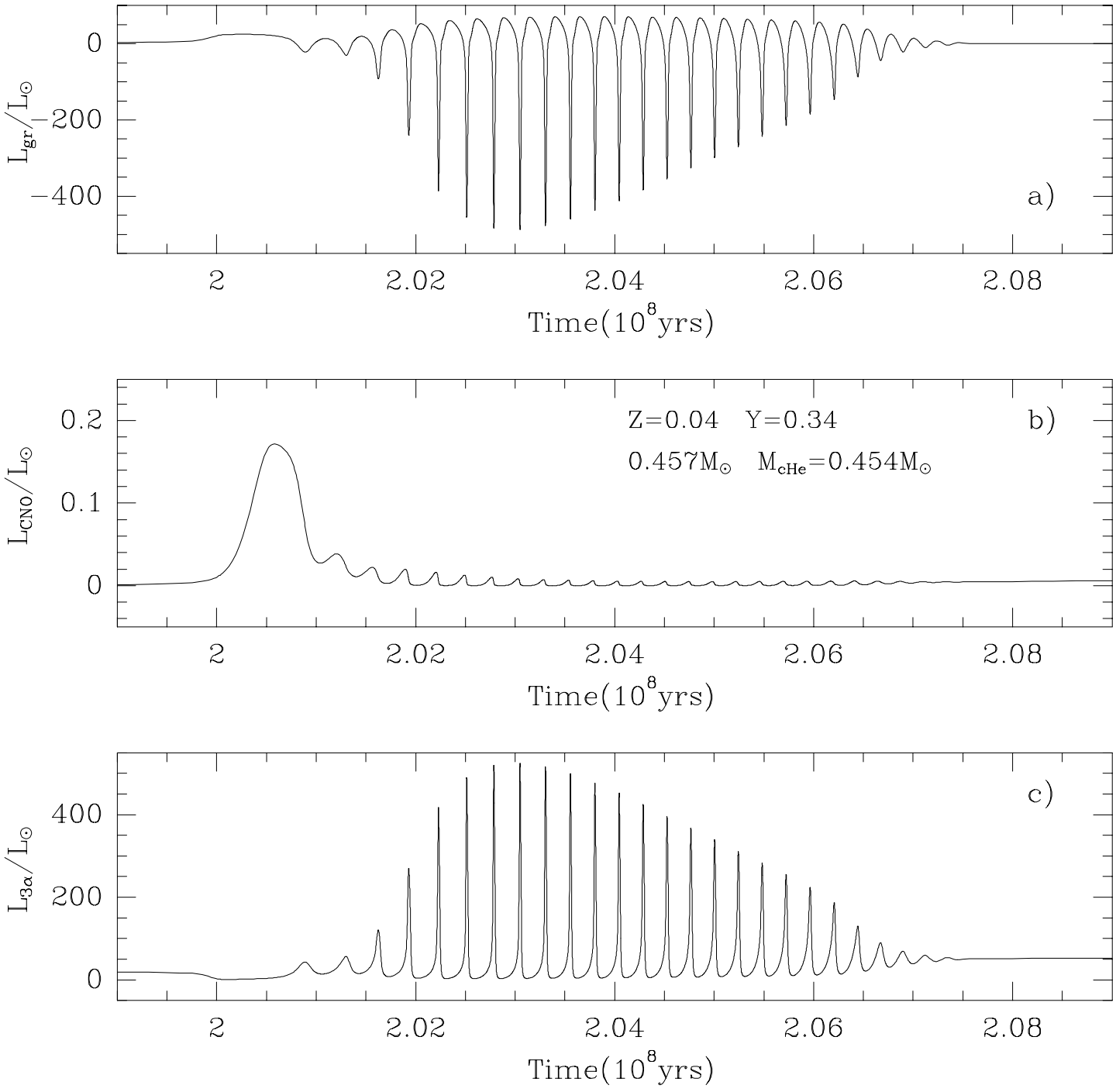
0
−200
−400
$L_{gr}/L_{\odot}$
a)
2
2.02
2.04
2.06
2.08
Time(10^8yrs)
0.2
0.1
0
$L_{CNO}/L_{\odot}$
Z=0.04 Y=0.34
0.457$M_{\odot}$ M_{cHe}=0.454$M_{\odot}$
b)
2
2.02
2.04
2.06
2.08
Time(10^8yrs)
400
200
0
$L_{3\alpha}/L_{\odot}$
c)
2
2.02
2.04
2.06
2.08
Time(10^8yrs)

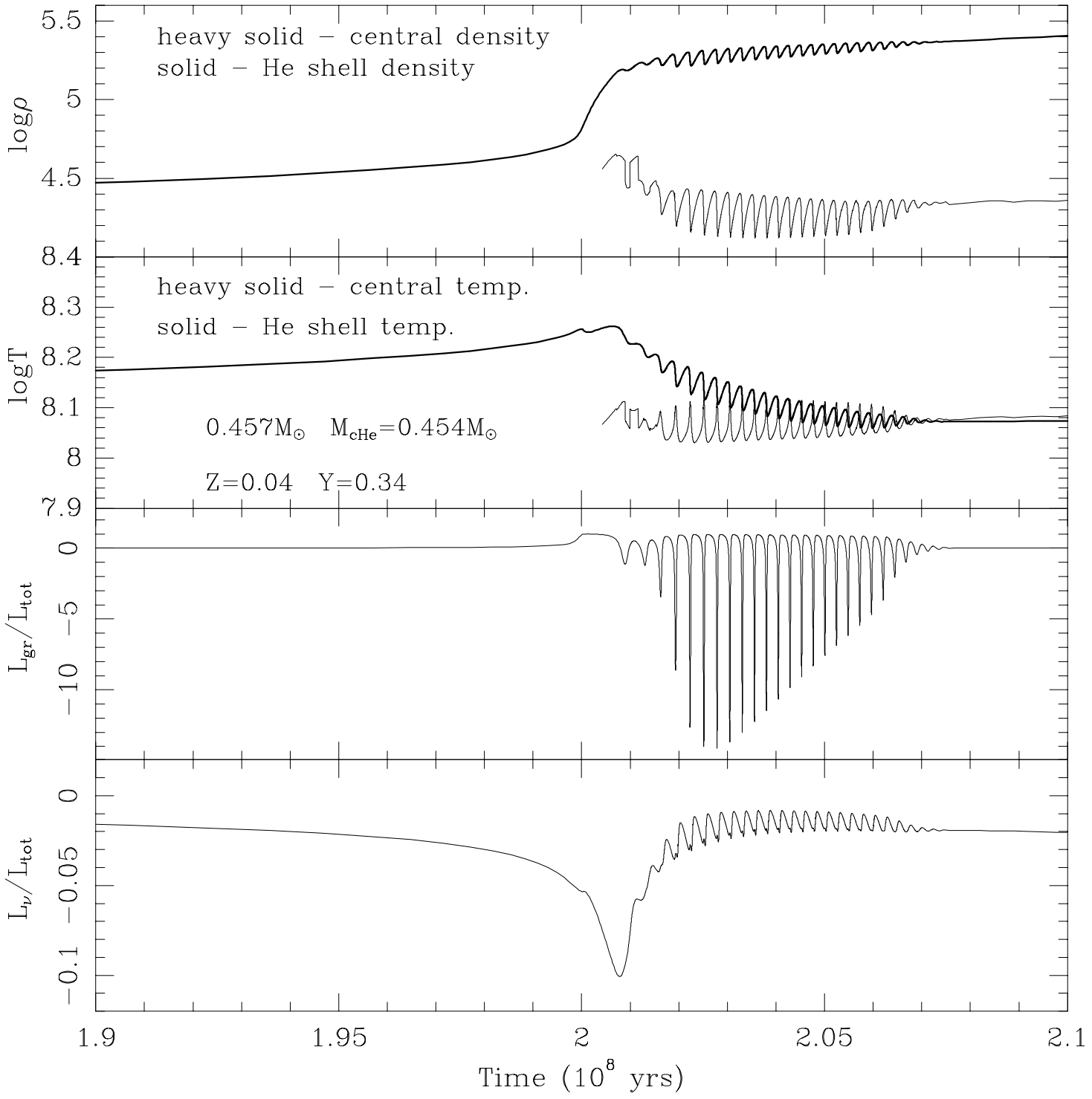
heavy solid – central density
solid – He shell density
logρ
heavy solid – central temp.
solid – He shell temp.
logT
0.457M⊙ M_cHe=0.454M⊙
Z=0.04 Y=0.34
L_gr/L_tot
L_ν/L_tot
Time (10^8 yrs)

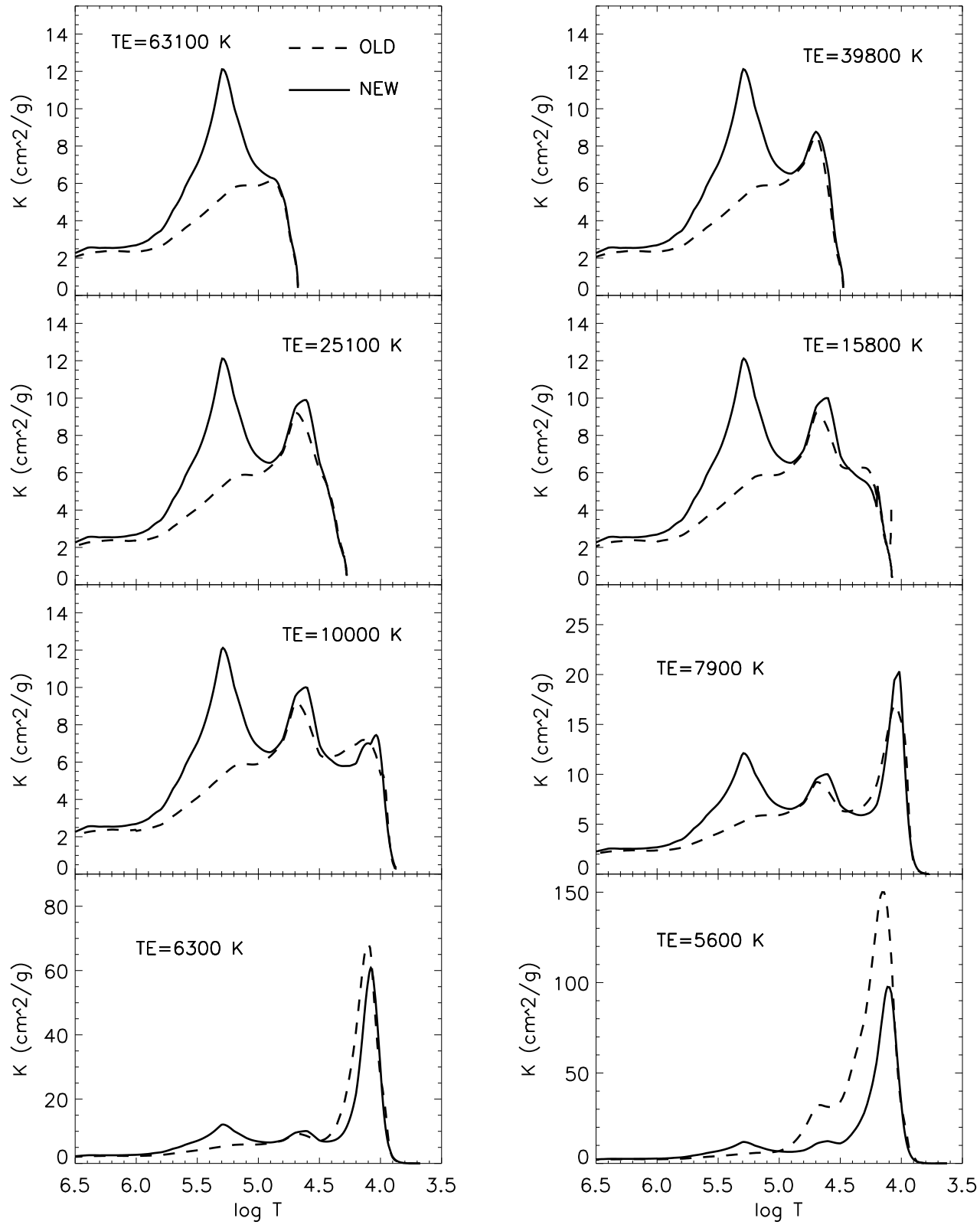
TE=63100 K
OLD
NEW
TE=39800 K
TE=25100 K
TE=15800 K
TE=10000 K
TE=7900 K
TE=6300 K
TE=5600 K
K (cm^2/g)
log T